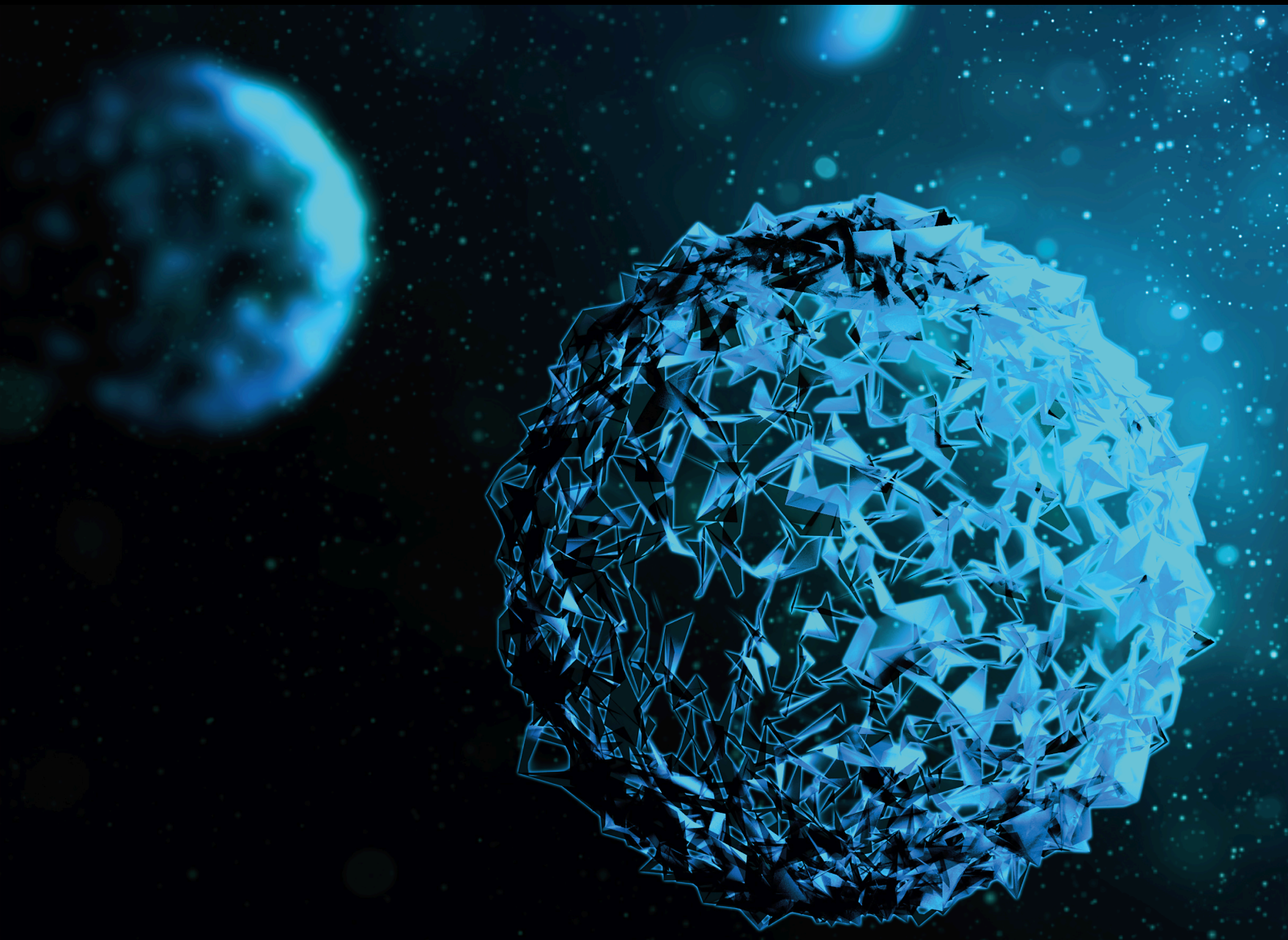


Mechanisms of Stress Adaptation in Cancer and Unraveling Promising Therapeutic Opportunities

Lead Guest Editor: Hai-Feng Zhang

Guest Editors: Amal EL-Naggar and Chengsheng Wu





Mechanisms of Stress Adaptation in Cancer and Unraveling Promising Therapeutic Opportunities

BioMed Research International

Mechanisms of Stress Adaptation in Cancer and Unraveling Promising Therapeutic Opportunities

Lead Guest Editor: Hai-Feng Zhang

Guest Editors: Amal EL-Naggar and Chengsheng
Wu



Copyright © 2020 Hindawi Limited. All rights reserved.



This is a special issue published in "BioMed Research International." All articles are open access articles distributed under the Creative Commons Attribution License, which permits unrestricted use, distribution, and reproduction in any medium, provided the original work is properly cited.

Section Editors

Penny A. Asbell, USA
David Bernardo , Spain
Gerald Brandacher, USA
Kim Bridle , Australia
Laura Chronopoulou , Italy
Gerald A. Colvin , USA
Aaron S. Dumont, USA
Pierfrancesco Franco , Italy
Raj P. Kandpal , USA
Fabrizio Montecucco , Italy
Mangesh S. Pednekar , India
Letterio S. Politi , USA
Jinsong Ren , China
William B. Rodgers, USA
Harry W. Schroeder , USA
Andrea Scribante , Italy
Germán Vicente-Rodriguez , Spain
Momiao Xiong , USA
Hui Zhang , China

Academic Editors

Oncology

Fawzy A.S., Australia
Gitana Maria Aceto , Italy
Amedeo Amedei, Italy
Aziz ur Rehman Aziz , China
Riadh Badraoui , Tunisia
Stergios Boussios , Greece
Alberto Briganti, Italy
Franco M. Buonaguro , Italy
Xianbin Cai , Japan
Melchiorre Cervello , Italy
Winson Cheung, Canada
Somchai Chutipongtanate , Thailand
Kate Cooper, USA
Enoc Mariano Cortes-Malagon , Mexico
Alessandro De Vita , Italy
Hassan, El-Abid, Morocco
Yujiang Fang , USA


Zhien Feng , China
Stefano Gambardella , Italy
Dian Gao , China
Piotr Gas , Poland
Nebu Abraham George, India
Xin-yuan Guan, Hong Kong
Hirotaka Iwase, Japan
Arumugam R. Jayakumar , USA
Mitomu Kioi , Japan
Krzysztof Ksiazek , Poland
Yuan Li , China
Anna Licata , Italy
Wey-Ran Lin , Taiwan
César López-Camarillo, Mexico
João F Mota , Brazil
Rakesh Sathish Nair , USA
Peter J. Oefner, Germany
Mana Oloomi , Iran
Vera Panzarella , Italy
Pierpaolo Pastina , Italy
Georgios G. Pissas, Greece
Kyoung-Ho Pyo , Republic of Korea
Giandomenico Roviello , Italy
Daniele Santini, Italy
Wen Shi , USA
Krzysztof Siemianowicz , Poland
Henrique César Santejo Silveira , Brazil
Himangshu Sonowal, USA
Maurizio Soresi, Italy
Kenichi Suda , Japan
Farzad Taghizadeh-Hesary, Iran
Seyithan Taysi , Turkey
Fernando Toshio Ogata , Sweden
Abhishek Tyagi , USA
Marco A. Velasco-Velázquez , Mexico
Thirunavukkarasu Velusamy , India
Navin Viswakarma , USA
Ya-Wen Wang , China
Hushan Yang , USA
Zongguo Yang , China
Hui Yu, USA
Baotong Zhang , USA
Yi Zhang , China



Eugenio Zoni , Switzerland

Contents

Evaluation of the Role of Human DNAJAs in the Response to Cytotoxic Chemotherapeutic Agents in a Yeast Model System

Aurellia Whitmore, Devon Freeny, Samantha J. Sojourner, Jana S. Miles, Willie M. Graham, and Hernan Flores-Rozas 



Research Article (14 pages), Article ID 9097638, Volume 2020 (2020)

A Novel Three-Gene Model Predicts Prognosis and Therapeutic Sensitivity in Esophageal Squamous Cell Carcinoma

Fa-Min Zeng, Jian-Zhong He, Shao-Hong Wang, De-kai Liu, Xiu-E. Xu, Jian-Yi Wu, En-Min Li , and Li-Yan Xu 




Research Article (12 pages), Article ID 9828637, Volume 2019 (2019)

A Novel Clinical Six-Flavoprotein-Gene Signature Predicts Prognosis in Esophageal Squamous Cell Carcinoma

Liu Peng, Jin-Cheng Guo, Lin Long, Feng Pan, Jian-Mei Zhao, Li-Yan Xu , and En-Min Li 




Research Article (13 pages), Article ID 3869825, Volume 2019 (2019)

Spica Prunellae Extract Enhances Fluorouracil Sensitivity of 5-Fluorouracil-Resistant Human Colon Carcinoma HCT-8/5-FU Cells via TOP2 α and miR-494

Yi Fang , Chi Yang, Ling Zhang, Lihui Wei, Jiumao Lin , Jinyan Zhao, and Jun Peng 

Research Article (12 pages), Article ID 5953619, Volume 2019 (2019)

Risk of Developing Hepatocellular Carcinoma following Depressive Disorder Based on the Expression Level of Oatp2a1 and Oatp2b1

Yan Chen , Jiongshan Zhang, Mengting Liu, Zengcheng Zou, Fenglin Wang, Hao Hu, Baoguo Sun , and Shijun Zhang 

Research Article (11 pages), Article ID 3617129, Volume 2019 (2019)

Research Article

Evaluation of the Role of Human DNAJAs in the Response to Cytotoxic Chemotherapeutic Agents in a Yeast Model System

Aurellia Whitmore, Devon Freeny, Samantha J. Sojourner, Jana S. Miles, Willie M. Graham, and Hernan Flores-Rozas 

College of Pharmacy and Pharmaceutical Sciences, Florida A&M University, Tallahassee, FL, USA

Correspondence should be addressed to Hernan Flores-Rozas; hernan.floresrozas@famuedu

Received 25 September 2019; Revised 3 January 2020; Accepted 9 January 2020; Published 14 February 2020

Guest Editor: Chengsheng Wu

Copyright © 2020 Aurellia Whitmore et al. This is an open access article distributed under the Creative Commons Attribution License, which permits unrestricted use, distribution, and reproduction in any medium, provided the original work is properly cited.

Heat-shock proteins (HSPs) play a crucial role in maintaining protein stability for cell survival during stress-induced insults. Overexpression of HSPs in cancer cells results in antiapoptotic activity contributing to cancer cell survival and restricting the efficacy of cytotoxic chemotherapy, which continues to play an important role in the treatment of many cancers, including triple-negative breast cancer (TNBC). First-line therapy for TNBC includes anthracycline antibiotics, which are associated with serious dose-dependent side effects and the development of resistance. We previously identified *YDJ1*, which encodes a heat-shock protein 40 (HSP40), as an important factor in the cellular response to anthracyclines in yeast, with mutants displaying over 100-fold increased sensitivity to doxorubicin. In humans, the DNAJA HSP40s are homologues of *YDJ1*. To determine the role of DNAJAs in the cellular response to cytotoxic drugs, we investigated their ability to rescue *ydj1Δ* mutants from exposure to chemotherapeutic agents. Our results indicate that DNAJA1 and DNAJA2 provide effective protection, while DNAJA3 and DNAJA4 did not. The level of complementation was also dependent on the agent used, with DNAJA1 and DNAJA2 rescuing the *ydj1Δ* strain from doxorubicin, cisplatin, and heat shock. DNAJA3 and DNAJA4 did not rescue the *ydj1Δ* strain and interfered with the cellular response to stress when expressed in wild type background. DNAJA1 and DNAJA2 protect the cell from proteotoxic damage caused by reactive oxygen species (ROS) and are not required for repair of DNA double-strand breaks. These data indicate that the DNAJAs play a role in the protection of cells from ROS-induced cytotoxic stress.

1. Introduction

Despite advances in targeted therapy of cancer, cytotoxic chemotherapy remains an essential therapeutic alternative. Targeted and cytotoxic chemotherapy are two distinctive modes of cancer treatment with each associating to certain benefits and limitations. Targeted therapies are used to kill tumor cells based on the presence of cancer-specific molecules, whereas cytotoxic chemotherapy has a nonselective mechanism of action aimed at proliferating cells. However, both approaches may result in therapeutic resistance.

Some cancers lack therapeutic targets or lose them during cancer progression and therefore rely solely on cytotoxic chemotherapy as a means of treatment. This approach is used for triple-negative breast cancer (TNBC),

which lacks the estrogen, progesterone, and HER2 receptors required for targeted therapy [1], limiting its treatment to the use of cytotoxic chemotherapy such as anthracycline antibiotics [2]. Anthracycline antibiotics, specifically doxorubicin, are one of the most common and effective antineoplastic agents used in treatment of a large number of malignancies.

The effectiveness of doxorubicin can be attributed to its multiple mechanisms of actions. Doxorubicin poisons DNA topoisomerase II, resulting in DNA double-strand breaks (DSBs) leading to cell death [3]. In addition, in the cell, doxorubicin is oxidized to a semiquinone, an unstable metabolite, which is recycled in a process that releases reactive oxygen species (ROS) [3]. ROS can result in a variety of effects such as lipid peroxidation, membrane damage, and

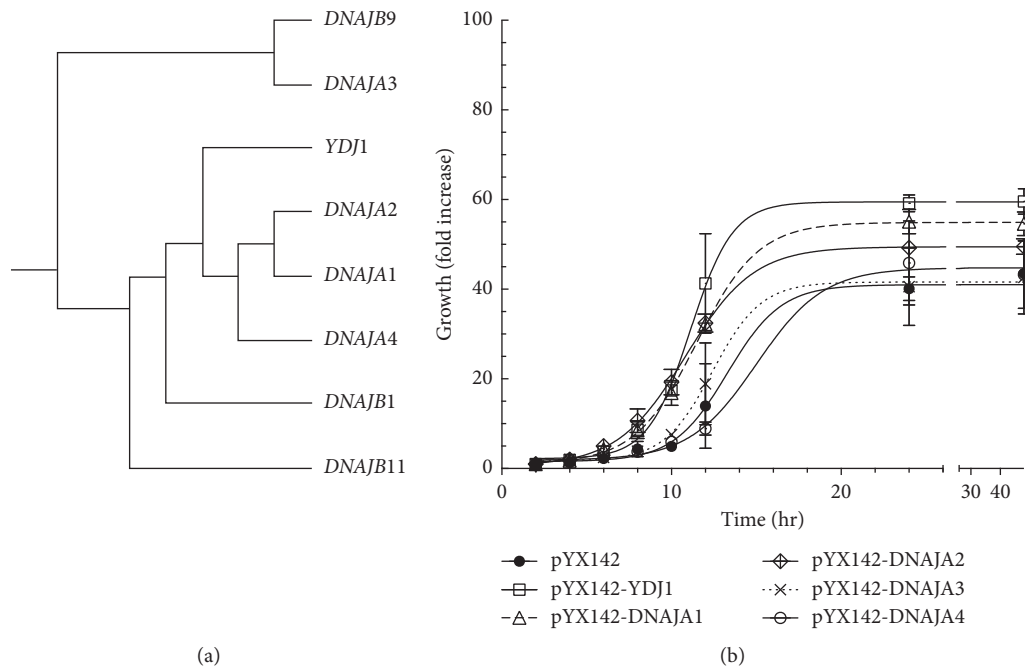


FIGURE 1: Rescue of the growth phenotype of *ydj1Δ* by the human DNAJAs. (a). Sequence comparison indicates that YDJ1 is more closely related to DNAJA1 and DNAJA 2, as indicated by the phylogenetic tree. The comparison included 49 human HSP40 sequences obtained from NCBI protein database. Comparison was performed using the Constraint-based Multiple Alignment Tool from NCBI (COBALT). (b). The growth of *ydj1Δ* complemented strains was evaluated by growing them in the absence of stressors, as described in the Materials and Methods section. The strains tested are as follows: *YDJ1* (open squares), *ydj1Δ* (closed circles), *ydj1Δ*-DNAJA1 (open triangles), *ydj1Δ*-DNAJA2 (open rhombus), *ydj1Δ*-DNAJA3 (---X---), and *ydj1Δ*-DNAJA4 (open circles). Growth was monitored at specified intervals by measuring and aliquot of the culture at OD₆₀₀. The fold increase, relative to the initial OD₆₀₀ of the culture, is presented.

DNA damage. Anthracycline-induced ROS can result in the development of cardiotoxicity, which can be partially managed by chelation of intracellular iron [3]. Doxorubicin-induced ROS trigger apoptotic pathways in nondividing cells contributing to its side effects [4]. Although effective, drug resistance to anthracyclines can develop during treatment. This resistance cannot be overcome by increasing the dose, due to potential development of cardiotoxicity [4].

Attempts to maintain efficacy while reducing toxicity of anthracyclines has been a major focus of research [5]. We have previously identified YDJ1, a homologue of the DNAJA family of Hsp40s, as a crucial factor for the protection of cells under cytotoxic stress displaying hypersensitivity (100–1000x) to protein folding from doxorubicin [6]. YDJ1 is the yeast *S. cerevisiae* HSP40 and functions as a cochaperone to HSP70. HSP40 and HSP70 together protect thermally damaged proteins from aggregation, dissociating aggregated protein complexes, refolding damaged proteins in an ATP-dependent manner, or targeting them for efficient degradation [7].

There are 3 types of DNAJ proteins, classified based on the presence of the DNAJ domain, a zinc finger motif, a glycine/phenylalanine rich region, and a C-terminal domain. YDJ1 is most closely related to the type I subfamily DNAJA, which contains all domains/motifs [8]. Type II (DNAJB) lacks the zinc finger motif, while type III (DNAJC) only contains the J domain. There are four DNAJAs in humans, DNAJA1, DNAJA2, DNAJA3, and DNAJA4. Sequence analysis by constraint-based multiple alignment tool (NCBI,

COBALT) indicates that the yeast YDJ1 is most closely related to DNAJA1 and DNAJA2 (Figure 1(a)). Pairwise analysis using the NCBI blastp suite indicates that YDJ1 is 46.23%, 46.12%, 30.95%, and 43.21% identical to DNAJA1, DNAJA2, DNAJA3, and DNAJA4, respectively.

Although a number of reports indicate that the heat-shock response prevents cytotoxic effects of doxorubicin, these have mostly focused on Hsp70 and Hsp27 [9, 10]. The role of the DNAJAs in the response to cytotoxic chemotherapy has not been investigated. Interestingly, HSP40s, including the DNAJAs, are overexpressed in multiple cancers, and recently, a report indicates that the DNAJAs have high levels of expression in breast cancer after treatment [11]. Recent work from our laboratory indicates that YDJ1, a type I HSP40 in yeast, plays a critical role in the protection from ROS stress from anthracycline exposure [12].

To determine the role of DNAJAs in the cellular response to cytotoxic drugs, we investigated their ability to rescue *ydj1Δ* mutants from exposure to chemotherapeutic agents. Mutant strains complemented by the DNAJAs were exposed to chemotherapy agents: doxorubicin, cisplatin, and etoposide, as well as oxidative stress agent menadione. Our results indicate that the different DNAJAs provide distinct levels of protection, with DNAJA1 and DNAJA2 being more effective at complementation while DNAJA3 and DNAJA4 did not complement. Deletion *ydj1Δ* strains expressing DNAJA1 or DNAJA2 survived to exposure to doxorubicin, cisplatin, and heat shock, comparable to the strain expressing the wild type YDJ1. DNAJA1 and DNAJA2

also rescued the growth phenotype of the *ydj1* Δ strain and were essential in the protection of the *ydj1* Δ strain to reactive oxygen species (ROS) generated by menadione, consistent with our previous observation in yeast [12]. Conversely, *ydj1* Δ strains harboring DNAJA3 and DNAJA4 displayed reduced survival when exposed to cytotoxic stress and did not rescue the growth phenotype of *ydj1* Δ , and in some cases, they appeared more sensitive than the noncomplemented strain. In fact, expression of DNAJA3 and DNAJA4 was detrimental to the growth of the wild type strain and sensitized it to both doxorubicin and heat shock, suggesting that DNAJA3 and DNAJA4 interfere with the normal heat-shock response in yeast. Our results indicate that DNAJA1 and DNAJA2 are functional homologues of yeast YDJ1 and play a role in the protection of cells from cytotoxic stresses such as those exerted by cancer chemotherapeutic agents.

2. Materials and Methods

2.1. Media and Chemicals. *E. coli* strains were grown in LB broth or on LB agar, both supplemented with 100 μ g/ml ampicillin (Sigma-Aldrich) for plasmid maintenance, when appropriate. Yeast strains were grown in leucine drop-out media (Leu⁻) for plasmid selection, containing 0.67% yeast nitrogen base, 2% agar, 2% glucose (dextrose) or 2% galactose, and 0.087% amino acid drop-out mix [13, 14]. When required, etoposide (Chem-Impex International Inc.) was included in Leu⁻ selective media at 1 mM concentration. Doxorubicin-HCl (2 mg/mL) was purchased from MP Biomedicals (Irvine, CA, USA); cisplatin (1 mg/mL) was purchased from Calbiochem; menadione (Vitamin K3) was purchased from Enzo Life Sciences (Farmingdale, NY); etoposide was purchased from Chem-Impex International Inc (Wood Dale, IL).

2.2. *S. cerevisiae* Strains. The genotypes of all strains used in these studies are shown in Table 1. Homozygous haploid deletion strains library (parental strain BY4741: *MATa his3 Δ 1 leu2 Δ 0 met15 Δ 0 ura3 Δ 0*) was obtained from Thermo Fisher Scientific (Waltham, MA). The gene deletion present in the strains used in this study have been validated by polymerase chain reaction (data not shown).

2.3. Molecular Biology. The *YDJ1* gene was PCR-amplified using genomic DNA from wild type strain BY4741 as the template and cloned into the EcoRI/SacI restriction sites of the pXY142 yeast expression vector (Ingenious, 2 μ , LEU2, TPI constitutive expression promoter). Correct clone was confirmed by DNA sequencing (MCLAB, San Francisco, CA). The DNAJAs 1 to 4 were PCR-amplified from plasmids harboring the genes (Dharmacon, Lafayette, CO) and cloned into the NcoI/SacI restriction sites of pXY142. Correct clones were confirmed by DNA sequence.

2.4. Yeast Genetics and Cytotoxic Stress Sensitivity Assays. HSP40s-expressing plasmids were transformed into *ydj1* Δ or wild type strains, as previously described [1, 6, 15–19]. The *rad52* Δ deletion strain was transformed with pXY142 empty

vector to provide LEU2 selectivity and served as a control for sensitivity to DNA double-strand breaks (DSBs) by etoposide.

For the growth rate analysis, cells harboring the expression plasmid were cultured overnight in selective media as described above (at 30°C, for approximately 16 hours) to saturation, and then new cultures were started by inoculating with the overnight culture to a dilution of OD₆₀₀ = 0.04. The cultures were started (30°C, with shaking) and aliquots were taken to measure the OD₆₀₀, at timed intervals and observed under the microscope to exclude bacterial contamination. In the cytotoxic stress survival assay, the concentration of the drugs used for strain exposure was determined experimentally using the WT parental strain BY4741 and sensitive strain *ydj1* Δ , as previously described [6]. Single colonies were grown overnight in liquid Leu⁻ media, at 30°C with shaking. Cells were then washed and resuspended in ultrapure sterile water. Strains were then separated into control and treatment groups and exposed to drug or vehicle for 1–3 h depending on the agent. After exposure, the cells were once again washed and suspended in sterile water. Serial dilutions (20 μ L) were spotted onto Leu⁻ agar plates and incubated at 30°C. Heat-shock treatment was performed by plating serial dilutions of the strains and incubating at 37°C. Cell growth was monitored daily, and colonies were counted at day 3. Survival was calculated relative to the corresponding untreated control, and sensitivity was determined relative to the survival of the *ydj1* Δ -complemented strain (YDJ1). Survival, as indicated in the Results section, is specific for that drug concentration. Each trial involved the testing of five independent colonies for each cytotoxic agent, and a minimum of three trials were performed. The survival of the untreated strain was defined as 100%.

2.5. Statistical Analysis. Data analysis and graphing was performed using the GraphPad Prism 7 software package. Specific analysis for each experiment is indicated in the respective figure. The mean of at least three trials is plotted, together with the SEM. Differences between mean values and multiple groups were analyzed by one-way analysis of variance (ANOVA). Statistical significance was set at $p < 0.05$. Fitting and interpolation of the sigmoidal growth curve were performed using the model Sigmoidal, 4PL, X is log (concentration) from GraphPad Prism 7.

3. Results

3.1. Rescue of *ydj1* Δ Growth Phenotype by the Human DNAJAs. The *ydj1* Δ strain displays a growth defect, which results in slow growth, longer doubling time, and small colonies relative to the wild type. To determine if the human DNAJAs can rescue the growth defect of *ydj1* Δ , the strain was transformed with yeast expression plasmids expressing each DNAJA (1–4) as well as *YDJ1* (positive control) and empty vector (negative control) and cultured as described in Materials and Methods section. Growth showed a typical sigmoidal curve with varying lag time, slope, and plateau,

TABLE 1: Yeast strains used in this study.

Strain	Genotype	Description
Wild type (WT)	<i>MATa his3-1 leu2Δ met15Δ ura3Δ [pYX142 LEU2]</i>	Parental <i>S. cerevisiae</i> strain (BY4741)
<i>ydj1Δ</i>	<i>MATa his3-1 leu2Δ met15Δ ura3Δ ydj1Δ [pYX142 LEU2]</i>	<i>ydj1</i> deletion strain
YDJ1	<i>MATa his3-1 leu2Δ met15Δ ura3Δ ydj1Δ [pYX142-YDJ1 LEU2]</i>	<i>ydj1</i> deletion strain complemented with wild type <i>YDJ1</i> gene
<i>ydj1</i> -DNAJA1	<i>MATa his3-1 leu2Δ met15Δ ura3Δ ydj1Δ [pYX1423-ydj1-DNAJA1 LEU2]</i>	<i>ydj1</i> deletion strain complemented with human DNAJA1 gene
<i>ydj1</i> -DNAJA2	<i>MATa his3-1 leu2Δ met15Δ ura3Δ ydj1Δ [pYX142-ydj1-DNAJA2 LEU2]</i>	<i>ydj1</i> deletion strain complemented with human DNAJA2 gene
<i>ydj1</i> -DNAJA3	<i>MATa his3-1 leu2Δ met15Δ ura3Δ ydj1Δ [pYX142-ydj1-DNAJA3 LEU2]</i>	<i>ydj1</i> deletion strain complemented with human DNAJA3 gene
<i>ydj1</i> -DNAJA4	<i>MATa his3-1 leu2Δ met15Δ ura3Δ ydj1Δ [pYX142-ydj1-DNAJA4 LEU2]</i>	<i>ydj1</i> deletion strain complemented with human DNAJA4 gene
<i>rad52</i>	<i>MATa his3-1 leu2Δ met15Δ ura3Δ rad52Δ [pYX142 LEU2]</i>	<i>rad52</i> deletion strain
WT + DNAJA3	<i>MATa his3-1 leu2Δ met15Δ ura3Δ ydj1Δ [pYX142- DNAJA3 LEU2]</i>	Wild type strain expressing the human DNAJA3 gene
WT + DNAJA4	<i>MATa his3-1 leu2Δ met15Δ ura3Δ ydj1Δ [pYX142- DNAJA4 LEU2]</i>	Wild type strain expressing the human DNAJA4 gene

depending on the strain. Several parameters, including top plateau, Growth₅₀, hill slope, and span (see Table 2), were derived using the Sigmoidal 4PL model equation from GraphPad Prism 7, where X is the log (concentration). As shown in Figure 1, the *ydj1Δ* strain shows a long lag time, compared to the complemented strain (*YDJ1*), with slow growth rate at exponential phase (hill slope of 0.281 vs 0.347), slower half maximum growth (growth 50%), achieved in 13.2 vs 11.11 hours, respectively, and lower maximum growth (plateau) (40.2-fold increase vs 59.4-fold, respectively) (Table 2). Interestingly, DNAJA1 and DNAJA2 effectively complemented the *ydj1Δ* strain, achieving similar maximum growth (55.2-fold and 49.4-fold increase, respectively) compared to the *YDJ1* complemented strain (59.4). They achieved half maximum growth at similar times (11.5 h and 10.8 h) to the *ydj1Δ*-complemented strain (*YDJ1*, 11.1 h), although they showed slightly lower growth rate at the exponential phase (0.238 and 0.217, respectively). The span, which represents the difference between the top and the bottom plateau, shows that the overall performance of each strain corresponds to the maximum growth they can achieve. However, strains expressing DNAJA3 and DNAJA4 resembled more the *ydj1Δ* strain, achieving low maximum growth (38.9-fold increase for DNAJA3 and 44.0 for DNAJA4) and long half maximum growth time (12.3 h). This is more evident in the DNAJA4-complemented strain, with half maximum growth time of 15.0 h.

3.2. Complementation of the sensitivity of the *ydj1Δ* mutant strain to chemotherapeutic agents doxorubicin and cisplatin by human DNAJAs. We have previously shown yeast strains deleted in the HSP40 *YDJ1* to be highly sensitive to cytotoxic stress [6]. To evaluate the ability of DNAJAs to complement the sensitivity of *ydj1Δ*, we determined the survival of the *ydj1Δ* strains expressing each human DNAJA exposed to chemotherapeutic agents doxorubicin and cisplatin. The concentration of the drugs used in the assays was determined empirically using the wild type strain (not sensitive

control) and *ydj1Δ* (sensitive control). Strains were grown in Leu- selective media to maintain the expression plasmid, treated and washed to remove the drug as described in Material and Methods section. Serial dilutions were spotted in Leu- agar plates to count colonies and to determine survival. When exposed to doxorubicin (20 μM), the strain harboring a wild type copy of *YDJ1* displayed 63% survival relative to the untreated strain. As expected, the *ydj1Δ* strain was highly sensitive with 6.4% survival, which is 10-fold more sensitive than the complemented strain (*YDJ1*) (Figures 2(a) and 2(b) and Table 3). Interestingly, both DNAJA1 and DNAJA2 were effective at complementing the *ydj1Δ* mutant, displaying similar levels of survival to the strain expressing the wild type gene (66% and 85% survival for DNAJA1 and DNAJA2, respectively). However, the strains expressing DNAJA3 and DNAJA4 were sensitive to doxorubicin (4% and 1.7% survival, respectively), similar to the noncomplemented *ydj1Δ* strain. In fact, the strain expressing DNAJA4 appears more sensitive (37-fold higher sensitivity compared to the *YDJ1* strain) (Figures 2(a) and 2(b) and Table 3). While the survival of *YDJ1*- and DNAJA1-complemented strains is not statistically significantly different ($p > 0.05$) among each other, they are significantly different to the *ydj1Δ* strain ($p < 0.05$). Interestingly, the DNAJA2-complemented strain displays higher survival indicating that DNAJA2 provides more fitness than the wild type *YDJ1* itself.

Exposure of the strains to cisplatin (80 μM) indicates that both the DNAJA1- and DNAJA2-complemented strains rescued the sensitivity of the *ydj1Δ* mutation ($p < 0.05$). While DNAJA1 displayed a survival similar to that of the strain complemented by *YDJ1* (38% vs 27%, respectively), the DNAJA2-complemented strain was significantly more resistant to cisplatin (72% survival) (Figures 3(a) and 3(b) and Table 3). As with doxorubicin, the strains expressing DNAJA3 and DNAJA4 failed to complement the *ydj1Δ* mutation, with the DNAJA3 strain showing significant sensitivity (1% survival) which is 27-fold more sensitive than the *YDJ1*-complemented strain and ~3-fold more sensitive

TABLE 2: Growth Analysis of the HSP40s expressing strains.

Strain	Max growth (fold increase)	Growth ₅₀ (h)	Hill slope	Span
<i>ydj1Δ</i>	40.2	13.2	0.281	38.6
YDJ1	59.4	11.1	0.347	57.2
<i>ydj1</i> -DNAJA1	55.2	11.5	0.238	54.1
<i>ydj1</i> -DNAJA2	49.4	10.8	0.217	48.8
<i>ydj1</i> -DNAJA3	40.6	12.3	0.307	38.9
<i>ydj1</i> -DNAJA4	44.0	15.0	0.102	40.8

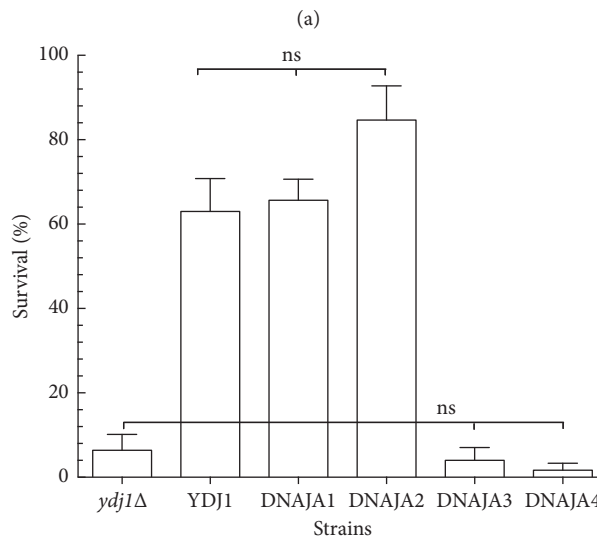
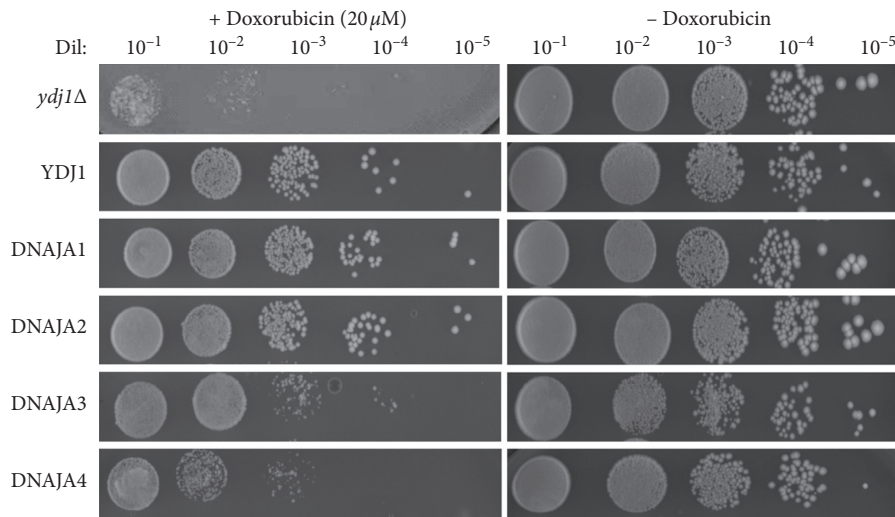


FIGURE 2: Sensitivity of the DNAJAs-expressing strains to doxorubicin. (a) The survival of the strains to 20 μM doxorubicin was determined as described in the “Materials and Methods” section. Serial dilutions (1 : 10⁻¹ : 10⁻⁵) of the treated cultures were spotted onto Leu⁻ + glucose plates. Growth was scored after 3 days of incubation at 30°C. The serial dilutions of the strains are shown. (b) Quantification of the survival of the tested strains. Survival was determined by counting the number of colonies in the respective dilutions and calculated on the basis of the growth of strains not treated with doxorubicin. At least three sets of experiments were used in the statistical analysis. Average survival plus standard deviation is shown. Dil: serial dilutions; Doxo: doxorubicin; ns: not significantly different.

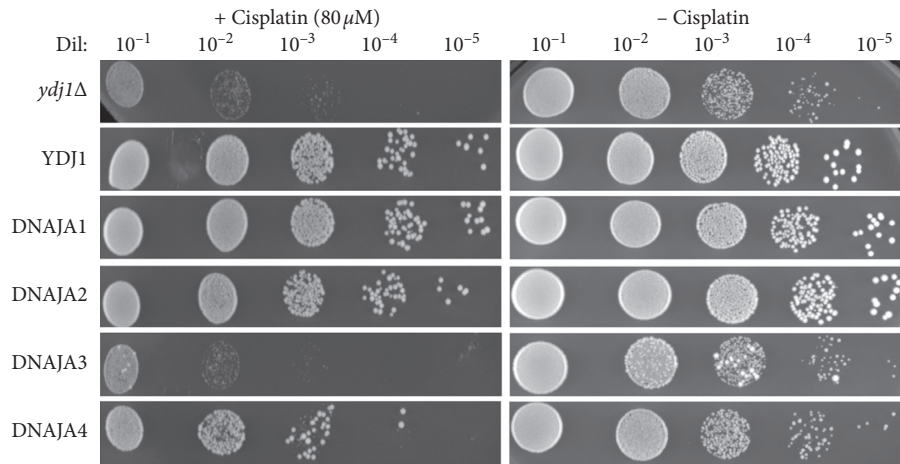
than the *ydj1Δ* strain (Table 3). The DNAJA4-expressing strain was similar to *ydj1Δ* (3.7% vs 4% survival, respectively) (Figures 3(a) and 3(b) and Table 3).

The role of YDJ1 in the heat-shock response has been clearly described. The *ydj1Δ* deletion strain is highly

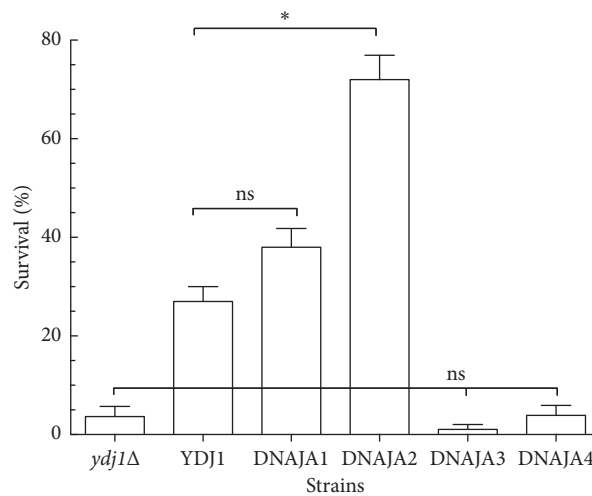
sensitive to heat shock and does not survive exposure to 37°C (heat shock for yeast). We tested the ability of the human DNAJAs to rescue the heat-sensitive phenotype of *ydj1Δ*. As shown in Figures 4(a) and 4(b), the *ydj1Δ* strain shows no growth upon heat shock, while complementation with YDJ1,

TABLE 3: Sensitivity of the HSP40s expressing strains to chemotherapeutic agents and heat shock.

Strain	Doxorubicin		Cisplatin		Heat shock	
	Survival (% ± SEM)	Sensitivity (fold)	Survival (% ± SEM)	Sensitivity (fold)	Survival (% ± SEM)	Sensitivity (fold)
<i>ydj1Δ</i>	6.4 ± 3.8	10	3.7 ± 2.0	7.3	0 ± 0	—
YDJ1	63.0 ± 7.8	1	27.0 ± 3.0	1.0	89 ± 26	1
DNAJA1	66.0 ± 5.0	1	38.0 ± 3.8	0.7	119 ± 5	0.7
DNAJA2	85.0 ± 8.0	0.7	72.0 ± 5.0	0.4	201 ± 24	0.4
DNAJA3	4.0 ± 3.0	15.8	1.0 ± 1.0	27.0	5 ± 5	18
DNAJA4	1.7 ± 2.0	37	4.0 ± 2.0	6.8	0 ± 0	—



(a)



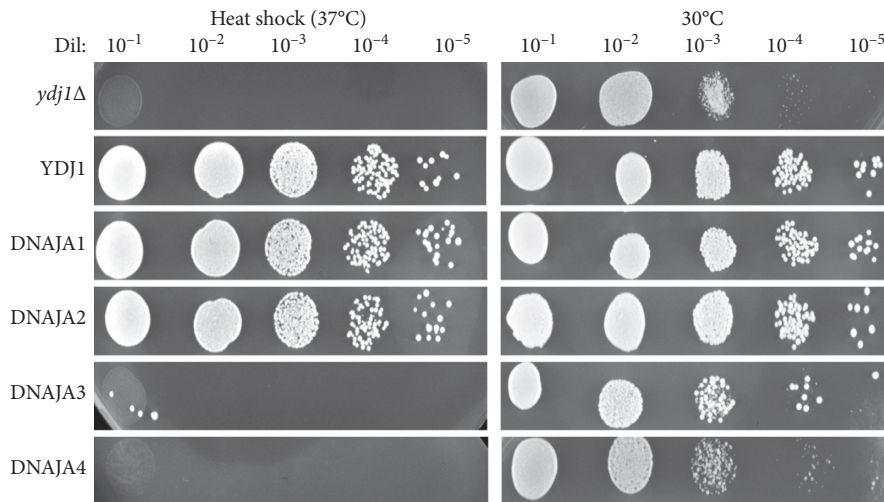
(b)

FIGURE 3: Sensitivity of the DNAJAs-expressing strains to cisplatin. (a) Strains were exposed to 80 μ M cisplatin. Serial dilutions (1:10–1:105) of the treated cultures were spotted onto Leu⁻ + glucose plates. Growth was scored after 3 days of incubation at 30°C. The serial dilutions of the strains are shown. (b) Quantification of the survival of the tested strains. Survival was determined by counting the number of colonies in the respective dilutions and calculated on the basis of the growth of strains not treated with cisplatin. At least three sets of experiments were used in the statistical analysis. Average survival plus standard deviation is shown. Dil: serial dilutions; Cis: cisplatin; ns: not significantly different. *Significantly different.

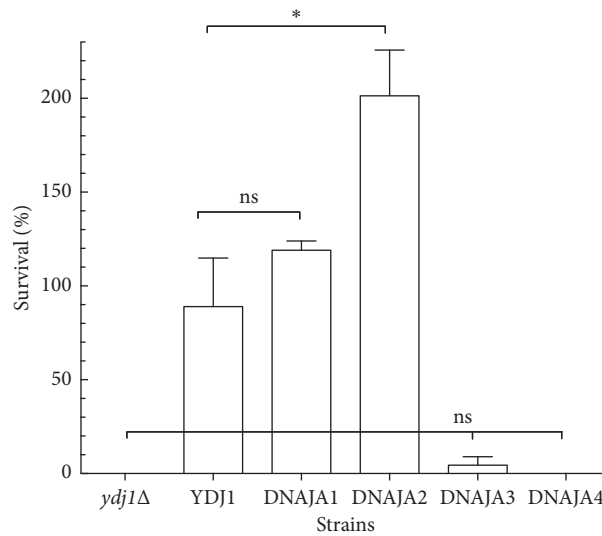
DNAJA1, and DNAJA2 rescues the phenotype. In fact, the DNAJA2-expressing strain grows significantly better at 37°C (Figures 4(a) and 4(b) and Table 3). Conversely, DNAJA3 and DNAJA4 failed to rescue *ydj1* from heat shock and similarly showed no growth at 37°C (Figures 4(a) and 4(b) and Table 3). These data suggest that both DNAJA1 and DNAJA2

are functional homologs of *YDJ1* and can substitute it effectively, rescuing the defects of the deletion strain.

3.3. Sensitivity of DNAJA1- and DNAJ2-Expressing Strains to Menadione and Etoposide. Doxorubicin exerts its



(a)



(b)

FIGURE 4: Sensitivity of the DNAJAs-expressing strains to heat shock. (a) The survival of the strains was tested for heat sensitivity. Serial dilutions of the cells were plated onto Leu⁻ + glucose plates and incubated at 30°C (untreated controls) and at 37°C (heat shock). Growth was scored at 72 hours. YDJ1 is the positive control, resistant to heat shock, and *ydj1Δ* is the negative control, sensitive to heat-shock. (b) Survival was determined by growth of the heat-shocked strain relative to the growth of nonheat-shocked cells. At least three sets of experiments were used in the statistical analysis. Average survival plus standard deviation is shown. Dil: serial dilutions; ns: not significantly different. *Significantly different.

antineoplastic activity through two main mechanisms: (i) DNA damage (generation of DSBs) and (ii) by the generation of reactive oxygen species (ROS) [4]. Our results indicate that both DNAJA1 and DNAJA2 were more effective at protecting the *ydj1Δ* strain from doxorubicin. To further investigate if the protection was specific to DSBs or ROS, we tested the sensitivity of the strains to the oxidative stress generating agent menadione and to the DNA-topoisomerase II inhibitor, etoposide.

Menadione is commonly used in research as a ROS-producing agent and shares the same quinone ring as doxorubicin [4]. As shown in Figure 5(a), the strains that displayed the highest levels of protection from exposure to menadione were those expressing DNAJA2 (109% survival) and DNAJA1 (47%

survival), corresponding to 0.3-fold and 0.8-fold sensitivity relative to the YDJ1 (37%), respectively. The *ydj1Δ* strain is highly sensitive to oxidative stress, displaying 10% survival (>3-fold more sensitive than YDJ1). Addition of ROS scavenger agent N-acetylcysteine (NAC) significantly increased the survival of the *ydj1Δ* strain (21%), confirming that this strain is sensitive to ROS (Table 4, Figures 5(a) and 5(b)). However, in HSP40-complemented strains (YDJ1, DNAJA1, and DNAJA2), NAC only had a marginal effect (~20% increase in survival, Figures 5(a) and 5(b)). Our results indicate that DNAJA1 and DNAJA2 protect the cell viability from exposure to ROS-generating agents such as menadione.

As doxorubicin, the topoisomerase II inhibitor etoposide generates DSBs that require homologous recombination for

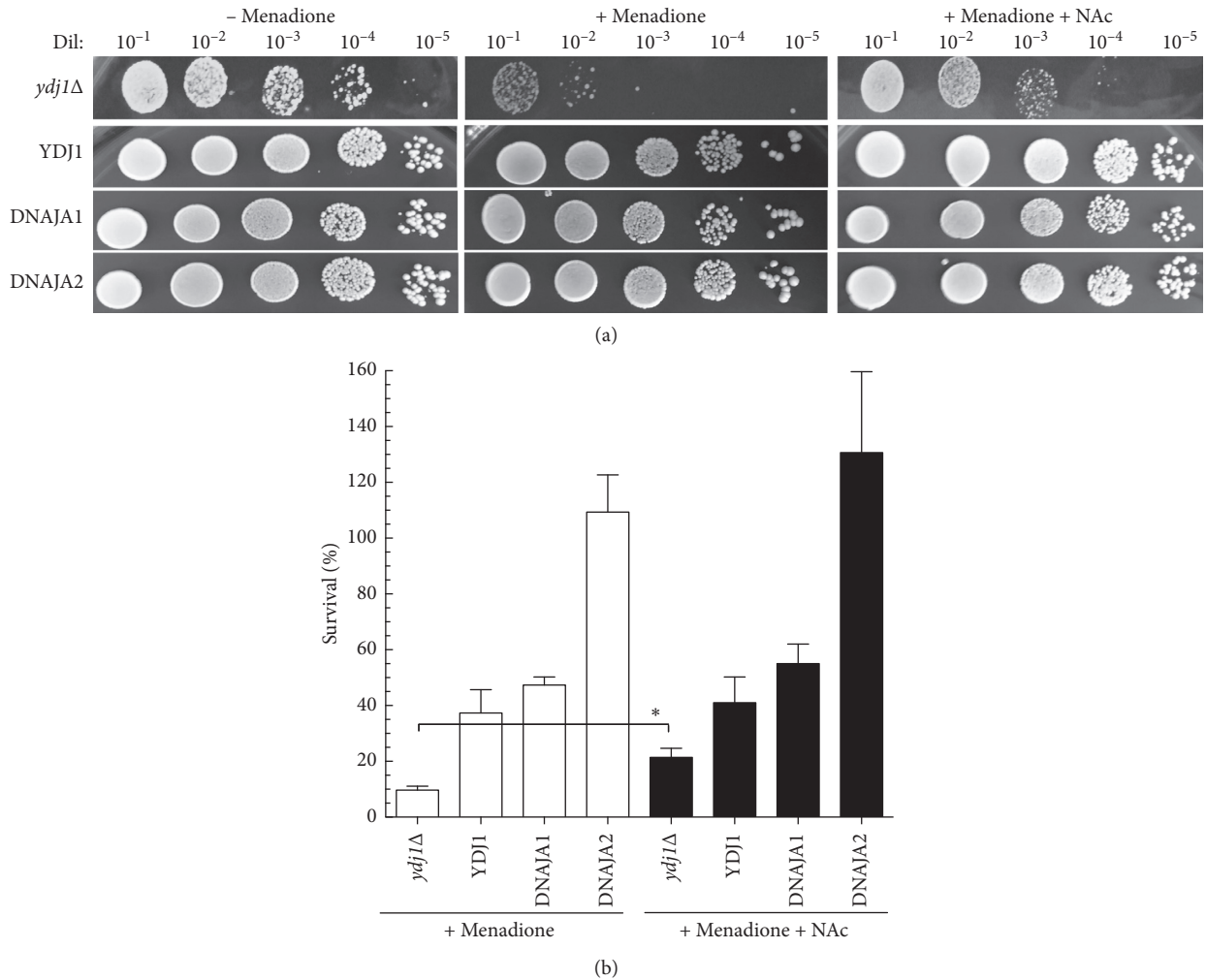


FIGURE 5: Sensitivity of the DNAJAs-expressing strains to menadione. (a) DNAJA1- and DNAJA2-expressing strains showed the most resistance to doxorubicin and cisplatin and were therefore exposed to 6.6 mM menadione (1 h at 30°C) to determine survival. Cells were washed with sterile water and serial dilutions (1 : 10⁻¹ : 10⁻⁵) of the treated cultures were spotted onto Leu⁻ + glucose plates. Growth was scored after 3 days of incubation at 30°C. The serial dilutions of the strains are shown. N-acetylcysteine (NAC, 20 mM) was added as cotreatment with menadione to the indicated strains. (b) Quantification of the survival of the tested strains. Survival was determined by counting the number of colonies in the respective dilutions and calculated on the basis of the growth of strains not treated with menadione. At least three sets of experiments were used in the statistical analysis. Average survival plus standard deviation is shown. Dil: serial dilutions. *Significantly different.

TABLE 4: Sensitivity of the HSP40s expressing strains to etoposide and menadione.

Strain	Etoposide		Menadione			
	Survival (% ± SEM)	Sensitivity (fold)	-NAC		+NAC	
			Survival (% ± SEM)	Sensitivity (fold)	Survival (% ± SEM)	Sensitivity (fold)
<i>ydj1Δ</i>	104 ± 7.7	1	10 ± 2.5	3.7	21 ± 5.7	2.0
YDJ1	139 ± 6.4	1	37 ± 14.5	1	41 ± 16	1
DNAJA1	135 ± 3.3	1	47 ± 5.0	0.8	55 ± 7.0	0.8
DNAJA2	184 ± 8.0	0.7	109 ± 23.0	0.3	131 ± 29	0.3
<i>rad52Δ</i>	5 ± 4.8	29				

repair. As expected, the homologous recombination defective mutant *rad52Δ* is highly sensitive to the drug (5% survival) (Figures 6(a) and 6(b), Table 4). However, the

ydj1Δ strain does not show sensitivity to etoposide (104% survival) and the expression of the wild type *YDJ1*, or *DNAJA1* and *DNAJA2*, does not negatively affect this

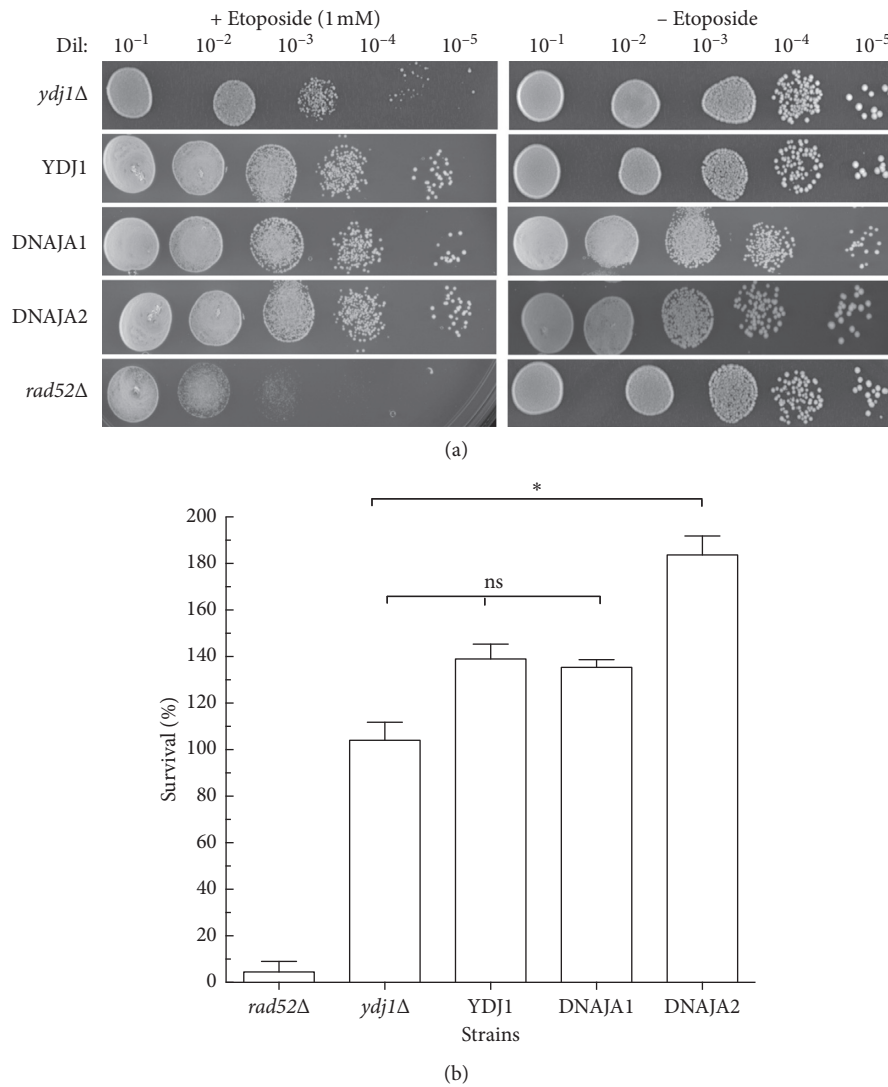


FIGURE 6: Sensitivity of the DNAJAs-expressing strains to etoposide. (a) The survival of DNAJA1 and DNAJA2 strains was determined through exposure to etoposide. Serial dilutions of the treated strains were spotted onto Leu⁻ + glucose plates containing etoposide (1 mM) and incubated at 30°C. Growth was scored at 72 hours. Positive controls sensitive to etoposide is the *rad52Δ* deletion strain. (b) Survival was determined by growth of the treated strain relative to the growth of its untreated control. At least three sets of experiments were used in the statistical analysis. Average survival plus standard deviation is shown. Dil: serial dilutions; ns: not significantly different. *Significantly different.

survival (139%, 135%, and 184%, respectively), with DNAJA1 not statistically significantly different to the strain complemented with wild type YDJ1. The survival of the DNAJA2-complemented strain was significantly higher than that of YDJ1-complemented strain (Figures 6(a) and 6(b) and Table 4).

Together, these data indicate that DNAJA1 and DNAJA2 are effective at complementing the *ydj1Δ* mutation, rescuing it from its sensitivity to doxorubicin, cisplatin, and heat shock, most likely through its chaperone activity.

3.4. Distant DNAJA3 and DNAJA4 Interfere with YDJ1 in Wild Type Cells. Our results indicate that both DNAJA3 and DNAJA4 fail to complement the *ydj1Δ* mutant as DNAJA1 and DNAJA2 do. In fact, strains expressing DNAJA3 and

DNAJA4 appear as sensitive or more sensitive than the deletion strain. Based on these results, it is possible that DNAJA3 and DNAJA4, which are more distant homologs of YDJ1 than DNAJA1 and DNAJA2, may be interfering in YDJ1-dependent functions. To confirm this possibility, we proceeded to express DNAJA3 and DNAJA4 in a wild type background with functional YDJ1. As shown in Figure 7, expression of DNAJA3 or DNAJA4 considerably reduced the growth rate of the wild type strain, with a hill slope, at the exponential phase, of 0.18 for wild type and 0.04 and 0.10 for WT + DNAJA3 and WT + DNAJA4, respectively. The time to get to 50% growth is also extended from 11.34 h for wild type to ~14 h and 16 h for WT + DNAJA3 and WT + DNAJA4, respectively. To evaluate if these distant DNAJAs affect the response of wild type cells to cytotoxic stressors, we determined the survival of WT + DNAJA3 and

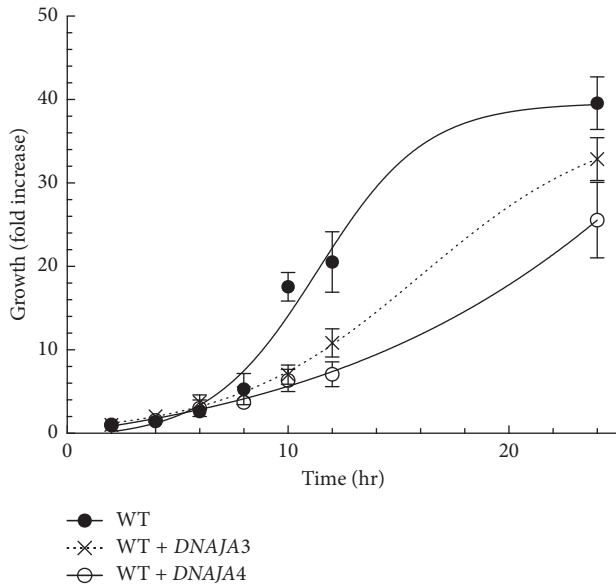


FIGURE 7: Effect of DNAJA3 and DNAJA4 in the growth of cells with wild type YDJ1. Growth of DNAJA3- and DNAJA4-expressing cells was evaluated under nonstress conditions. Wild type cells contained an empty plasmid to provide selection (black circles), a plasmid expressing DNAJA3 (—X—), or a plasmid expressing DNAJA4 (open circles). Growth was monitored at specified intervals by measuring and aliquot of the culture at OD₆₀₀. The fold increase, relative to the initial OD₆₀₀ of the culture, is presented.

WT + DNAJA4 strains after exposure to doxorubicin and heat shock (Figures 8(a) and 8(b)). Expression of DNAJA3 or DNAJA4 significantly reduced the survival of the wild type strain from 63% to 20% for WT + DNAJA3 (3-fold more sensitive, Table 5) and 4% for WT + DNAJA4 (15-fold more sensitive, Table 5), both significantly different than the wild type ($p < 0.05$).

The expression of DNAJA3 and DNAJA4 in a wild type background also interfered with the response to heat shock (Figures 9(a) and 9(b)). Both the WT + DNAJA3 and WT + DNAJA4 strains did not survive the heat shock (0% survival) compared to the wild type (104% survival). Our data confirm that the expression of the distant HSP40s, DNAJA3 and DNAJA4, interferes with a functional YDJ1 affecting the response of the cell to stress and displaying a phenotype similar to that of the *ydj1Δ* strain.

4. Discussion

Cytotoxic therapeutic agents, such as doxorubicin and cisplatin, are commonly used as sole agents or in combination therapy in cancers that lack biological targets. However, their nonselective mechanism of action against cancer cells also results in serious side effects such as cardiotoxicity, nephrotoxicity, and diverse injuries to healthy tissues that can lead to necrosis [20]. Significant effort in the field of cancer therapeutics is aimed at increasing the effects of cytotoxic agents to cancer cells while mitigating their toxic effects.

One approach to the goal of increasing therapeutic efficacy of anthracyclines, while decreasing toxic effects, is through the hypersensitization of cancer cells. A study in 2001 described high levels of Hsp40 in the serum of lung cancer patients compared to the serum of patients with no lung cancer [21]. Moreover, there is increasing evidence of HSP40s overexpression in a plethora of metastatic tumors including, among others, those of the breast, prostate, brain, and lung [22]. It has been suggested that the proteins in cancer cells depend heavily on HSPs due to protein misfolding brought in by acquired mutations that result in altered protein structure. This is critical for factors necessary to support rapid proliferation and survival of cancer cells driven by oncoproteins promoting metastatic growth [1]. Understanding the role of Hsp40s is vital for targeted inhibition of their overexpression as a potential therapeutic option. Reducing the levels of overexpressed HSP40s would sensitize cancer cells to therapeutic agent and lead to a lower effective therapeutic dosage of cytotoxic drugs resulting in less toxicity and thus enhancing the patient's quality of life.

Previous work in our lab identified YDJ1, a homologue of the DNAJA-type Hsp40s, as a crucial factor for survival under doxorubicin stress. We have extended our investigation by evaluating the role of all human DNAJAs (DNAJA1, DNAJA2, DNAJA3, and DNAJA4) in the response of cells to cancer therapeutic agents, such as doxorubicin, cisplatin, and etoposide, and to define cytotoxic stresses such as ROS and heat shock.

While YDJ1 is more closely related to the DNAJA subfamily of HSP40s, than to DNAJB and DNAJC subfamilies, there are differences between the homology of YDJ1 and the DNAJA subfamily members. Phylogenetic analysis indicates that DNAJA1 and DNAJA2 are closer sequence homologues, while DNAJA3 and DNAJA4 are more distantly related. In order to determine functional homology, we tested if the DNAJAs could rescue the phenotype of the *ydj1Δ* deletion strain by expressing them in this strain and exposing them to diverse cytotoxic stresses. As described in the Results section, DNAJA1 and DNAJA2 displayed the highest levels of complementation and were found to consistently protect cells from all agents tested to levels similar to those of wild type YDJ1. The requirement for HSP40s in normal cell growth has been well documented [16]. In fact, cells lacking YDJ1 display a slow growth phenotype, as indicated by a longer doubling time, reduced maximal growth in culture, and formation of smaller colonies on solid agar plates. Once again, DNAJA1 and DNAJA2 could rescue the growth phenotype, while DNAJA3 and DNAJA4 could not. Consistently, DNAJA3 and DNAJA4 failed to complement the *ydj1Δ* strain, and when expressed in wild type cells, they interfered with the endogenous pathway, affecting cell growth and sensitizing the cell to stress. It is possible that DNAJA3 and DNAJA4 form nonproductive interactions with components of the heat-shock response (namely, HSP70s), sequestering and preventing them from performing YDJ1 independent functions that are crucial for cell growth. In fact, there are at least 22 HSP40s [23] and multiple HSP70s [24] which do not have exclusive partners and interact with each other.

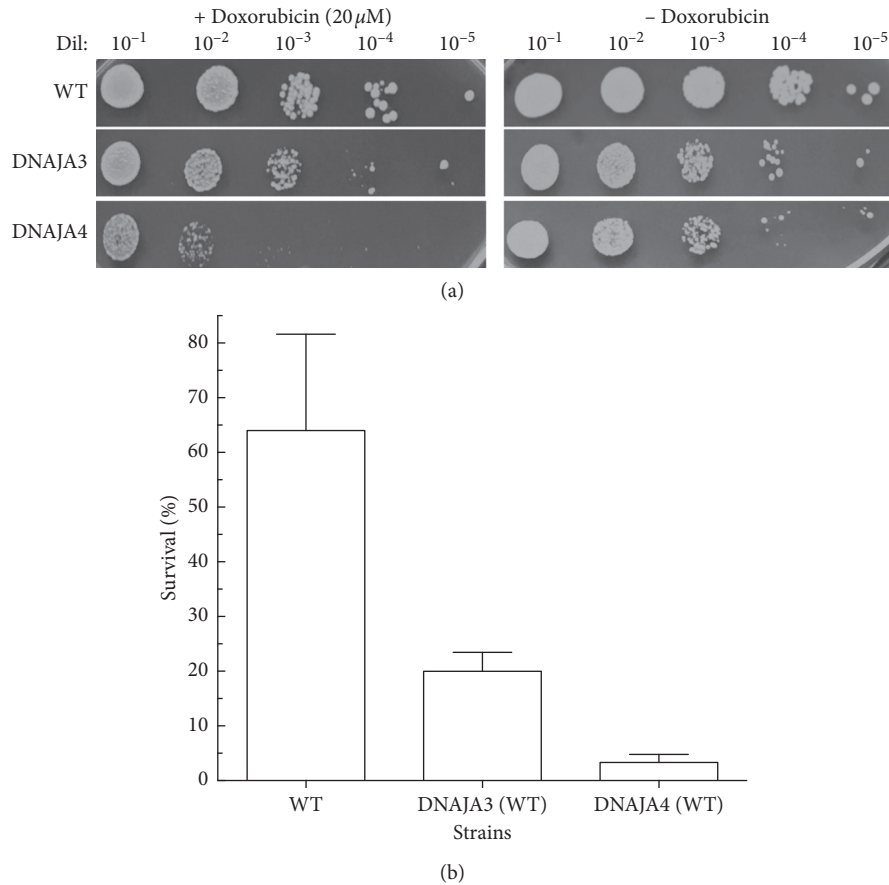


FIGURE 8: Effect of DNAJA3 and DNAJA4 expression in cells with wild type YDJ1 to exposure to doxorubicin. (a) The survival to doxorubicin exposure of the DNAJA3- and DNAJA4-expressing wild type cells was determined. Serial dilutions (1 : 10⁻¹ : 10⁻⁵) of the treated cultures were spotted onto Leu⁻ + glucose plates. Growth was scored after 3 days of incubation at 30°C. The serial dilutions of the strains are shown. (b) Quantification of the survival of the tested strains. Survival was determined by counting the number of colonies in the respective dilutions and calculated on the basis of the growth of strains not treated with doxorubicin. At least three sets of experiments were used in the statistical analysis. Average survival plus standard deviation is shown. Dil: serial dilutions; Doxo, doxorubicin.

TABLE 5: Effect of DNAJA3 and DNAJA4 expression in a wild type background.

Strain	Doxorubicin		Heat shock	
	Survival (% ± SEM)	Sensitivity (fold)	Survival (% ± SEM)	Sensitivity (fold)
WT	63.3 ± 18.6	1	104 ± 4	1
WT-DNAJA3	20 ± 2.9	3.2	0 ± 0	—
WT-DNAJA4	4 ± 1.8	15.8	0 ± 0	—

As expected, the HSP40s are not required for the repair of DSBs, since the *ydj1Δ* deletion strain was not sensitive to etoposide. However, they are essential for the survival to exposure to ROS-generating agent menadione, indicating that ROS-induced protein damage is processed by DNAJA1 and DNAJA2.

While the HSP40s have not been as extensively studied as HSP90 and the HSP70s, recent interest in these chaperones has increased our knowledge of their function and the cellular processes they are involved in, besides their protein folding roles. DNAJA1, as all DNAJA members, is induced by heat shock factor 1 (HSF1). DNAJA1 negatively regulates the translocation of BAX from the cytosol to mitochondria in response to cellular stress, thereby protecting cells against

apoptosis, and has subcellular localization within the nucleus, mitochondria, and endoplasmic reticulum [25]. It is known for binding to ubiquitin protein ligase and chaperone activity [26]. There are several DNAJA1 isoforms, one of which, isoform 2, is highly expressed in the testes and lung [27].

DNAJA2 has been shown to play a role in the positive regulation of cellular proliferation and the refolding of proteins and subcellular localizations within the cytosol [28]. It catalyzes unfolded protein binding and heat shock protein binding activity [29]. DNAJA2 is highly expressed in the adrenal gland, duodenum, kidney tubules, testis seminiferous ducts, and follicle ovarian cells [30].

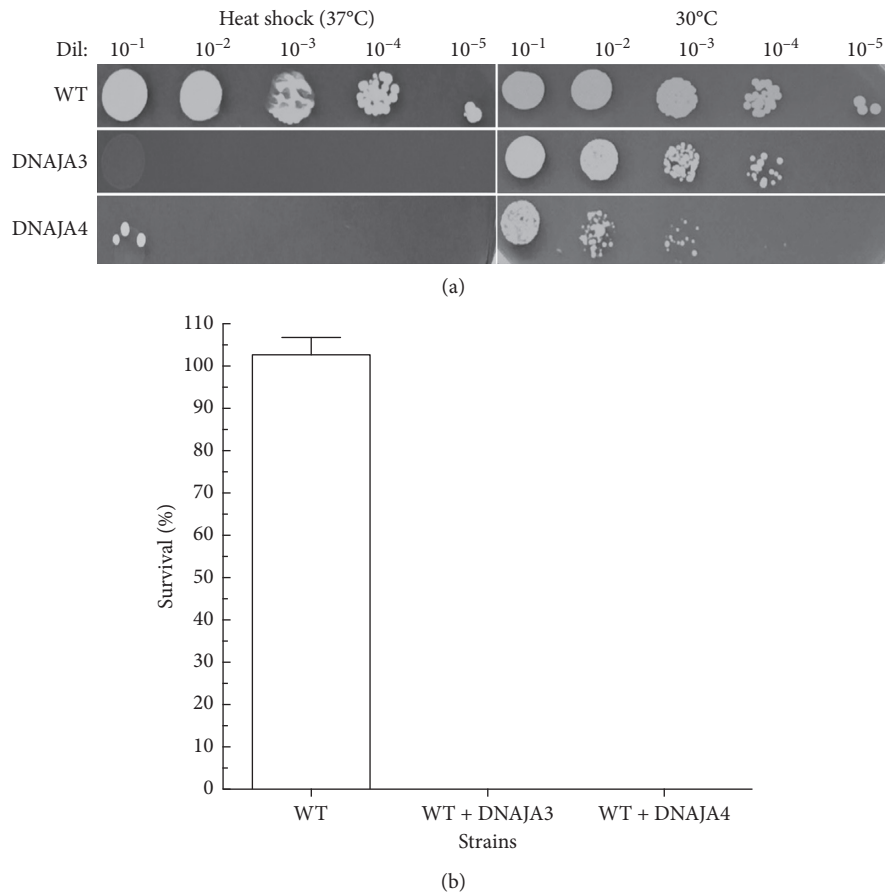


FIGURE 9: Effect of the expression of DNAJA3 and DNAJA4 in cells with wild type YDJ1 exposed to heat shock. (a) The survival to heat shock of the DNAJA3- and DNAJA4-expressing wild type cells containing was determined. Serial dilutions of the cells were plated onto Leu⁻ + glucose plates and incubated at 30°C (untreated controls) and at 37°C (heat shock). Growth was scored at 72 hours. WT is the positive control, resistant to heat shock. (b) Survival was determined by growth of the heat-shocked strain relative to the growth of nonheat-shocked cells. At least three sets of experiments were used in the statistical analysis. Average survival plus standard deviation is shown. Dil: serial dilutions; Doxo, doxorubicin.

DNAJA3 is localized to mitochondria and mediates several cellular processes including proliferation, survival, and apoptotic signal transduction [31]. It plays a critical role in tumor suppression through interactions with oncogenic proteins including ErbB2 and the p53 tumor suppressor protein [32]. DNAJA3 has been found to bind to protein kinase [33]. Its subcellular locations include postsynaptic plasma membrane, cytosol, and mitochondria. Its expression is high within the heart, liver, lung, and skeletal muscles with expression in keratinocytes. DNAJA3 has been shown to play a crucial role in preventing dilated cardiomyopathy [34].

DNAJA4 has negative regulation of inclusion body assembly [35]1). It interacts with nonstructure 2 protein of classical swine fever virus by 2-hybrid system [36]. It has been shown to be involved in cholesterol biosynthesis as a SREBP-regulated chaperone [37]. DNAJA4, as well as DNAJA1 and DNAJA2, acts in concert with Hsc70 to regulate the maturation and trafficking of hERG potassium channels [38].

Molecular chaperones such as DNAJAs are involved in the regulation of kinases, caspases, and other protein

remodeling events, and it has been proposed that altered levels of HSP expression in cancer could lead to the loss of control of cell growth and inhibitory effects on apoptosis [17]. In fact, altered expression of HSPs has been reported for almost all classes of tumors, and because of their role in the control of cell growth, they could serve as biomarkers for cancer diagnosis and therapy [17].

The role of the DNAJAs in the response to stress may be associated to the specific client proteins they interact with and the biological processes they participate in. The role of the heat shock response in preventing cytotoxicity of doxorubicin has been reported; however, these studies have mostly focused on Hsp70 and Hsp27 [9]. Our study has identified the *YDJ1* homologues DNAJA1 and DNAJA2 as crucial factors for survival from doxorubicin and cisplatin stress. Interestingly, while anthracyclines act through a combination of DNA damage and generation of ROS, preventing the cell from responding to ROS-induced protein damage is sufficient sensitize it. Additionally, increasing the expression of these DNAJAs may provide protection in noncancerous sensitive tissue. Future research will elucidate the role of these genes in mammalian cells. Targeting these

factors for chemotherapeutic sensitization of cancer cells may have potential in the development of alternative therapeutic treatments.

Data Availability

Data will be available by contacting the corresponding author. All strains and reagents used in the studies are available upon request.

Conflicts of Interest

The authors declare that there are no conflicts of interest regarding the publication of this paper.

Acknowledgments

The authors are grateful for the support provided by the Gene and Cell Manipulation Facility and the CARE² Tissue Modeling Core of Florida A&M University. This project was supported by the National Institute on Minority Health and Health Disparities of the National Institute of Health under grant no. U54MD007582.

References

- [1] S. Chatterjee and T. F. Burns, "Targeting heat shock proteins in cancer: a promising therapeutic approach," *International Journal of Molecular Sciences*, vol. 18, no. 9, 2017.
- [2] J. V. McGowan, R. Chung, A. Maulik, I. Piotrowska, J. M. Walker, and D. M. Yellon, "Anthracycline chemotherapy and cardiotoxicity," *Cardiovascular Drugs and Therapy*, vol. 31, no. 1, pp. 63–75, 2017.
- [3] G. Minotti, P. Menna, E. Salvatorelli, G. Cairo, and L. Gianni, "Anthracyclines: molecular advances and pharmacologic developments in antitumor activity and cardiotoxicity," *Pharmacological Reviews*, vol. 56, no. 2, pp. 185–229, 2004.
- [4] G. Minotti, S. Recalcati, P. Menna, E. Salvatorelli, G. Corna, and G. Cairo, "Doxorubicin cardiotoxicity and the control of iron metabolism: quinone-dependent and independent mechanisms," *Quinones and Quinone Enzymes, Part A*, vol. 378, pp. 340–361, 2004.
- [5] M. Volkova and R. Russell 3rd, "Anthracycline cardiotoxicity: prevalence, pathogenesis and treatment," *Current Cardiology Reviews*, vol. 7, no. 4, pp. 214–220, 2011.
- [6] L. Xia, L. Jaafar, A. Cashikar, and H. Flores-Rozas, "Identification of genes required for protection from doxorubicin by a genome-wide screen in *Saccharomyces cerevisiae*," *Cancer Research*, vol. 67, no. 23, pp. 11411–11418, 2007.
- [7] J. Verghese, J. Abrams, Y. Wang, and K. A. Morano, "Biology of the heat shock response and protein chaperones: budding yeast (*Saccharomyces cerevisiae*) as a model system," *Microbiology and Molecular Biology Reviews*, vol. 76, no. 2, pp. 115–158, 2012.
- [8] M. Reidy, R. Sharma, B.-L. Roberts, and D. C. Masison, "Human J-protein DnaJB6b cures a subset of *Saccharomyces cerevisiae* Prions and selectively blocks assembly of structurally related amyloids," *Journal of Biological Chemistry*, vol. 291, no. 8, pp. 4035–4047, 2016.
- [9] Z. N. Demidenko, C. Vivo, H. D. Halicka et al., "Pharmacological induction of Hsp70 protects apoptosis-prone cells from doxorubicin: comparison with caspase-inhibitor- and cycle-arrest-mediated cytoprotection," *Cell Death & Differentiation*, vol. 13, no. 9, pp. 1434–1441, 2006.
- [10] R. K. Hansen, "Hsp27 overexpression inhibits doxorubicin-induced apoptosis in human breast cancer cells," *Breast Cancer Research and Treatment*, vol. 56, no. 2, pp. 187–196, 1999.
- [11] R. Kumar, A. Sharma, and R. Tiwari, "Application of microarray in breast cancer: an overview," *Journal of Pharmacy and Bioallied Sciences*, vol. 4, no. 1, pp. 21–26, 2012.
- [12] J. S. Miles, "The role of protein chaperones in the survival from anthracycline-induced oxidative stress in *Saccharomyces cerevisiae*," *International Journal of Advanced Research*, vol. 6, pp. 144–152, 2018.
- [13] R. D. Kolodner and E. Alani, "Mismatch repair and cancer susceptibility," *Current Opinion in Biotechnology*, vol. 5, no. 6, pp. 585–594, 1994.
- [14] D. X. Tishkoff, A. L. Boerger, P. Bertrand et al., "Identification and characterization of *Saccharomyces cerevisiae* EXO1, a gene encoding an exonuclease that interacts with MSH2," *Proceedings of the National Academy of Sciences*, vol. 94, no. 14, pp. 7487–7492, 1997.
- [15] M. D. Freeman, "Inactivation of chromatin remodeling factors sensitizes cells to selective cytotoxic stress," *Biologics*, vol. 8, pp. 269–280, 2014.
- [16] G. Jego, A. Hazoume, R. Seigneuric, and C. Garrido, "Targeting heat shock proteins in cancer," *Cancer Letters*, vol. 332, no. 2, pp. 275–285, 2013.
- [17] C. Jolly and R. I. Morimoto, "Role of the heat shock response and molecular chaperones in oncogenesis and cell death," *Journal of the National Cancer Institute*, vol. 92, no. 19, pp. 1564–1572, 2000.
- [18] Z. Nahleh, A. Tfayli, A. Najm, A. El Sayed, and Z. Nahle, "Heat shock proteins in cancer: targeting the chaperones," *Future Medicinal Chemistry*, vol. 4, no. 7, pp. 927–935, 2012.
- [19] R. E. Wang, "Targeting heat shock proteins 70/90 and proteasome for cancer therapy," *Current Medicinal Chemistry*, vol. 18, no. 18, pp. 4250–4264, 2011.
- [20] G. Barrera, "Oxidative stress and lipid peroxidation products in cancer progression and therapy," *ISRN Oncol*, vol. 2012, 2012.
- [21] M. Oka, S.-i. Sato, H. Soda et al., "Autoantibody to heat shock protein Hsp40 in sera of lung cancer patients," *Japanese Journal of Cancer Research*, vol. 92, no. 3, pp. 316–320, 2001.
- [22] G. D. Lianos, G. A. Alexiou, A. Mangano et al., "The role of heat shock proteins in cancer," *Cancer Letters*, vol. 360, no. 2, pp. 114–118, 2015.
- [23] X.-B. Qiu, Y.-M. Shao, S. Miao, and L. Wang, "The diversity of the DnaJ/Hsp40 family, the crucial partners for Hsp70 chaperones," *Cellular and Molecular Life Sciences*, vol. 63, no. 22, pp. 2560–2570, 2006.
- [24] S. K. Lotz, L. E. Knighton, fnm Nitika, G. W. Jones, and A. W. Truman, "Not quite the SSAME: unique roles for the yeast cytosolic Hsp70s," *Current Genetics*, vol. 65, no. 5, pp. 1127–1134, 2019.
- [25] T. Gotoh, K. Terada, S. Oyadomari, and M. Mori, "hsp70-DnaJ chaperone pair prevents nitric oxide- and CHOP-induced apoptosis by inhibiting translocation of Bax to mitochondria," *Cell Death & Differentiation*, vol. 11, no. 4, pp. 390–402, 2004.
- [26] G. C. Meacham, C. Patterson, W. Zhang, J. M. Younger, and D. M. Cyr, "The Hsc70 co-chaperone CHIP targets immature CFTR for proteasomal degradation," *Nature Cell Biology*, vol. 3, no. 1, pp. 100–105, 2001.

- [27] Y. Gao, "Distinct roles of molecular chaperones HSP90alpha and HSP90beta in the biogenesis of KCNQ4 channels," *PLoS One*, vol. 8, no. 2, Article ID e57282, 2013.
- [28] M. C. Edwards, "Human CPR (cell cycle progression restoration) genes impart," 1997.
- [29] J. N. Rauch and J. E. Gestwicki, "Binding of human nucleotide exchange factors to heat shock protein 70 (Hsp70) generates functionally distinct complexes in vitro," *Journal of Biological Chemistry*, vol. 289, no. 3, pp. 1402–1414, 2014.
- [30] P. A. Gonzales, T. Pisitkun, J. D. Hoffert et al., "Large-scale proteomics and phosphoproteomics of urinary exosomes," *Journal of the American Society of Nephrology*, vol. 20, no. 2, pp. 363–379, 2009.
- [31] I. Dhennin-Duthille, R. Nyga, S. Yahiaoui et al., "The tumor suppressor hTid1 inhibits STAT5b activity via functional interaction," *Journal of Biological Chemistry*, vol. 286, no. 7, pp. 5034–5042, 2011.
- [32] H. Cheng, C. Cenciarelli, Z. Shao et al., "Human T cell leukemia virus type 1 Tax associates with a molecular chaperone complex containing hTid-1 and Hsp70," *Current Biology*, vol. 11, no. 22, pp. 1771–1775, 2001.
- [33] J. H. Choi, D.-K. Choi, K.-C. Sohn et al., "Absence of a human DnaJ protein hTid-1SCorrelates with aberrant actin cytoskeleton organization in lesional psoriatic skin," *Journal of Biological Chemistry*, vol. 287, no. 31, pp. 25954–25963, 2012.
- [34] M. Hayashi, K. Imanaka-Yoshida, T. Yoshida et al., "A crucial role of mitochondrial Hsp40 in preventing dilated cardiomyopathy," *Nature Medicine*, vol. 12, no. 1, pp. 128–132, 2006.
- [35] J. Hageman, M. A. W. H. van Waarde, A. Zylicz, D. Walerych, and H. H. Kampinga, "The diverse members of the mammalian HSP70 machine show distinct chaperone-like activities," *Biochemical Journal*, vol. 435, no. 1, pp. 127–142, 2011.
- [36] K. Kang, K. Guo, Q. Tang et al., "Interactive cellular proteins related to classical swine fever virus non-structure protein 2 by yeast two-hybrid analysis," *Molecular Biology Reports*, vol. 39, no. 12, pp. 10515–10524, 2012.
- [37] C. Robichon, M. Varret, X. Le Liepvre et al., "DnaJA4 is a SREBP-regulated chaperone involved in the cholesterol biosynthesis pathway," *Biochimica et Biophysica Acta (BBA)—Molecular and Cell Biology of Lipids*, vol. 1761, no. 9, pp. 1107–1113, 2006.
- [38] E. B. J. Ahrendt and J. E. A. Braun, "Channel triage: emerging insights into the processing and quality control of hERG potassium channels by DnaJA proteins 1, 2 and 4," *Channels*, vol. 4, no. 5, pp. 335–336, 2010.

Research Article

A Novel Three-Gene Model Predicts Prognosis and Therapeutic Sensitivity in Esophageal Squamous Cell Carcinoma

Fa-Min Zeng,^{1,2,3} Jian-Zhong He,^{1,2,4} Shao-Hong Wang,⁵ De-kai Liu,^{1,2,6} Xiu-E. Xu,^{1,2}
Jian-Yi Wu,^{1,2} En-Min Li ^{1,2} and Li-Yan Xu ^{1,2}

¹The Key Laboratory of Molecular Biology for High Cancer Incidence Coastal Chaoshan Area, Shantou University Medical College, Shantou, Guangdong, China

²Department of Biochemistry and Molecular Biology, Shantou University Medical College, Shantou, Guangdong, China

³Guangdong Provincial Engineering Research Center of Molecular Imaging, The Fifth Affiliated Hospital, Sun Yat-sen University, Zhuhai, Guangdong, China

⁴Department of Pathology, The Fifth Affiliated Hospital, Sun Yat-sen University, Zhuhai, Guangdong, China

⁵Department of Pathology, Shantou Central Hospital, Affiliated Shantou Hospital of Sun Yat-sen University, Shantou, Guangdong, China

⁶Department of Medical Records Management, Shenzhen People's Hospital, Shenzhen, Guangdong, China

Correspondence should be addressed to En-Min Li; nmli@stu.edu.cn and Li-Yan Xu; lyxu@stu.edu.cn

Received 25 September 2019; Accepted 7 November 2019; Published 25 November 2019

Guest Editor: Amal El-Naggar

Copyright © 2019 Fa-Min Zeng et al. This is an open access article distributed under the Creative Commons Attribution License, which permits unrestricted use, distribution, and reproduction in any medium, provided the original work is properly cited.

To precisely predict the clinical outcome and determine the optimal treatment options for patients with esophageal squamous cell carcinoma (ESCC) remains challenging. Prognostic models based on multiple molecular markers of tumors have been shown to have superiority over the use of single biomarkers. Our previous studies have identified the crucial role of ezrin in ESCC progression, which prompted us to hypothesize that ezrin-associated proteins contribute to the pathobiology of ESCC. Herein, we explored the clinical value of a molecular model constructed based on ezrin-associated proteins in ESCC patients. We revealed that the ezrin-associated proteins (MYC, PDIA3, and ITGA5B1) correlated with the overall survival (OS) and disease-free survival (DFS) of patients with ESCC. High expression of MYC was associated with advanced pTNM-stage ($P = 0.011$), and PDIA3 and ITGA5B1 were correlated with both lymph node metastasis (PDIA3: $P < 0.001$; ITGA5B1: $P = 0.001$) and pTNM-stage (PDIA3: $P = 0.001$; ITGA5B1: $P = 0.009$). Furthermore, we found that, compared with the current TNM staging system, the molecular model elicited from the expression of MYC, PDIA3, and ITGA5B1 shows higher accuracy in predicting OS ($P < 0.001$) or DFS ($P < 0.001$) in ESCC patients. Moreover, ROC and regression analysis demonstrated that this model was an independent predictor for OS and DFS, which could also help determine a subgroup of ESCC patients that may benefit from chemoradiotherapy. In conclusion, our study has identified a novel molecular prognosis model, which may serve as a complement for current clinical risk stratification approaches and provide potential therapeutic targets for ESCC treatment.

1. Introduction

Esophageal cancer is the sixth leading cause of cancer-related deaths and the eighth most common type of malignant gastrointestinal cancer in the world [1, 2]. Adenocarcinoma and squamous cell carcinoma (ESCC) are the two major types of esophageal cancer, with the latter accounting for the 90% of cases worldwide [3]. In China, ESCC still remains the highest incidence and cancer-induced mortality rates, and

the long-term prognosis of patients with ESCC is less than 20%, despite improvements in treatments such as surgical resection and adjuvant chemoradiation [4, 5]. This poor prognosis for ESCC patients is highly associated with the difficult nature of diagnosing early-stage ESCC and the frequent occurrence of local invasion and distant metastasis [5]. In addition, conventional chemotherapy and radiotherapy treatments are relatively ineffective [6]. Therefore, seeking novel molecular prognostic markers that can help

identify patients at high risk and improving their prognosis are urgent needs in the clinic.

However, signal molecular marker cannot meet the clinical requirements for biomarkers, such as high sensitivity and specificity, and it is more accurate than the current clinical staging system [7]. In the last few years, studies have demonstrated that combinations of multiple biomarkers were more sensitive and reliable than single molecular marker. Although several prognostic biomarkers for ESCC have been reported [8–12], there is still no ideal biomarker for clinical use.

Ezrin as a member of the ezrin/radixin/moesin (ERM) protein family plays an important role in regulating the growth and metastatic of cancer [13, 14]. In our previous studies, we showed that ezrin was upregulated in ESCC and promoted cellular proliferation and invasiveness of ESCC cells [15]. Furthermore, Ezrin might be a new prognostic molecular marker for ESCC patients [16]. Ezrin was also known as a key molecule connected with many other molecules in the biology of tumor development [17]. In these ezrin-related proteins, our previous studies identified that three proteins, i.e., MYC, PDIA3, and ITGA5B1, correlated with patients' survival [11, 12]. MYC, a protooncogene, plays an integral role in a variety of normal cellular functions [18]. MYC amplification is a recurrent event in many tumors and contributes to tumor development and progression [19–22]. The progress of MYC-induced tumorigenesis in prostate cancer cells entails MYC binding to the ezrin gene promoter and the induction of its transcription [23]. Meanwhile, the induction of ezrin expression is essential for MYC-stimulated invasion [23]. PDIA3 (protein disulfide isomerase family A, member 3), also known as ERp57, is one of the main members of the protein disulfide isomerase (PDI) gene family and is identified primarily as enzymatic chaperones for reconstructing misfolded proteins within the endoplasmic reticulum (ER) [24]. Several studies have linked PDIA3 to different types of cancer, including breast [25], ovarian [26], and colon [27] cancers. In ESCC, we found that PDIA3 interacted with ezrin, and it was not only involved in the development and progression of ESCC but also related to OS and DFS of ESCC patients [12]. ITGA5B1 is a member of the integrin family which plays a significant role in cell adhesion to the extracellular matrix (ECM) [28, 29]. In ESCC, ITGA5B1 upregulates the expression of ezrin through the L1CAM [30].

Although ezrin plays a pivotal role in ESCC progression, the clinical significance of ezrin-related proteins (MYC, PDIA3, and ITGA5B1) has not been thoroughly investigated in ESCC patients. Clinicopathological analyses of these ezrin-interacting proteins may further our understanding of the function of ezrin and provide therapeutic targets for ESCC. In the current study, we found that a three-gene signature comprised of MYC, PDIA3, and ITGA5B1 could independently predict ESCC patient survival.

2. Materials and Methods

2.1. Patients and Specimens. For this retrospective study, 284 cases of formalin-fixed, paraffin-embedded ESCC tissue were collected from the Shantou Central Hospital between November 2007 and January 2010. All patients underwent

curative resection and were confirmed as having ESCC by pathologists in the Clinical Pathology Department of the Hospital. Information on age, gender, and histopathological factors was obtained from the medical records and shown in Table 1. An independent validation set (GSE53622 and GSE5364) was obtained from the publicly available GEO database (<https://www.ncbi.nlm.nih.gov/>). We excluded the ESCC patients without clinical survival information, and the clinicopathological information was shown in Table S1. Overall survival (OS) was defined as the interval between surgery and death from tumors or between surgery and the last observation taken for surviving patients. Disease-free survival (DFS) was defined as the interval between surgery and diagnosis of relapse or death. Ethical approval was obtained from the ethical committee of the Central Hospital of Shantou City and the ethical committee of the Medical College of Shantou University, and only resected samples from surgical patients giving written informed consent were included for use in research.

2.2. Tissue Microarrays (TMAs) and Immunohistochemistry (IHC). TMAs were constructed based on standard techniques as previously described [12]. IHC was performed using the PV-9000 2-step Polymer Detection System (ZSGB-BIO, Beijing, China) and Liquid DAB Substrate Kit (Invitrogen, San Francisco, CA) according to the manufacturer's instructions and has been described in our previous studies [12]. The primary mouse monoclonal MYC antibody (1 : 100 dilution; Santa Cruz Biotechnology, USA), anti-PDIA3 antibody (polyclonal, 1 : 700 dilution; sigma, Saint Louis, MO), and anti-ITGA5B1 antibody (monoclonal, 1 : 50 dilution; millipore, USA) were used in this study.

2.3. Evaluation of IHC Variables. The protein expression was evaluated by an automated quantitative pathology imaging system (PerkinElmer, Waltham, MA, USA), as described previously [11]. Briefly, as shown in Figure S1, the automated image acquisition and color images were obtained using Vectra 2.0.8 software. Subsequently, the spectral libraries were constructed using Nuance 3.0 software. And then, the color images were evaluated by Inform 1.2 software as follows: (1) segmentation of the tumor region from the tissue compartments, (2) segmentation of the tumor region from the tumor region, and (3) H score calculation ($= (\% \text{ at } 0) * 0 + (\% \text{ at } 1+) * 1 + (\% \text{ at } 2+) * 2 + (\% \text{ at } 3+) * 3$) based on the optical density which produces a continuous protein expression value in the range of 0 to 300.

2.4. Construction of a Survival Predictive Model. Firstly, we used a univariate Cox proportional hazards regression analysis to evaluate the correlation between survival and each protein. Subsequently, we constructed a predictive model by the summation of the expression of each biomarker (high = 1, low = 0) multiplied by its regression coefficient, as described in the following equation: $Y = (\beta_1) \times \text{MYC} + (\beta_2) \times \text{PDIA3} + (\beta_3) \times \text{ITGA5B1}$ [9]. Patients were then divided into three groups (high-risk, medium-risk, and low-risk) by the cut-off value generated by X-tile software [31].

TABLE 1: The clinicopathological characteristics of generation dataset of patients with ESCC.

Clinical and pathological indexes	Case no.	5-year OS (%)	<i>P</i> *	5-year DFS (%)	<i>P</i> *
Specimens	284				
Mean age	58.7				
Age (year)					
≤58	148	48.1	0.036	43.4	0.207
>58	136	39.1		35.8	
Gender					
Male	220	44.8	0.387	40.5	0.915
Female	64	40.2		37.2	
Therapies					
Only surgery	160	45.2	0.080	42.0	0.070
Surgery + radiotherapy	39	53.6		51.3	
Surgery + chemotherapy	57	46.2		36.4	
Surgery + chemoradiotherapy	28	17.9		17.9	
Tumor size					
≤3 cm	67	55.6	0.057	54.4	0.021
3–5 cm	134	43.5		37.9	
>5 cm	83	34.7		31.1	
Tumor location					
Upper	16	33.5	0.463	25.0	0.127
Middle	122	45.6		44.8	
Lower	146	43.3		37.2	
Histologic grade					
G1	45	57.7	0.001	57.7	<0.001
G2	219	43.5		38.3	
G3	20	15.0		15.0	
Invasive depth					
T1	13	84.6	0.005	84.6	0.013
T2	42	50.0		45.2	
T3	229	40.2		36.2	
Lymph node metastasis					
N0	141	58.1	<0.001	53.5	<0.001
N1	81	44.0		39.0	
N2	46	15.2		13.0	
N3	16	0.0		0.0	
pTNM-stage					
I	23	82.6	<0.001	82.6	<0.001
II	131	54.2		49.2	
III	130	26.4		22.6	

* Log-rank test of Kaplan–Meier method; $P < 0.05$ was considered significant. All patients underwent surgical treatment. OS: overall survival. DFS: disease-free survival.

2.5. Statistical Analysis. The SPSS v19.0 program was used for statistical analysis. Cumulative survival time was calculated by the Kaplan–Meier (K-M) method and analyzed by the log-rank test. The association of biomarkers and clinicopathological factors was evaluated by Fisher’s exact test. The Cox proportional hazards regression model was used for univariate and multivariate analyses. The predictive value of the parameters was determined by receiver operating characteristic (ROC) curve analysis. $P < 0.05$ was considered to be statistically significant.

3. Results

3.1. Immunohistochemical Characteristics of 3 Biomarkers. The expression levels of MYC, PDIA3, and ITGA5B1 protein in ESCC were examined by IHC. As shown in Figure 1(a), MYC, PDIA3, and ITGA5B1 were mainly localized in the cytoplasm. We further investigated the association between

the expression of these 3 biomarkers and clinicopathological parameters. There was no significant correlation between the 3 markers and age, gender, tumor size, histologic grade, or invasive depth, etc. Nonetheless, low-expression of PDIA3 or high expression of ITGA5B1 significantly correlated with lymph node (LN) metastasis, whereas no correlation was found between MYC and LN metastasis (Table 2). In addition, PDIA3 had a negative correlation while MYC and ITGA5B1 had a positive correlation with pTNM-stage (Table 2). In support of these correlation analyses, MYC and ITGA5B1 showed increased expression in tumors with high clinical stage; in contrast, PDIA3 expression was down-regulated in stage III tumors compared with those with stages I and II (Figure 1(b)).

3.2. Prognostic Significance of MYC, PDIA3, and ITGA5B1 in Patients with ESCC. To further explore the clinical

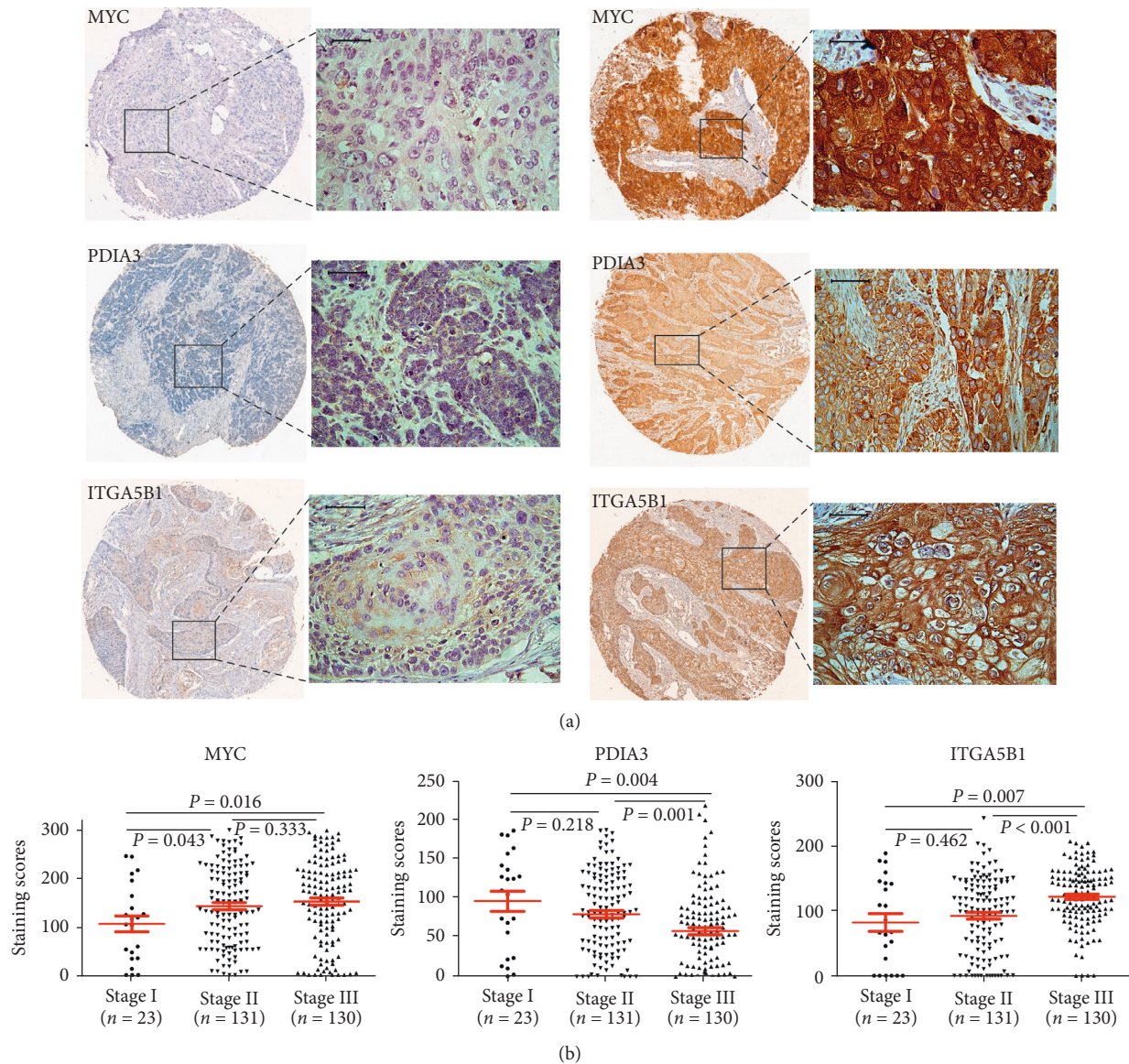


FIGURE 1: Expression of MYC, PDIA3, and ITGA5B1 in ESCC. (a) Representative images of IHC staining for MYC, PDIA3, and ITGA5B1 in ESCC samples (scale bars = 50 μ m). (b) The H scores of MYC, PDIA3, and ITGA5B1 in different clinical stages (stages I, II, and III) of ESCC were shown by scatter diagram ($P < 0.05$, independent-samples t -test).

significance of MYC, PDIA3, and ITGA5B1 in ESCC patients, Kaplan-Meier analysis and log-rank test were performed. As shown in Figure 2, high expression of MYC or ITGA5B1 was significantly associated with poor prognosis (MYC: OS, $P = 0.024$, DFS, $P = 0.024$; ITGA5B1: OS, $P = 0.001$, DFS, $P = 0.009$, Figures 2(a) and 2(c)). However, the overexpression of PDIA3 trended to predict a favorable OS ($P = 0.002$) and DFS ($P = 0.003$, Figure 2(b)). Besides, because ITGA5B1 is a heterodimer of alpha and beta subunit, we used the expression level of ITGA5 instead of ITGA5B1 in microarray data, and the predictive value of MYC, PDIA3, and ITGA5 was further validated in an independent cohort (GSE53622 and GSE5364).

The results for validation set were in line with those in generation set (Supplementary Figure S2(a)). Univariate

Cox regression analysis further identified that these 3 molecules were significantly associated with OS (MYC: $P = 0.026$; PDIA3: $P = 0.003$; ITGA5B1: $P = 0.001$) and DFS (MYC: $P = 0.026$; PDIA3: $P = 0.004$; ITGA5B1: $P = 0.010$, Table 3).

3.3. A Molecular Prognostic Model of the 3 Biomarkers Signature. We then evaluated the prognostic value of a molecular model that takes consideration of all the 3 biomarkers. To this end, we calculated the risk score $Y = (\beta_1) * (\text{MYC}) + (\beta_2) * (\text{PDIA3}) + (\beta_3) * (\text{ITGA5B1})$. In this dataset, the regression coefficients ($\beta_1 = 0.347$, $\beta_2 = -0.482$, $\beta_3 = 0.501$) were calculated by univariate Cox proportional hazards analysis. All patients were divided into

TABLE 2: The correlation between 3 markers and clinicopathological characteristics in ESCC.

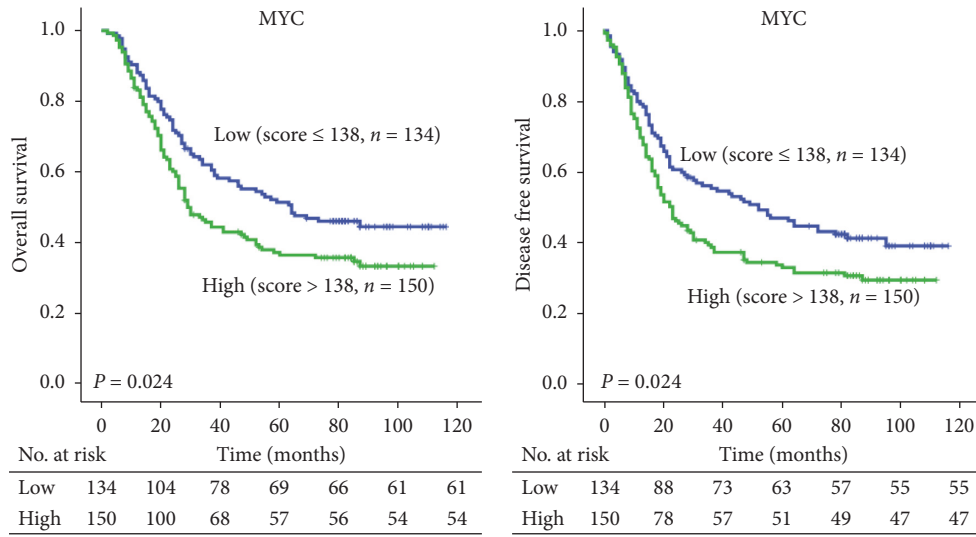
Variables	MYC ^a		P*	PDIA3 ^b		P*	ITCA5B1 ^c		P*
	Low	High		Low	High		Low	High	
Age (year)									
≤58	67	81	0.425	84	64	0.725	92	56	0.334
>58	68	68		80	56		92	44	
Gender									
Male	109	111	0.208	127	93	0.990	137	83	0.100
Female	26	38		37	27		47	17	
Therapies									
Only surgery	85	75	0.067	97	63	0.588	107	53	0.849
Surgery + radiotherapy	14	25		20	19		25	14	
Surgery + chemotherapy	21	36		30	27		35	22	
Surgery + radiochemotherapy	15	13		17	11		17	11	
Tumor size									
≤3 cm	39	28	0.101	41	26	0.303	43	24	0.489
3–5 cm	62	72		71	63		83	51	
>5 cm	34	49		52	31		58	25	
Tumor location									
Upper	6	10	0.307	9	7	0.383	8	8	0.395
Middle	64	58		65	57		82	40	
Lower	65	81		90	56		94	52	
Histologic grade									
G1	25	20	0.499	20	25	0.054	32	13	0.588
G2	101	118		129	90		140	79	
G3	9	11		15	5		12	8	
Invasive depth									
T1 + T2	32	23	0.078	37	18	0.111	34	21	0.607
T3 + T4	103	126		127	102		150	79	
Lymph node metastasis									
N0	73	68	0.156	64	77	<0.001	105	36	0.001
N1 + N2 + N3	62	81		100	43		79	64	
pTNM-stage									
I	17	6	0.011	10	13	0.001	16	7	0.009
II	65	66		64	67		96	35	
III	53	77		90	40		72	58	

*Fisher's exact test. P value < 0.05 was considered significant.

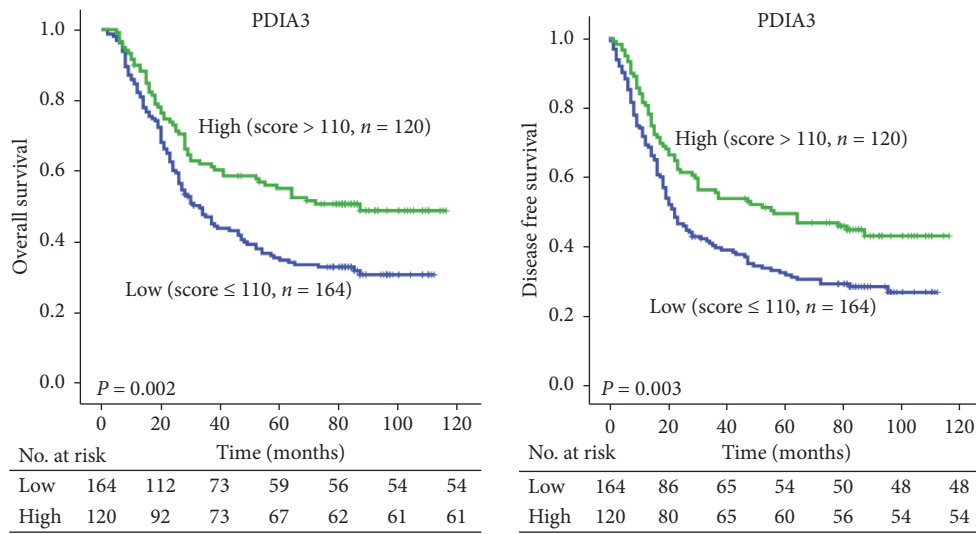
low-, medium-, and high-risk groups based on the Y scores, and the optimal cut-off values were determined by the X-tile software based on patients' prognosis [31]. Kaplan–Meier analysis further demonstrated that patients in the low-risk group indeed had markedly prolonged survival (OS: $P < 0.001$; DFS: $P < 0.001$, Figure 3(a)). The 5-year OS for low-, medium-, and high-risk groups was 62.9%, 41.3%, and 24.5%, respectively. Similar results were obtained for 5-year DFS in those groups, which were 56.0%, 37.4%, and 24.5%, respectively (Figure 3(a)). To validate whether this molecular prognostic model can serve as an independent predictor for OS and DFS, we carried out both univariate and multivariate analyses. As shown in Table 3, our newly defined molecular prognostic model, along with pTNM-stage and tumor size, was independent prognostic factors (Table 3). Moreover, receiver operating characteristic (ROC) analysis indicated that the predictive power of this molecular prognostic model was higher compared to each biomarker individually or the pTNM-stage (Figure 3(b)). The predictive value and power

of molecular model for OS also yielded similar results from validation set as shown in Figure S2(b).

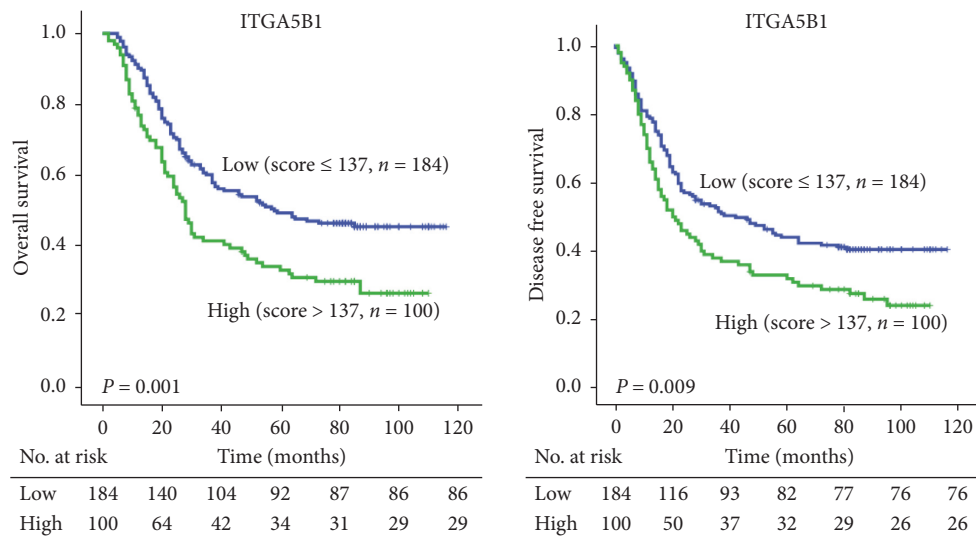
3.4. The Potential of the Molecular Prognostic Model in Identifying ESCC Patients Who Can Benefit from Chemoradiotherapy. As shown in Table 1, chemoradiotherapy did not markedly prolong the OS and DFS of ESCC patients. To test the utility of the molecular prognostic model for predicting therapeutic efficacy, we performed K-M survival analysis. Our results showed that the OS and DFS of patients who were treated with surgery only were higher compared with those who received surgery + radiotherapy or surgery + chemotherapy in the low-risk group (Figure 4(a)). However, the opposite was true for patients in the high-risk group, in which ESCC patients who received only surgery had an unfavorable outcome (Figure 4(c)). Radiotherapy and chemotherapy tended to prolong patients' survival as the risk went up as determined



(a)



(b)



(c)

FIGURE 2: K-M survival analysis in ESCC patients based on the expression of MYC, PDIA3, and ITGA5B1. The H scores of each protein were divided into low and high groups as determined by X-tile, and the number of patients who were at risk at specific times was labeled under the x-axis ($P < 0.05$, log-rank test).

TABLE 3: Univariate and multivariate analyses of factors associated with overall survival (OS) and disease-free survival (DFS) in patients with ESCC.

Variables	Univariate analysis				Multivariate analysis			
	OS		DFS		OS		DFS	
	HR (95% CI)	P	HR (95% CI)	P	HR (95% CI)	P	HR (95% CI)	P
Age (>58 vs. ≤58)	1.376 (1.017 to 1.861)	0.039	1.203 (0.900 to 1.609)	0.213	1.498 (1.082 to 2.073)	0.015		
Gender (female vs. male)	0.857 (0.603 to 1.219)	0.391	0.981 (0.693 to 1.390)	0.916				
Therapies		0.090		0.080				
(Surgery + radiotherapy vs. only surgery)	0.799 (0.492 to 1.296)	0.363	0.893 (0.557 to 1.432)	0.639				
(Surgery + chemotherapy vs. only surgery)	0.918 (0.642 to 1.423)	0.825	1.225 (0.847 to 1.770)	0.281				
(Surgery + radiochemotherapy vs. only surgery)	0.918 (1.036 to 2.550)	0.035	1.701 (1.087 to 2.662)	0.020				
Tumor size		0.062		0.025		0.045		0.021
3–5 cm vs. ≤3 cm	1.285 (0.860 to 1.921)	0.222	1.404 (0.948 to 2.077)	0.090	1.378 (0.915 to 2.075)	0.124	1.432 (0.964 to 2.130)	0.076
>5 cm vs. ≤3 cm	1.657 (1.082 to 2.539)	0.020	1.787 (1.176 to 2.716)	0.007	1.730 (1.124 to 2.664)	0.013	1.821 (1.193 to 2.779)	0.005
pTNM-stage (III vs. I + II)	2.087 (1.443 to 3.019)	<0.001	1.956 (1.376 to 2.780)	<0.001	1.876 (1.267 to 2.778)	0.002	1.689 (1.162 to 2.456)	0.006
MYC	1.415 (1.043 to 1.920)	0.026	1.397 (1.041 to 1.874)	0.026				
PDIA3	0.618 (0.450 to 0.848)	0.003	0.638 (0.471 to 0.864)	0.004				
ITGA5B1	1.651 (1.216 to 2.241)	0.001	1.477 (1.098 to 1.986)	0.010				
Molecular prognostic model		<0.001		<0.001		0.001		0.006
Medium-risk vs. ≤low-risk	1.830 (1.215 to 2.758)	0.004	1.625 (1.111 to 2.378)	0.012	1.577 (1.036 to 2.402)	0.034	1.493 (1.010 to 2.208)	0.045
High-risk vs. ≤low-risk	2.914 (1.828 to 4.680)	<0.001	2.457 (1.580 to 3.823)	<0.001	2.539 (1.556 to 4.141)	<0.001	2.122 (1.338 to 3.367)	0.001

Note. Multivariate analysis, Cox proportional hazards regression model. Variables were adopted for their prognostic significance by univariate analysis.

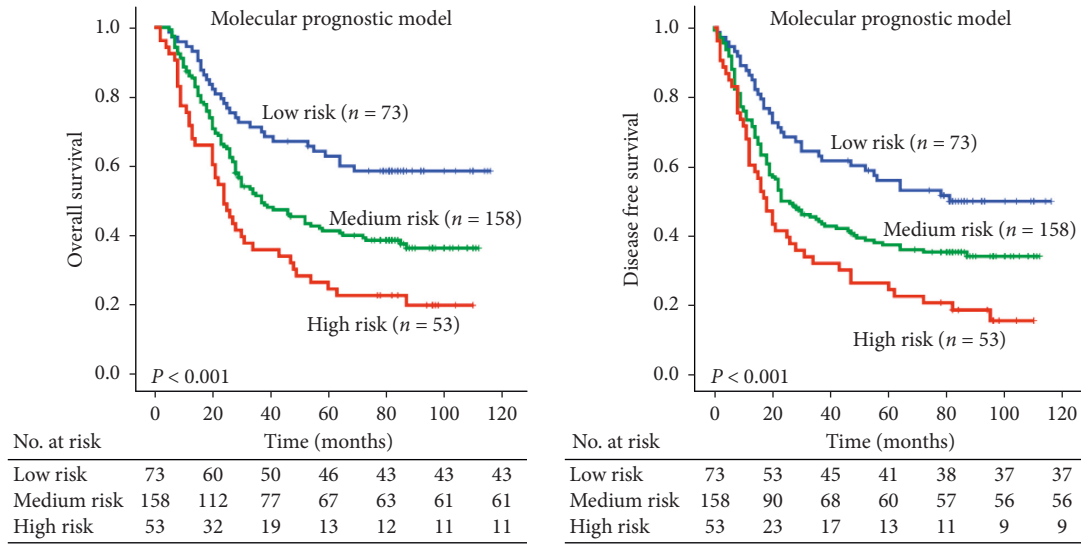
by our molecular prognostic model. In particular, patients treated with surgery + chemotherapy in the high-risk group had the most favorable OS and DFS compared with surgery alone and surgery + radiotherapy (Figure 4).

4. Discussion

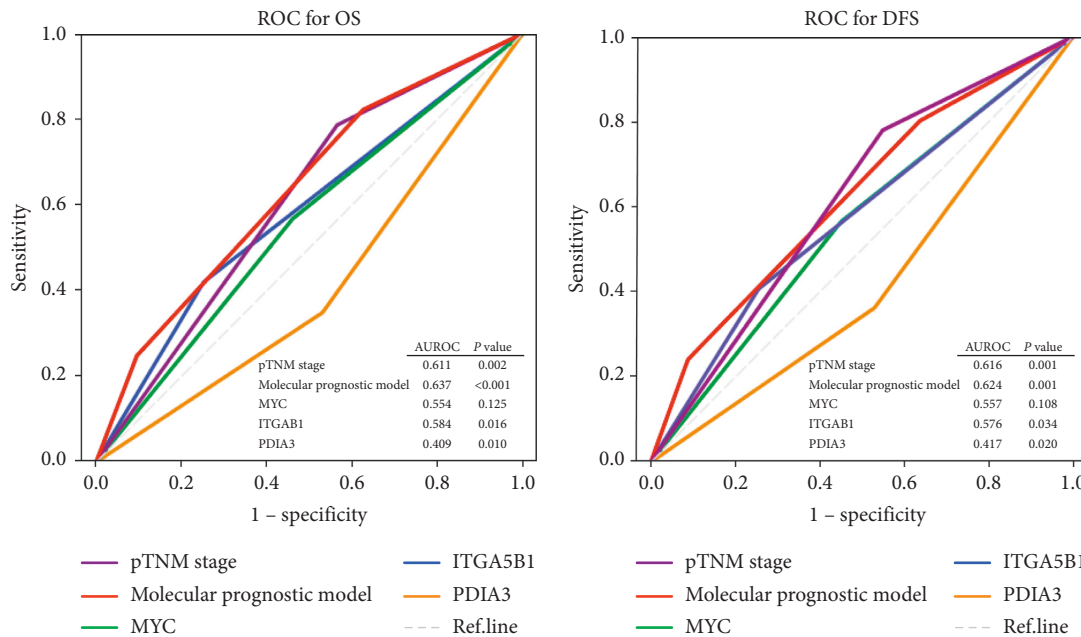
ESCC is one of the most prevalent and lethal cancers in Asian [4]; however, there is no effective molecular signatures for predicting the effectiveness of adjuvant treatments and prognosis in the clinic. Previous studies demonstrated that the cytoskeleton changes are intimately associated with cancer invasion and metastasis [32]. In support of this notion, our research has confirmed that the membrane-cytoskeletal linking protein ezrin contributes significantly to ESCC progression [15]. In this study, we attempted to generate an effective molecular model based on ezrin-related proteins (MYC, PDIA3, and ITGA5B1) for potential clinical applications. Our data highlight that a molecular model elicited from MYC, PDIA3, and ITGA5B1 has superior prognostic values compared with pTNM-stage, which also facilitates the identification of ESCC patients who may benefit from chemoradiotherapy.

Ezrin, a membrane-cytoskeleton linker, plays a major role in promoting tumor progression [23, 33]. Our previous study has identified the mislocalization of ezrin during ESCC development, in which membranous ezrin in normal epithelial cells becomes cytoplasmic in ESCC [34]. This abnormal localization changes the interacting proteins of ezrin, which has been shown to be critical for regulating tumor cell survival, invasion, and metastasis [12, 17]. The expressions of MYC, PDIA3, and ITGA5B1 have been demonstrated to play critical roles in various malignant tumors and are independent prognostic factors in certain cancers [12, 35, 36].

It is important to note that although ESCC patients with higher risk predicted by our three-protein molecular model had poor prognosis, these patients might benefit from adjuvant therapies such as chemoradiotherapy, which improved their survival compared with surgical treatment alone. Compared with the model using three different genes (PPARG, MDM2, and NANOG), which we reported in 2015 [9], the current molecular model not only accurately predicts the OS of patients with ESCC but also predicts the DFS and sensitivity to chemoradiation. This makes it much more practical for clinical application. Our results are in line with



(a)



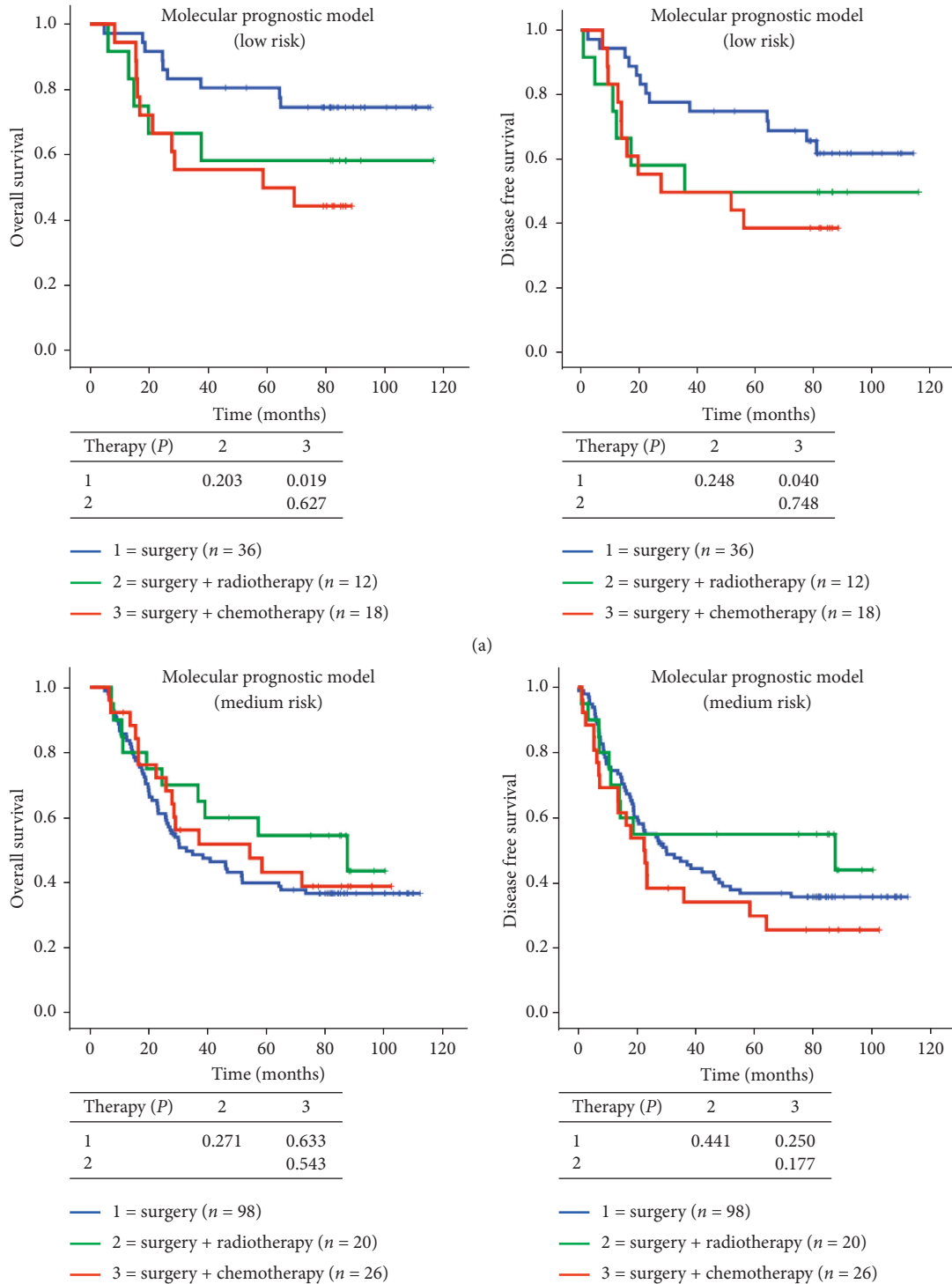
(b)

FIGURE 3: Predictive value of the molecular model. (a) K-M survival curves showing that the OS and DFS had a striking contrast between the ESCC patients in low-, medium-, and high-risk groups. (b) Receiver operating characteristic (ROC) curve was used to evaluate the ability of the molecular model for OS or DFS compared with each biomarker alone or the pTMN-stage.

other clinical studies, which have shown that high expression and rearrangement of MYC are associated with better response to chemoradiotherapy compared with patients without these abnormalities [37, 38]. The mechanism behind this observation is probably related to the biological function of MYC in promoting DNA replication and cell cycle distribution [39]. As chemoradiotherapy utilizes the effects of DNA damage-induced cytotoxicity in neoplastic cells, it is not surprising to see an association between MYC and chemo/radiosensitivity in ESCC patients. Indeed, overexpression of MYC has been shown to render tumor cells susceptible to chemotherapeutics, such as etoposide, doxorubicin, and

camptothecin [40]. Nevertheless, MYC remains an attractive molecular target for therapy due to its high oncogenic properties [41]. Antisense oligonucleotides (ASOs) targeting MYC have been shown to block cell proliferation and induce apoptosis in solid and hematologic tumors [41, 42].

Compared with MYC, relatively little is known about the biological function of ITGA5B1 in carcinoma. Recent studies suggest that ITGA5B1 can prevent cell anoikis through suppressing inflammation- and oxidative stress-related genes [43, 44]. ITGA5B1 is especially more noticeable in regulating cell adhesion [45], and it can promote early peritoneal metastasis in serous ovarian cancer [46]. In



(b)
 FIGURE 4: Continued.

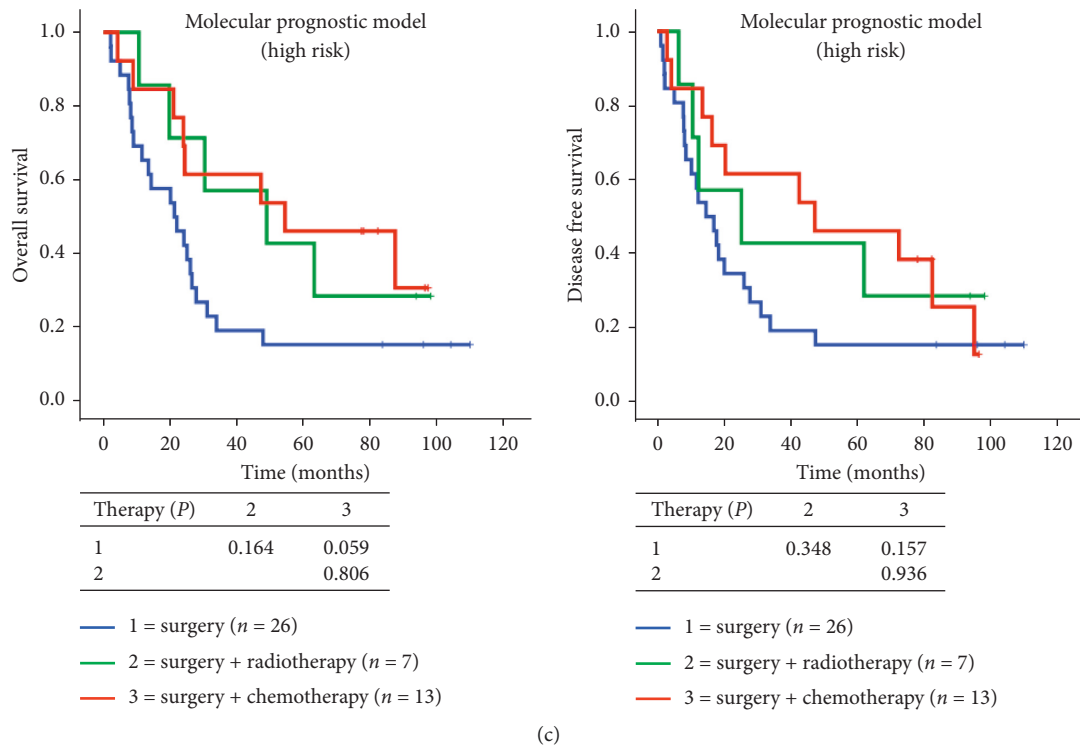


FIGURE 4: K-M survival curves indicate that radiotherapy and chemotherapy prolonged patients' OS and DFS in high-risk group but shortened patients' survival in low-risk group.

line with the protumorigenic role of ITGA5B1, we are the first to uncover the high expression of this protein in more advanced and metastatic ESCC tumors with unfavorable prognosis. Further studies are needed to delineate the mechanisms behind the deregulation of ITGA5B1 and its biological function in ESCC. PDIA3 has been shown to confer chemo/radioresistance to various types of tumor cells such as ovarian carcinoma [47, 48]. PDIA3 expression level is correlated with the clinical outcome of patients with ovarian carcinoma who receive chemoradiotherapy, and the sensitivity to paclitaxel can be enhanced by PDIA3 silencing [47, 48]. In ESCC, we found that PDIA3 decreased gradually with the progress of stage and related to favorable prognosis, which was in accord with the findings in gastric cancer [49], but contrary to those in hepatocellular carcinoma [50]. The favorable prognostic value of PDIA3 in ESCC implies that ESCC patients with high expression of PDIA3 may be more sensitive to chemotherapy such as paclitaxel, but further studies are warranted. These contrasting observations can be attributed to the differences in the carcinogenic machinery between ESCC and other carcinomas.

Taken together, these data suggest that MYC, PDIA3, and ITGA5B1 may serve as potential therapeutic targets for ESCC treatment, and cotargeting of these biomarkers might be more effective than targeting a single biomarker alone. Importantly, this study provides a clinically applicable molecular model that can more precisely predict clinical outcome than pTNM-stage, which may also facilitate the identification of ESCC patients who can benefit from radiotherapy or chemotherapy.

Data Availability

The clinical data and protein expression used to support the findings of this study are available from the corresponding author upon request.

Conflicts of Interest

The authors declare no conflicts of interest.

Acknowledgments

The authors thank all the research staff for their contributions to this project. This work was supported in part by the Natural Science Foundation of China-Guangdong Joint Fund (no. U1601229), the National Science Foundation of China (nos. 81772532 and 81472613), the National Cohort of Esophageal Cancer of China (Grant no. 2016YFC09014000), the Guangdong Esophageal Cancer Institute Science and Technology Program (no. M201714), and the Department of Education, Guangdong Government under the Top-tier University Development Scheme for Research and Control of Infectious Diseases.

Supplementary Materials

Figure S1: representative images showing the scoring process by the automated quantitative pathology imaging system. Figure S2: predictive value of three genes and the molecular model in validation dataset. Table S1: the clinicopathological

characteristics of validation dataset of patients with ESCC. (*Supplementary Materials*)

References

- [1] S. McGuire, "World cancer report 2014. Geneva, Switzerland: World Health Organization, International Agency for Research on Cancer, WHO Press, 2015," *Advances in Nutrition*, vol. 7, no. 2, pp. 418-419, 2016.
- [2] R. L. Siegel, K. D. Miller, and A. Jemal, "Cancer statistics, 2016," *CA: A Cancer Journal for Clinicians*, vol. 66, no. 1, pp. 7-30, 2016.
- [3] F. Kamangar, G. M. Dores, and W. F. Anderson, "Patterns of cancer incidence, mortality, and prevalence across five continents: defining priorities to reduce cancer disparities in different geographic regions of the world," *Journal of Clinical Oncology*, vol. 24, no. 14, pp. 2137-2150, 2006.
- [4] W. Chen, R. Zheng, P. D. Baade et al., "Cancer statistics in China, 2015," *CA: A Cancer Journal for Clinicians*, vol. 66, no. 2, pp. 115-132, 2016.
- [5] P. C. Enzinger and R. J. Mayer, "Esophageal cancer," *New England Journal of Medicine*, vol. 349, no. 23, pp. 2241-2252, 2003.
- [6] M. Tachibana, S. Kinugasa, N. Hirahara, and H. Yoshimura, "Lymph node classification of esophageal squamous cell carcinoma and adenocarcinoma," *European Journal of Cardio-Thoracic Surgery*, vol. 34, no. 2, pp. 427-431, 2008.
- [7] S. Benowitz, "Revised guidelines signal that gene expression profiles are coming of age," *JNCI: Journal of the National Cancer Institute*, vol. 100, no. 13, pp. 916-917, 2008.
- [8] Y. Zhu, M.-X. Zhu, X.-D. Zhang et al., "SMYD3 stimulates EZR and LOXL2 transcription to enhance proliferation, migration, and invasion in esophageal squamous cell carcinoma," *Human Pathology*, vol. 52, pp. 153-163, 2016.
- [9] L.-L. Sun, J.-Y. Wu, Z.-Y. Wu et al., "A three-gene signature and clinical outcome in esophageal squamous cell carcinoma," *International Journal of Cancer*, vol. 136, no. 6, pp. E569-E577, 2015.
- [10] C. He, J. Xu, J. Zhang et al., "High expression of trimethylated histone H3 lysine 4 is associated with poor prognosis in hepatocellular carcinoma," *Human Pathology*, vol. 43, no. 9, pp. 1425-1435, 2012.
- [11] W. Liu, J.-Z. He, S.-H. Wang et al., "MASAN: a novel staging system for prognosis of patients with oesophageal squamous cell carcinoma," *British Journal of Cancer*, vol. 118, no. 11, pp. 1476-1484, 2018.
- [12] J.-Z. He, Z.-Y. Wu, S.-H. Wang et al., "A decision tree-based combination of ezrin-interacting proteins to estimate the prognostic risk of patients with esophageal squamous cell carcinoma," *Human Pathology*, vol. 66, pp. 115-125, 2017.
- [13] B. Bruce, G. Khanna, L. Ren et al., "Expression of the cytoskeleton linker protein ezrin in human cancers," *Clinical & Experimental Metastasis*, vol. 24, no. 2, pp. 69-78, 2007.
- [14] M. Curto and A. I. McClatchey, "Ezrin... a metastatic determinant?," *Cancer Cell*, vol. 5, no. 2, pp. 113-114, 2004.
- [15] J.-J. Xie, L.-Y. Xu, Y.-M. Xie et al., "Roles of ezrin in the growth and invasiveness of esophageal squamous carcinoma cells," *International Journal of Cancer*, vol. 124, no. 11, pp. 2549-2558, 2009.
- [16] J.-J. Xie, L.-Y. Xu, Z.-Y. Wu et al., "Prognostic implication of ezrin expression in esophageal squamous cell carcinoma," *Journal of Surgical Oncology*, vol. 104, no. 5, pp. 538-543, 2011.
- [17] M. Arpin, D. Chirivino, A. Naba, and I. Zwaenepoel, "Emerging role for ERM proteins in cell adhesion and migration," *Cell Adhesion & Migration*, vol. 5, no. 2, pp. 199-206, 2014.
- [18] C. V. Dang, "c-MYC target genes involved in cell growth, apoptosis, and metabolism," *Molecular and Cellular Biology*, vol. 19, no. 1, pp. 1-11, 1999.
- [19] X. Wang, Y. Liu, D. Shao et al., "Recurrent amplification of MYC and TNFRSF11B in 8q24 is associated with poor survival in patients with gastric cancer," *Gastric Cancer*, vol. 19, no. 1, pp. 116-127, 2016.
- [20] K. S. Lee, Y. Kwak, K. H. Nam et al., "c-MYC copy-number gain is an independent prognostic factor in patients with colorectal cancer," *PLoS One*, vol. 10, no. 10, Article ID e0139727, 2015.
- [21] H. Sato, S. Minei, T. Hachiya, T. Yoshida, and Y. Takimoto, "Fluorescence in situ hybridization analysis of c-MYC amplification in stage T₃N₀M₀ prostate cancer in Japanese patients," *International Journal of Urology*, vol. 13, no. 6, pp. 761-766, 2006.
- [22] M. Jung, A. J. Russell, B. Liu et al., "A myc activity signature predicts poor clinical outcomes in myc-associated cancers," *Cancer Research*, vol. 77, no. 4, pp. 971-981, 2017.
- [23] Y.-C. Chuan, D. Iglesias-Gato, L. Fernandez-Perez et al., "Ezrin mediates c-MYC actions in prostate cancer cell invasion," *Oncogene*, vol. 29, no. 10, pp. 1531-1542, 2010.
- [24] E. Perri, S. Parakh, and J. Atkin, "Protein disulphide isomerases: emerging roles of PDI and ERp57 in the nervous system and as therapeutic targets for ALS," *Expert Opinion on Therapeutic Targets*, vol. 21, no. 1, pp. 37-49, 2017.
- [25] F. S. Ramos, L. T. R. Serino, C. M. S. Carvalho et al., "PDIA3 and PDIA6 gene expression as an aggressiveness marker in primary ductal breast cancer," *Genetics and Molecular Research*, vol. 14, no. 2, pp. 6960-6967, 2015.
- [26] M. Kullmann, G. V. Kalayda, M. Hellwig et al., "Assessing the contribution of the two protein disulfide isomerases PDIA1 and PDIA3 to cisplatin resistance," *Journal of Inorganic Biochemistry*, vol. 153, pp. 247-252, 2015.
- [27] A. Ménoret, D. A. Drew, S. Miyamoto, M. Nakanishi, A. T. Vella, and D. W. Rosenberg, "Differential proteomics identifies PDIA3 as a novel chemoprevention target in human colon cancer cells," *Molecular Carcinogenesis*, vol. 53, no. S1, pp. E11-E22, 2014.
- [28] K. R. Legate and R. Fassler, "Mechanisms that regulate adaptor binding to beta-integrin cytoplasmic tails," *Journal of Cell Science*, vol. 122, no. 2, pp. 187-198, 2009.
- [29] R. Zaidel-Bar, S. Itzkovitz, A. Ma'ayan, R. Iyengar, and B. Geiger, "Functional atlas of the integrin adhesome," *Nature Cell Biology*, vol. 9, no. 8, pp. 858-867, 2007.
- [30] J.-C. Guo, Y.-M. Xie, L.-Q. Ran et al., "L1CAM drives oncogenicity in esophageal squamous cell carcinoma by stimulation of ezrin transcription," *Journal of Molecular Medicine*, vol. 95, no. 12, pp. 1355-1368, 2017.
- [31] R. L. Camp, M. Dolled-Filhart, and D. L. Rimm, "X-tile: a new bio-informatics tool for biomarker assessment and outcome-based cut-point optimization," *Clinical Cancer Research*, vol. 10, no. 21, pp. 7252-7259, 2004.
- [32] C. M. Fife, J. A. McCarroll, and M. Kavallaris, "Movers and shakers: cell cytoskeleton in cancer metastasis," *British Journal of Pharmacology*, vol. 171, no. 24, pp. 5507-5523, 2014.
- [33] Y. Wang, Z. Lin, L. Sun et al., "Akt/ezrin Tyr353/NF-κB pathway regulates EGF-induced EMT and metastasis in tongue squamous cell carcinoma," *British Journal of Cancer*, vol. 110, no. 3, pp. 695-705, 2014.

- [34] H. Zeng, L. Xu, D. Xiao et al., "Altered expression of ezrin in esophageal squamous cell carcinoma," *Journal of Histochemistry & Cytochemistry*, vol. 54, no. 8, pp. 889–896, 2006.
- [35] D. Kienle, T. Katzenberger, G. Ott et al., "Quantitative gene expression deregulation in mantle-cell lymphoma: correlation with clinical and biologic factors," *Journal of Clinical Oncology*, vol. 25, no. 19, pp. 2770–2777, 2007.
- [36] W. Zheng, C. Jiang, and R. Li, "Integrin and gene network analysis reveals that ITGA5 and ITGB1 are prognostic in non-small-cell lung cancer," *OncoTargets and Therapy*, vol. 9, pp. 2317–2327, 2016.
- [37] A. M. Staiger, M. Ziepert, H. Horn et al., "Clinical impact of the cell-of-origin classification and the MYC/BCL2 dual expresser status in diffuse large B-cell lymphoma treated within prospective clinical trials of the German high-grade non-Hodgkin's lymphoma study group," *Journal of Clinical Oncology*, vol. 35, no. 22, pp. 2515–2526, 2017.
- [38] N. Gassler, I. Herr, M. Keith et al., "Wnt-signaling and apoptosis after neoadjuvant short-term radiotherapy for rectal cancer," *International Journal of Oncology*, vol. 25, no. 6, pp. 1543–1549, 2004.
- [39] Y. Kinoshita and E. M. Johnson, "Site-specific loading of an MCM protein complex in a DNA replication initiation zone upstream of the c-MYC gene in the HeLa cell cycle," *Journal of Biological Chemistry*, vol. 279, no. 34, pp. 35879–35889, 2004.
- [40] C. E. Nesbit, L. E. Grove, X. Yin, and E. V. Prochownik, "Differential apoptotic behaviors of c-myc, N-myc, and L-myc oncoproteins," *Cell Growth & Differentiation*, vol. 9, no. 9, pp. 731–741, 1998.
- [41] E. V. Prochownik, "c-MYC as a therapeutic target in cancer," *Expert Review of Anticancer Therapy*, vol. 4, no. 2, pp. 289–302, 2004.
- [42] E. Morelli, L. Biamonte, C. Federico et al., "Therapeutic vulnerability of multiple myeloma to MIR17PTi, a first-in-class inhibitor of pri-miR-17-92," *Blood*, vol. 132, no. 10, pp. 1050–1063, 2018.
- [43] Y. Zhang, J. Ding, C. Xu et al., "rBMSCs/ITGA5B1 promotes human vascular smooth muscle cell differentiation via enhancing nitric oxide production," *International Journal of Stem Cells*, vol. 11, no. 2, pp. 168–176, 2018.
- [44] H.-Y. Chen, L. Pan, H.-L. Yang et al., "Integrin alpha5beta1 suppresses rBMSCs anoikis and promotes nitric oxide production," *Biomedicine & Pharmacotherapy*, vol. 99, pp. 1–8, 2018.
- [45] S. M. Hrycaj, L. Marty-Santos, C. Cebrian et al., "Hox5genes direct elastin network formation during alveologenesis by regulating myofibroblast adhesion," *Proceedings of the National Academy of Sciences*, vol. 115, no. 45, pp. E10605–E10614, 2018.
- [46] Q. Gao, Z. Yang, S. Xu et al., "Heterotypic CAF-tumor spheroids promote early peritoneal metastasis of ovarian cancer," *The Journal of Experimental Medicine*, vol. 216, no. 3, pp. 688–703, 2019.
- [47] S. Li, X. Zhao, S. Chang, Y. Li, M. Guo, and Y. Guan, "ERp57small interfering RNA silencing can enhance the sensitivity of drug resistant human ovarian cancer cells to paclitaxel," *International Journal of Oncology*, vol. 54, no. 1, pp. 249–260, 2019.
- [48] H. Zou, C. Wen, Z. Peng et al., "P4HB and PDIA3 are associated with tumor progression and therapeutic outcome of diffuse gliomas," *Oncology Reports*, vol. 39, no. 2, pp. 501–510, 2018.
- [49] T. Shimoda, R. Wada, S. Kure et al., "Expression of protein disulfide isomerase A3 and its clinicopathological association in gastric cancer," *Oncology Reports*, vol. 41, no. 4, pp. 2265–2272, 2019.
- [50] R. Kondo, K. Ishino, R. Wada et al., "Downregulation of protein disulfide-isomerase A3 expression inhibits cell proliferation and induces apoptosis through STAT3 signaling in hepatocellular carcinoma," *International Journal of Oncology*, vol. 54, no. 4, pp. 1409–1421, 2019.

Research Article

A Novel Clinical Six-Flavoprotein-Gene Signature Predicts Prognosis in Esophageal Squamous Cell Carcinoma

Liu Peng,^{1,2} Jin-Cheng Guo,^{1,2} Lin Long,^{1,2} Feng Pan,^{1,2} Jian-Mei Zhao,^{1,2} Li-Yan Xu ^{1,3} and En-Min Li ^{1,2}

¹The Key Laboratory of Molecular Biology for High Cancer Incidence Coastal Chaoshan Area, Shantou University Medical College, Shantou 515041, Guangdong, China

²Department of Biochemistry and Molecular Biology, Shantou University Medical College, Shantou 515041, Guangdong, China

³Institute of Oncologic Pathology, Shantou University Medical College, Shantou 515041, Guangdong, China

Correspondence should be addressed to Li-Yan Xu; lyxu@stu.edu.cn and En-Min Li; nmli@stu.edu.cn

Received 4 July 2019; Revised 23 August 2019; Accepted 4 October 2019; Published 30 October 2019

Guest Editor: Amal El-Naggar

Copyright © 2019 Liu Peng et al. This is an open access article distributed under the Creative Commons Attribution License, which permits unrestricted use, distribution, and reproduction in any medium, provided the original work is properly cited.

Flavoproteins and their interacting proteins play important roles in mitochondrial electron transport, fatty acid degradation, and redox regulation. However, their clinical significance and function in esophageal squamous cell carcinoma (ESCC) are little known. Here, using survival analysis and machine learning, we mined 179 patient expression profiles with ESCC in GSE53625 from the Gene Expression Omnibus (GEO) database and constructed a signature consisting of two flavoprotein genes (GPD2 and PYROXD2) and four flavoprotein interacting protein genes (CTTN, GGH, SRC, and SYNJ2BP). Kaplan–Meier analysis revealed the signature was significantly associated with the survival of ESCC patients (mean survival time: 26.77 months in the high-risk group vs. 54.97 months in the low-risk group, $P < 0.001$, $n = 179$), and time-dependent ROC analysis demonstrated that the six-gene signature had good predictive ability for six-year survival for ESCC (AUC = 0.86, 95% CI: 0.81–0.90). We then validated its prediction performance in an independent set by RT-PCR (mean survival: 15.73 months in the high-risk group vs. 21.1 months in the low-risk group, $P = 0.032$, $n = 121$). Furthermore, RNAi-mediated knockdown of genes in the flavoprotein signature led to decreased proliferation and migration of ESCC cells. Taken together, CTTN, GGH, GPD2, PYROXD2, SRC, and SYNJ2BP have an important clinical significance for prognosis of ESCC patients, suggesting they are efficient prognostic markers and potential targets for ESCC therapy.

1. Introduction

Esophageal cancer has been ranked as the fifth most malignant disease, and it is the fourth leading cause of cancer death in China [1]. There are two main histological types of esophageal cancer: adenocarcinoma and squamous cell carcinoma [2]. Esophageal squamous cell carcinoma (ESCC) is the most common histologic type of esophageal cancer, accounting for approximately 90% of esophageal cancer tumors in China. Despite the advance in diagnosis, prognosis, and treatment, the early diagnosis for ESCC is poor, with a 5-year overall survival rate less than 20% [3]. It is widely believed that the occurrence and development of ESCC depends on alteration of multiple factors, multiple

stages, and multiple genes, making it very likely that both genetic and environmental factors contribute to this disease [4]. Further understanding of the molecular mechanism of ESCC and screening of more efficient clinical markers are crucial for the early diagnosis and improvement in prognosis of ESCC patients.

Riboflavin (vitamin B2) is an essential micronutrient for normal cellular function. Riboflavin is the precursor of both flavin adenine dinucleotide (FAD) and flavin mononucleotide (FMN), which play key roles in cell development and growth. Riboflavin participates in intermediary metabolism and is required for many metabolic reactions, such as mitochondrial electron transport, fatty acid degradation, and redox regulation [5, 6]. An increasing number of

researchers have found a positive correlation between riboflavin deficiency and cancer risk. Bassett et al. found that a higher intake of riboflavin is associated with decreased risk of breast cancer, and the same phenomenon has been observed for gastric, colorectal, and lung cancers [7–10]. Throughout recent years, there has been much research focused on the relationship between riboflavin and esophageal cancer. Siassi et al. suggested that riboflavin deficiency of residents is higher in areas with a high incidence of ESCC [11]. Our previous studies have shown that low plasma riboflavin levels are significantly associated with high risk and poor prognosis of ESCC patients, while after repletion of riboflavin can improve prognosis [4]. The above studies show that riboflavin deficiency is common in high-incidence areas of ESCC, suggesting that riboflavin dysfunction may be present in ESCC patients.

Deficiency of riboflavin can directly lead to the abnormal function of flavoproteins. Flavoproteins are a class of enzymes that catalyze a wide range of redox reactions through a variety of chemical mechanisms. This kind of protein must contain noncovalently bound FAD or FMN as a cofactor. Warburg et al. isolated the first flavoprotein from yeast (flavin phosphoric acid was its prosthetic group), and Banga et al. observed the presence of flavin in muscle tissue. So far, more than 160 kinds of flavoproteins have been isolated and characterized [12]. One of the most important characteristics of flavoproteins is the wide range of the catalytic reactions they performed, such as typical redox catalysis, DNA damage repair, or activation of dioxygen [13]. A number of recent studies indicate that abnormal expression of flavoproteins and their interacting proteins lead to a variety of clinical abnormalities, which range from degenerative changes in the skin lesions, to the growth retardation, or nervous system and peripheral neuropathy; it also affects the proliferation and mobility of various cancer cells [14–16]. However, the clinical significance and function of flavoproteins and their interacting proteins in ESCC still need to be evaluated. In this study, we obtained the expression level of flavoproteins and their interactors by re-annotating gene microarrays through analysis of the data and screened out a flavoprotein-related signature that can accurately predict overall survival of ESCC patients.

2. Materials and Methods

2.1. Flavoproteins and Their Interacting Proteins. We selected flavoproteins from the UniProt database (<http://www.uniprot.org/>) and identified their interacting proteins from the Human Protein Reference Database (<http://www.hprd.org/>) and BioGRID (<https://thebiogrid.org/>) database [17].

2.2. GEO Cancer mRNA Expression Data. The mRNA expression data and corresponding clinical data of 179 ESCC patients (GSE53625) were obtained from the GEO database (<https://www.ncbi.nlm.nih.gov/geo/>). We used this dataset as a training set [18] to analyze the correlation of flavoproteins and their interacting protein and the relationship

between flavoproteins and the survival of ESCC patients. Probe re-annotation pipeline was performed as previously described [17, 19]. The probes which were perfectly matched to a transcript were retained. And the probes which targeted both noncoding transcripts and coding cDNA sequences were removed. The gene expression values were log₂ transformed for all subsequent analysis.

2.3. Construction of a Weighted Overall Survival (OS) Predictive Score Algorithm. Firstly, we selected survival-related flavoproteins and their interacting genes by univariate Cox proportional hazards analysis ($P < 0.05$) and then used the random survival forests variable hunting (RSFVH) algorithm to filter out genes until 10 genes [18]. Subsequently, we developed a model to estimate prognosis risk as follows [18, 20, 21]:

$$\text{risk score (RS)} = \sum_{i=1}^N (\beta * \text{EXP}), \quad (1)$$

where N is the number of prognostic flavoproteins and their interacting genes, EXP is the gene's fold change value of expression, and β is the corresponding COX coefficient of the genes.

2.4. Tissue Sample Collection. ESCC tissues were obtained from the Department of Oncological Surgery of the Central Hospital of Shantou City, Guangdong Province, P.R. China, during 2012–2013 [22]. Tissues were collected from 121 ESCCs (Table 1) and confirmed by haematoxylin and eosin staining. This study was approved by the Ethics Committee of the Central Hospital of Shantou City.

2.5. RNA Extraction, cDNA Synthesis, and qRT-PCR. Total RNA from cells and tissues was extracted with TRIzol (Life Technologies, USA) according to the manufacturer's protocol. The purity and concentration of RNA were determined by OD₂₆₀/280 ratio using a NanoDrop spectrophotometer, cDNA was obtained from the total RNA using random hexamers, and real-time PCR was performed by using a SYBR® Premix Ex Taq™ kit (DRR037A, Takara). The primer sequences for CTTN (cortactin), GGH (gamma-glutamyl hydrolase), GPD2 (glycerol-3-phosphate dehydrogenase 2), PYROXD2 (pyridine nucleotide-disulphide oxidoreductase domain 2), SRC (non-receptor tyrosine kinase), and SYNJ2BP (synaptojanin 2 binding protein) for real-time RT-PCR are shown in Table 2, and β -actin was used for normalization. Quantitative RT-PCR (qRT-PCR) was repeated at least three times [23, 24].

2.6. Cell Culture and Small RNA Interference. Cell lines used in this study were previously described [25, 26]. In brief, KYSE150 and KYSE510 esophageal carcinoma cells were grown in RPMI 1640 medium (Thermo Fisher Scientific) supplemented with 10% fetal bovine serum (GIBCO), penicillin-G (100 units/mL), and streptomycin (100 μ g/mL). Cells were incubated at 37°C in 5% CO₂.

TABLE 1: Clinical characteristics of 121 ESCC patients used for validation experiments.

Clinical parameters	Number
Total cases	121
Status	
Deceased	54
Living	67
Mean age, year	57.8
Age	
<57.8	62
≥57.8	59
Gender	
Male	92
Female	29
pTNM stage	
I	6
II	57
III	58

TABLE 2: Primer sequences for qRT-PCR and siRNA sequences.

Gene	Sequence (5'-3')
	Primers for qRT-PCR
CTTN-qF	AACGATCTGGGGATCACAGC
CTTN-qR	CCAGCCGTCGTCAATCATC T
PXROXD2-qF	CAAGCTCAGCCACCACACAT
PXROXD2-qR	GCTTCTCACCTCTGTGCCAT
SYNJ2BP-qF	CTGCACCAGGATGCTGTAGAC
SYNJ2BP-qR	GAAAGCCAGGCTGTACCAT
GGH-qF	GATGGCATTTCATGCACC
GGH-qR	TGCTTCTCCTCTTCAGATTTCAG
GPD2-qF	GTGGCCAAAATGGCAAGTGT
GPD2-qR	AATCCTGGGTAGGGCTTCCT
SRC-qF	GTGGGAGAGAACCTGGTGTG
SRC-qR	GATGGTGAAGCGGCCATAGA
ACTB-qF	CAACTGGGACGACATGGAGAAA
ACTB-qR	GATAGCAACGTACATGGCTGGG
	siRNA target sequence
CTTN-Homo-449	CCAUGGCUAUGGAGGGAAATT
PYROXD2-Homo-1328	CCUCCUUAUCAGGCCUUUTT
SYNJ2BP-Homo-2746	GGACAAGUUGAAGACCCUUTT
GGH-Homo-338	GCGAGCCUCGAGCUGUCUATT
GPD2-Homo-494	GCAUUUCAGAACCAGUUAATT
SRC-Homo-937	GCCUCUCAGUGUCUGACUUTT
Negative control	UUCUCCGAACGUGUCACGUTT

In functional assays, KYSE150 and KYSE510 cells were seeded into plates and cultured for 12–24 h until 70–80% confluence. ESCC cells were transfected with 30 nM or 75 nM siRNA using Lipofectamine 3000 (Invitrogen) according to the manufacturer's instructions. Then, cells were cultured and used for further analysis. Short interfering RNAs for CTTN, GGH, GPD2, PYROXD2, SRC, and SYNJ2BP and a negative control (NC) siRNA were synthesized by GenePharma (Suzhou, Jiangsu, China). The siRNA sequences targeting the flavoprotein signature are described in Table 2.

2.7. Colony Formation Assay. A colony formation assay was performed as described previously [27]. In brief, transfected

cells were trypsinized and counted with a cell counter (Bio-Rad, Hercules, CA, USA). 1000–2000 cells per well were plated in a 6-well plate and incubated for 14 days at 37°C with 5% CO₂. After washing twice with 4°C precooled PBS, cultures were fixed with ice-cold methanol for 20 min and stained with haematoxylin for 15 min. Colonies were photographed using ChemiDoc Touch (Bio-Rad). Each experiment was performed in triplicate.

2.8. Wound Healing Assay. KYSE150 and KYSE510 cells were transfected with siRNAs targeting the flavoprotein signature, and then cells were starved in serum-free medium for 12 h after being transfected for 36 h. Circles 3 mm in diameter were marked on the bottom of each dish to identify the areas for image capture and ensure that measurements were taken at the same locations. A wound was made by scraping the cell monolayer with a 200 µL pipette tip. ESCC cells were maintained in RPMI 1640 medium with 2.5% fetal bovine serum. Images were captured at 0 and 36 h using a Leica DMI3000B inverted phase-contrast microscope (Leica Microsystems GmbH, Wetzlar, Germany). The wound closure rate was calculated from 6 images, using Image J (National Institutes of Health, Bethesda) analysis. Each experiment was performed in triplicate.

2.9. Transwell Assay. The transwell assay was performed as described previously [28]. KYSE150 and KYSE510 cells were starved in serum-free medium for 12 h after being transfected. A total of 5×10^4 cells were plated in medium without serum in the upper well of a transwell chamber of a 24-well transwell with 8 µm pores (BD Biosciences), which was placed in a bottom chamber containing medium supplemented with 10% fetal bovine serum. After 48 h, the membranes were fixed and stained with haematoxylin solution and scraped off the cells remaining in the upper chamber. The migration was quantified by counting 10 random fields under a Leica DMI3000B inverted phase-contrast microscope (400) with Image J. Each experiment was performed in triplicate.

2.10. Statistical Analysis. In training datasets, 179 ESCC patients were divided into low-risk (risk score ≤ 12.86) and high-risk groups (risk score > 12.86) by using the median as a cutoff value [3]. In the independent validation datasets, 121 ESCC patients were divided into low-risk (risk score ≤ 1.28) and high-risk (risk score > 1.28) groups by using the X-tile software [29]. Kaplan–Meier analysis was performed to test the survival distributions in the different groups. The sensitivity and specificity of the risk score for survival were compared by the receiver operating characteristic (ROC) curve [30]. All analyses were performed using the R program (www.r-project.org), including packages named pROC, survival, and randomForestSRC downloaded from Bio-conductor (<http://www.bioconductor.org/>). SPSS v13.0 software was used for statistical analysis. Where indicated, statistical analysis was performed by calculating means and SD. Graphs were mainly made by GraphPad Prism 6 (GraphPad, San

Diego, USA). Differences between groups were evaluated with Student's *t* test. Significance was defined as $P < 0.05$. Gene set enrichment analysis (GSEA) was performed by the GSEA software [31].

3. Results

3.1. Acquisition of Flavoproteins and Their Interacting Protein Expression Level via Re-Annotation of the Agilent Array. 179 ESCC samples (contained tumor tissues and adjacent normal tissues) from the GSE53625 dataset were selected according to the dataset screening criteria described in the Materials and Methods section. Several PCGs were identified by probe re-annotation of the Agilent-038314 CBC Homo sapiens lncRNA + mRNA microarray V2.0. We generated a new mRNA expression profile of the GSE53625 profiles by the following steps: First, we keep the probes which were mapped to the genomic coordinates of mRNAs uniquely. Second, we use the arithmetic mean to integrate the values of multiple probes mapping to the same mRNAs. Then, we identified 17434 PCGs in the dataset.

3.2. Selection of Flavoproteins and Interacting Protein Combinations for the Prognostic Signature in the Training Dataset. The experimental process is shown in Figure 1(a). We extracted 162 flavoproteins and 1133 interacting proteins from the protein database. The ESCC patient cohort with 179 patients of ESCC was downloaded from the GEO database (GSE53625) and was used to explore the correlation between 1295 flavoproteins and their corresponding interacting proteins. Firstly, the univariate Cox proportional hazards regression analysis identified a flavoprotein family set composed of 6 flavoproteins and 47 interacting proteins, which were associated with overall survival ($P < 0.05$), to serve as prognostic genes. Secondly, ten genes most related to the prognostic classification were selected among the flavoprotein family set according to the permutation importance score by using random survival forests variable hunting (RSFVH) algorithm (Figure 1(b)).

We compared the risk-score model of $2^{10}-1=1023$ combinations of the flavoprotein set by the ROC curve to elect a better prediction prognostic signature. All the risk scores of the flavoprotein signature are described in the Materials and Methods section. Then, the flavoprotein signature with the max AUC is selected. The signature was composed of two flavoprotein genes (GPD2 and PYROXD2) and four flavoprotein interacting protein genes (CTTN, GGH, SRC, and SYNJ2BP), and the risk score was obtained as follows: risk score = $(-0.77 \times \text{expression level of GPD2}) + (0.28 \times \text{expression level PYROXD2}) + (0.33 \times \text{expression level of CTTN}) + (-0.39 \times \text{expression level of GGH}) + (0.54 \times \text{expression level of SRC}) + (0.48 \times \text{expression level of SYNJ2BP})$. AUC of the flavoprotein signature in the prognostic model was 0.76 for survival status (Figure 1(c), Table 3), and time ROC analysis showed that AUC of the signature is 0.710 (95% CI: 0.643–0.822) at 3 years, 0.759 (95% CI: 0.696–0.822) at 4 years, 0.767 (95% CI: 0.697–0.836) at 5 years, and 0.857 (95% CI: 0.813–0.900) at 6 years (Figure 1(d)).

3.3. The Flavoprotein Signature Could Predict ESCC Patients' Survival in Training Dataset and Independent Validation Datasets. By using the median risk score of the flavoprotein signature as the cutoff point, 179 ESCC patients of the training dataset were divided into the high-risk group ($n=90$) and low-risk group ($n=89$). The high-risk group had a significantly shorter OS than the low-risk group ($P < 0.001$, mean survival time: 26.77 months vs. 54.97 months; Figure 1(e)).

To confirm the findings described above, we also evaluated the efficiency of the constructed expression-defined flavoprotein prognostic model in independent validation datasets ($n=121$). The same flavoprotein model was used to calculate the flavoprotein signature-based risk scores for 121 patients in this dataset. Figure 1(f) shows the Kaplan–Meier curves of the model in the validation datasets ($P = 0.032$, mean survival time: 15.73 months vs. 21.1 months).

3.4. Knocking Down the Flavoprotein Signature Components in ESCC Cell Lines Affects Cell Migration and Growth. To assess the effect of the flavoprotein signature expression in ESCC cells, siRNAs targeting the flavoprotein signature genes were transfected into KYSE510 cells and KYSE150 cells, and the silencing of the flavoprotein signature was determined by qRT-PCR. Figure 2(a) shows that the relative mRNA expression of the flavoprotein signature in KYSE150 cells and KYSE510 cells in the si-flavoprotein signature group was lower than the si-negative control (NC) group ($P < 0.01$). Colony formation assay showed that knockdown of the flavoprotein signature genes significantly inhibited the growth of KYSE150 cells and KYSE510 cells (Figure 2(b)). Compared with the siNC group, ESCC cell growth in the si-flavoprotein signature group was generally suppressed ($P < 0.0001$, one-way ANOVA). Migration of ESCC cells was examined in each group by wound healing and transwell assays. As shown in Figures 3 and 4, siRNA-mediated knockdown of CTTN, GGH, GPD2, PYROXD2, SRC, or SYNJ2BP in KYSE150 cells and KYSE510 cells conferred reduced migration, compared with the siNC group ($P < 0.01$, one-way ANOVA). However, six genes in the flavoprotein signature produce different degrees of effect on ESCC cell proliferation and migration. And six genes also play different roles in KYSE150 and KYSE510 cells. After knocking down the PYROXD2 gene in KYSE150 cells, the cell proliferation ability was most significantly reduced ($P < 0.0001$, one-way ANOVA), while wound healing and transwell assay showed that knockdown of the PYROXD2 gene in KYSE150 cells had the least effect on cell migration compared to other genes ($P < 0.01$, one-way ANOVA). In KYSE510 cells, the significant effect of inhibiting cell proliferation is knocking down the SYNJ2BP gene ($P < 0.0001$, one-way ANOVA). In KYSE150 and KYSE510 cells, the effect of GGH on cell proliferation was minimal compared to other genes ($P < 0.01$, one-way ANOVA). However, after knockdown of GGH, wound healing and transwell assay showed that the GGH gene has a great influence on the mobility of ESCC cells ($P < 0.0001$, one-way ANOVA). These results

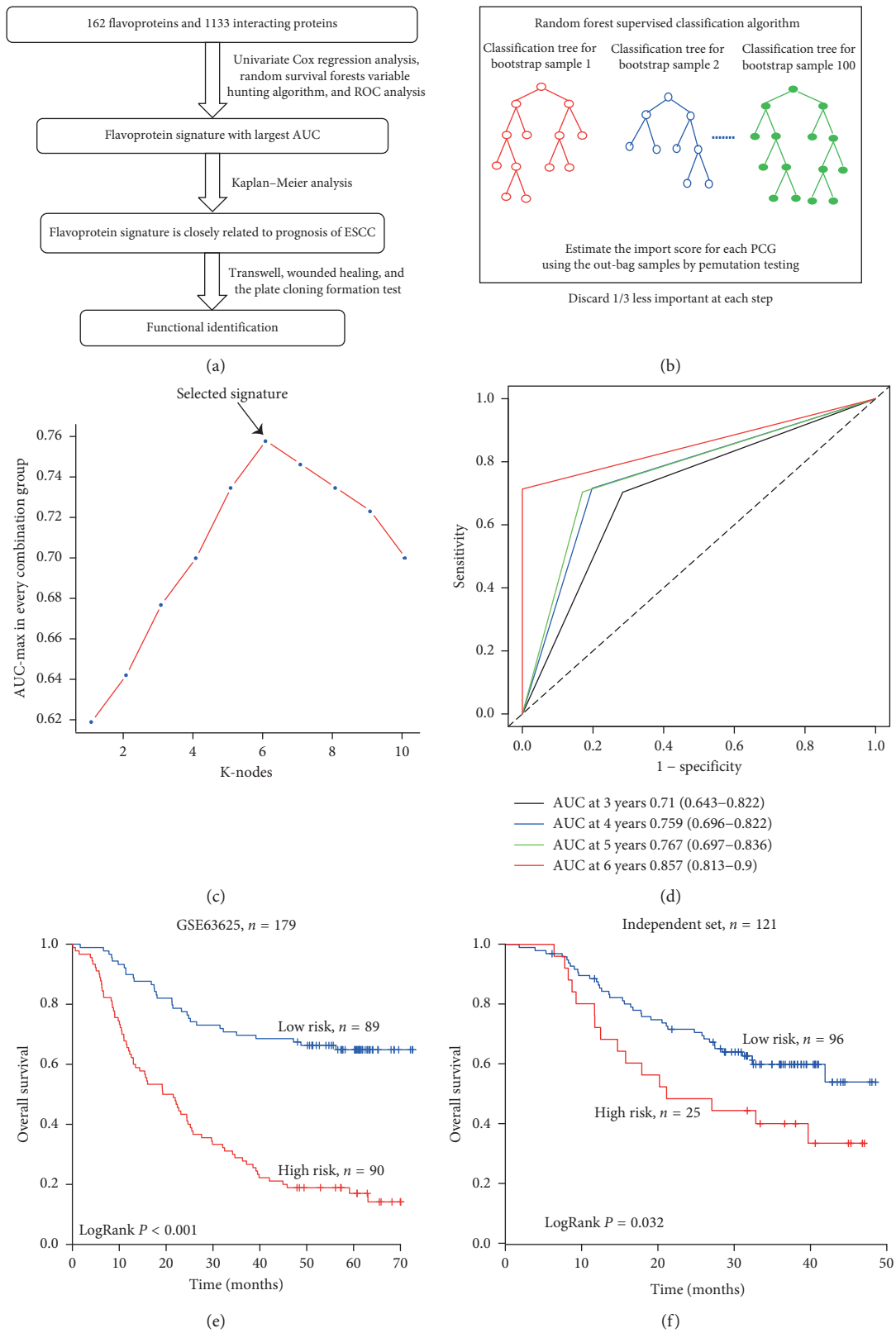


FIGURE 1: Identification of a flavoprotein signature predictive of overall survival of patients with ESCC. (a) Schematic diagram of the study. (b) Random forest supervised classification algorithm. (c) Procedure for identifying the final signature. The accuracies of all 1023 signatures were calculated, and the nine highest accuracies for $k = 1, 2, \dots, 10$ are shown in the plot and ROC for the flavoprotein signature prognostic model in the training dataset. (d) Time-dependent ROC for the flavoprotein signature prognostic model at 3–6 years in the training dataset. (e, f) Kaplan–Meier survival curves of patients classified into high- and low-risk groups, using the flavoprotein signature in the training and independent validation datasets. P values were calculated by the log-rank test.

TABLE 3: Identities of flavoproteins and their interacting proteins in the prognostic expression signature and their univariate Cox association with prognosis.

Ensembl ID	Gene symbol	Gene description	Coefficient ^a	P value ^a	Gene expression level association with prognosis	Chromosome location
ENSG00000115159	GPD2	Glycerol-3-phosphate dehydrogenase 2	-0.77	0.01	Low	2:156435290-156613735:1
ENSG00000119943	PYROXD2	Pyridine nucleotide-disulphide oxidoreductase domain 2	0.28	0.00	High	10:98383565-98415184:-1
ENSG00000085733	CTTN	Cortactin	0.33	0.00	High	11:70398404-70436584:1
ENSG00000137563	GGH	Gamma-glutamyl hydrolase	-0.39	0.01	Low	8:63015079-63039171:-1
ENSG00000197122	SRC	Non-receptor tyrosine kinase	0.54	0.02	High	20:37344685-37406050:1
ENSG00000213463	SYNJ2BP	Synaptojanin 2 binding protein	0.48	0.02	High	14:70366496-70417061:-1

^aDerived from the univariable Cox regression analysis in the training set.

imply that the flavoprotein signature plays important but different roles in the progression of ESCC.

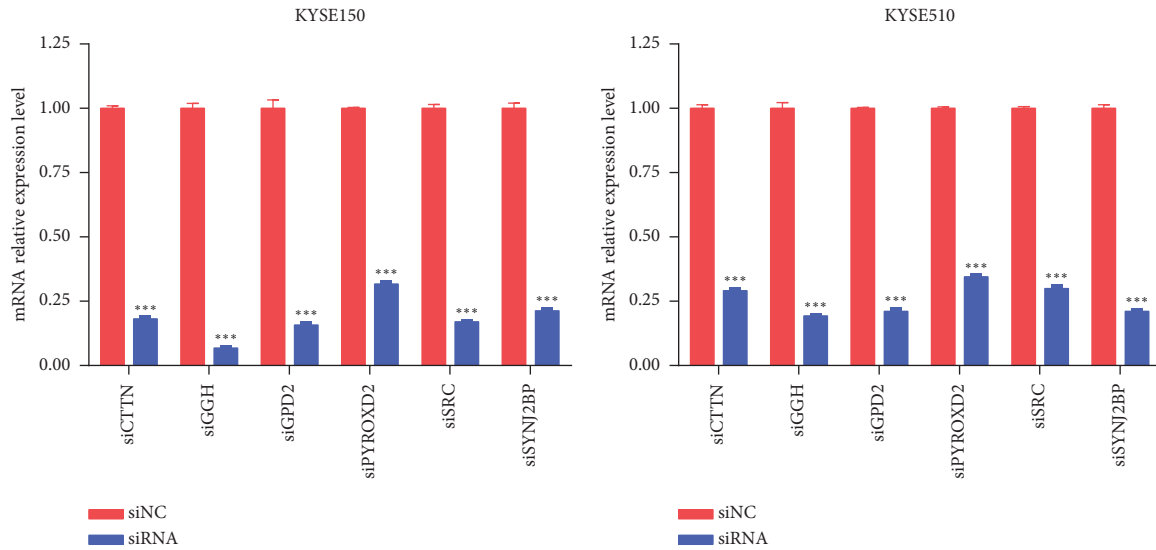
3.5. Functional Characterization of the Flavoprotein Signature. To further explore the potential biological function of this signature, we compared the gene expression profiles of ESCC patients classified as high-risk and low-risk by the flavoprotein signature in the training set (GSE53625). The gene sets with significantly different expression (FDR < 0.05) between high-risk and low-risk were selected for gene set enrichment analysis (GSEA). Several clusters of genes functionally related to more than 150 GO terms and 20 KEGG pathways were observed. These data suggest that the flavoprotein signature might affect tumorigenesis and development through interacting with many important biological processes, such as epithelial mesenchymal transition, focal adhesion, oxidative phosphorylation, and long chain fatty acid metabolism (Figure 5).

4. Discussion

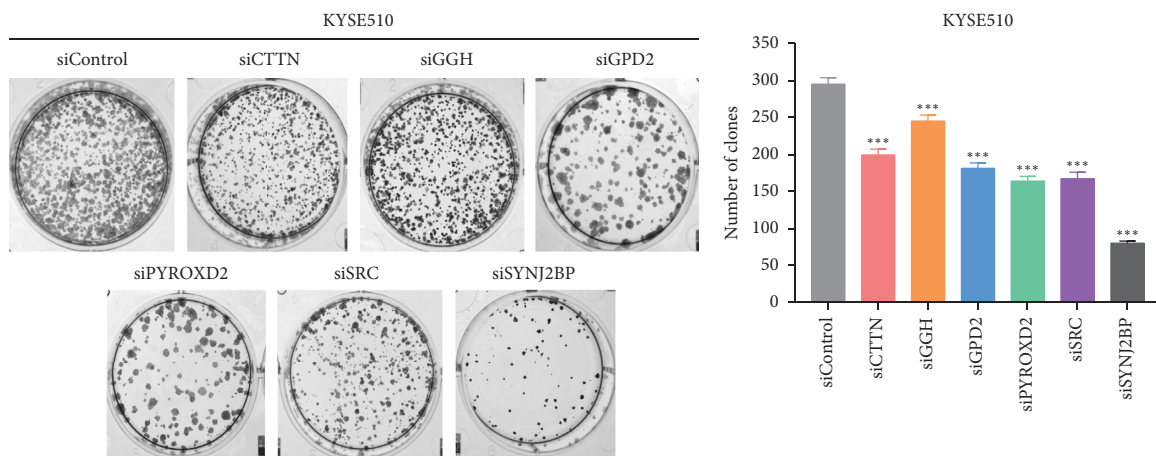
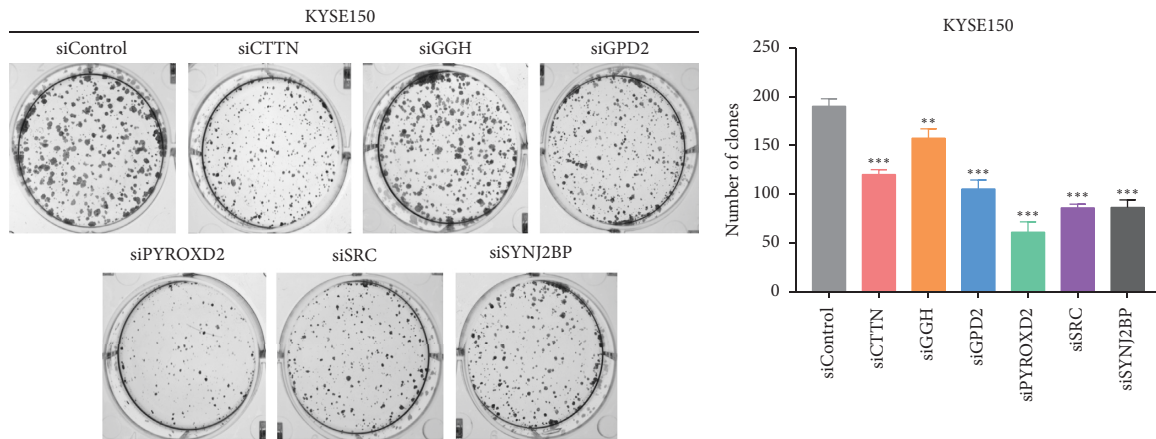
Esophageal cancer is the fifth most common and fourth most lethal malignant tumor in China [1]. Currently, the therapeutic efficacy of treatment is quite limited, with patients exhibiting a low five-year incidence of survival. In recent years, many reports have used gene arrays to analyze the gene expression profiles and predict prognostic signature in esophageal cancer. So far, however, there are no clinical predictive markers specific to the early diagnosis of ESCC. Therefore, the identification and validation of new novel biomarkers have vital significance in the diagnosis and treatment of esophageal cancer. Increasing evidences indicate that flavoproteins and their interacting proteins are involved in tumorigenesis and may serve as potential biomarkers [32, 33]. In this paper, we explored the clinical significance of flavoproteins (GPD2 and PYROXD2) and their interacting proteins (CTTN, GGH, SRC, and SYNJ2BP). The signature composed of six members is not

only involved in proliferation and migration of ESCC cells but also related with OS of ESCC patients. Furthermore, the combination of CTTN, GGH, GPD2, PYROXD2, SRC, and SYNJ2BP can accurately predict the prognosis of ESCC patients, with accuracies for predicting 6-year OS for ESCC patients (AUC = 0.857, 95% CI: 0.813–0.9). The signature composed of flavoproteins and their interacting proteins shows prognostic power in ESCC patients.

In this study, we used different statistics and machine learning methods to identify an expression signature, involving flavoproteins and their interacting proteins, that is associated with survival of ESCC patients. The six genes CTTN, GGH, GPD2, PYROXD2, SRC, and SYNJ2BP with the largest AUC were selected as the flavoprotein signature. CTTN and SRC are two of the most studied oncogenes. SRC is a non-receptor protein tyrosine kinase that is activated following engagement of many different classes of cellular receptors [34]. CTTN is a major substrate of the SRC tyrosine kinase and contributes to the organization of the actin cytoskeleton and cell shape [35]. CTTN and SRC have been implicated in cell proliferation, motility, and invasion in various types of cancer, such as esophageal cancer, colorectal cancer, laryngeal carcinoma, and lung cancer [36–41]. GPD2 and PYROXD2 are both flavoproteins that contain non-covalently bound FAD as cofactor. In later years, researchers found GPD2 is the target gene for many diseases, such as febrile seizures, nonspecific mental retardation, and diabetes [42–44]. Moreover, a study in Canada suggested that GPD2 can be a target for cancer therapeutics [45]. PYROXD2 is pyridine nucleotide-disulfide oxidoreductase domain 2 with oxidoreductase activity [46]. Montoliu et al. confirmed the effect of PYROXD2 polymorphisms on trimethylamine metabolism [47]. Hong et al. found that PYROXD2 can be a target gene for prostate cancer [48]. GGH plays an important role in the metabolism of pteroylpolyglutamates and antifolates [49]. Many reports have shown that GGH is involved in the ERG-negative prostate cancer and gastric cancer development by multiple methods [50, 51]. SYNJ2BP regulates endocytosis of activin type 2 receptor kinases through



(a)



(b)

FIGURE 2: Knockdown of the flavoprotein signature inhibits proliferation of ESCC cells. (a) siRNA-mediated knockdown of the flavoprotein signature was examined by using qRT-PCR. β -Actin served as the loading control. Negative control (NC) siRNA or siRNA targeting the flavoprotein signature (siRNA) was transfected into KYSE150 cells and KYSE510 cells. * $P < 0.05$, ** $P < 0.01$, *** $P < 0.001$, Student's t test. (b). Clone formation images and number of clones. Cell proliferation was determined in colony formation assays in which 2000 transfected cells were inoculated in each well of a six-well plate. Cultures were maintained for 2 weeks, and cells were then fixed, stained, and photographed. Each experiment was performed in triplicate, and results represent the mean \pm SD of three experiments. * $P < 0.05$, ** $P < 0.01$, *** $P < 0.001$, one-way ANOVA.

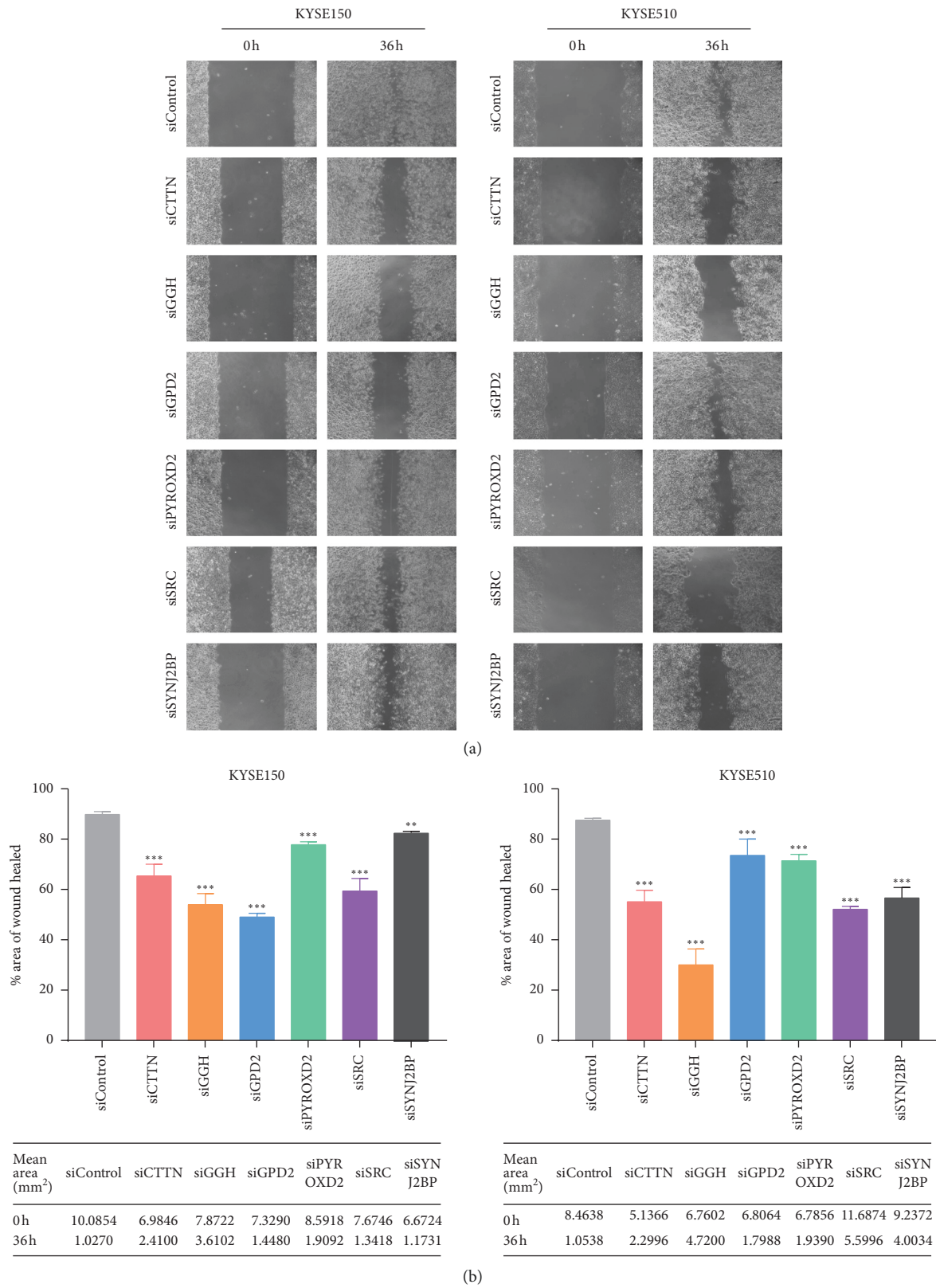


FIGURE 3: Knockdown of flavoprotein signature components reduces cell migration in a wound healing assay. (a). Wound healing images in KYSE150 and KYSE510 cells. (b) Top: rate of wound closure of KYSE150 and KYSE510 cells following transfection of siRNA and siNC. For quantification, the cells were counted in 6 random fields under a light microscope ($\times 400$). Data represent the mean \pm SD of triplicate. * $P < 0.05$, ** $P < 0.01$, *** $P < 0.001$, one-way ANOVA. Bottom: mean wound area (mm²) at 0 hours and 36 hours.

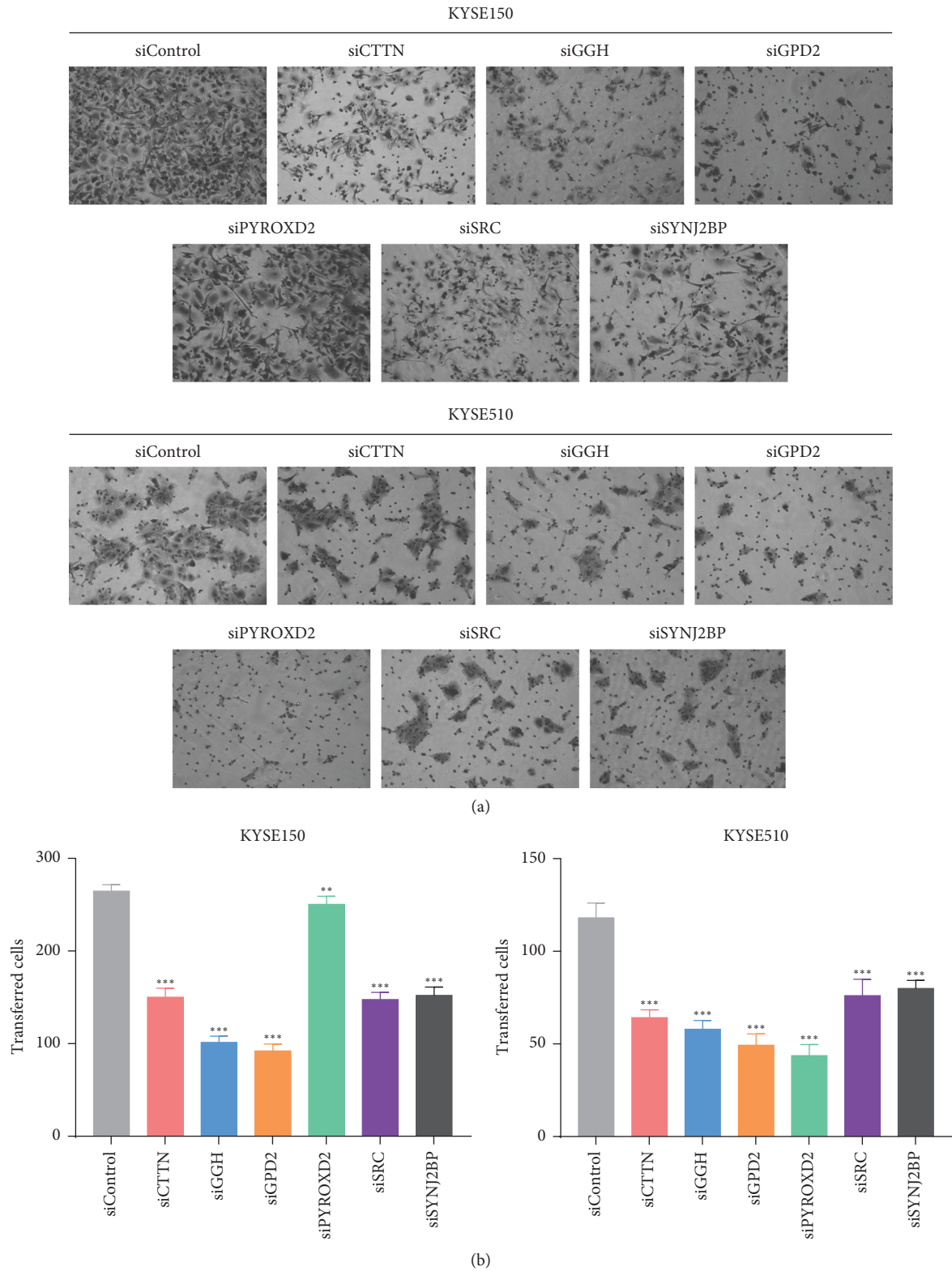


FIGURE 4: Knockdown of flavoprotein signature components reduces cell migration in a transwell assay. (a) Migratory images of KYSE150 and KYSE510 cells. (b) A transwell assay was used to determine the effects of siRNA-mediated knockdown of flavoprotein signature components on cell migration. Migrating cells were fixed and stained, and representative fields were photographed. For quantification, cells were counted in 10 random fields under a light microscope ($\times 400$). Data represent mean \pm SD of triplicate. * $P < 0.05$, ** $P < 0.01$, *** $P < 0.001$; one-way ANOVA.

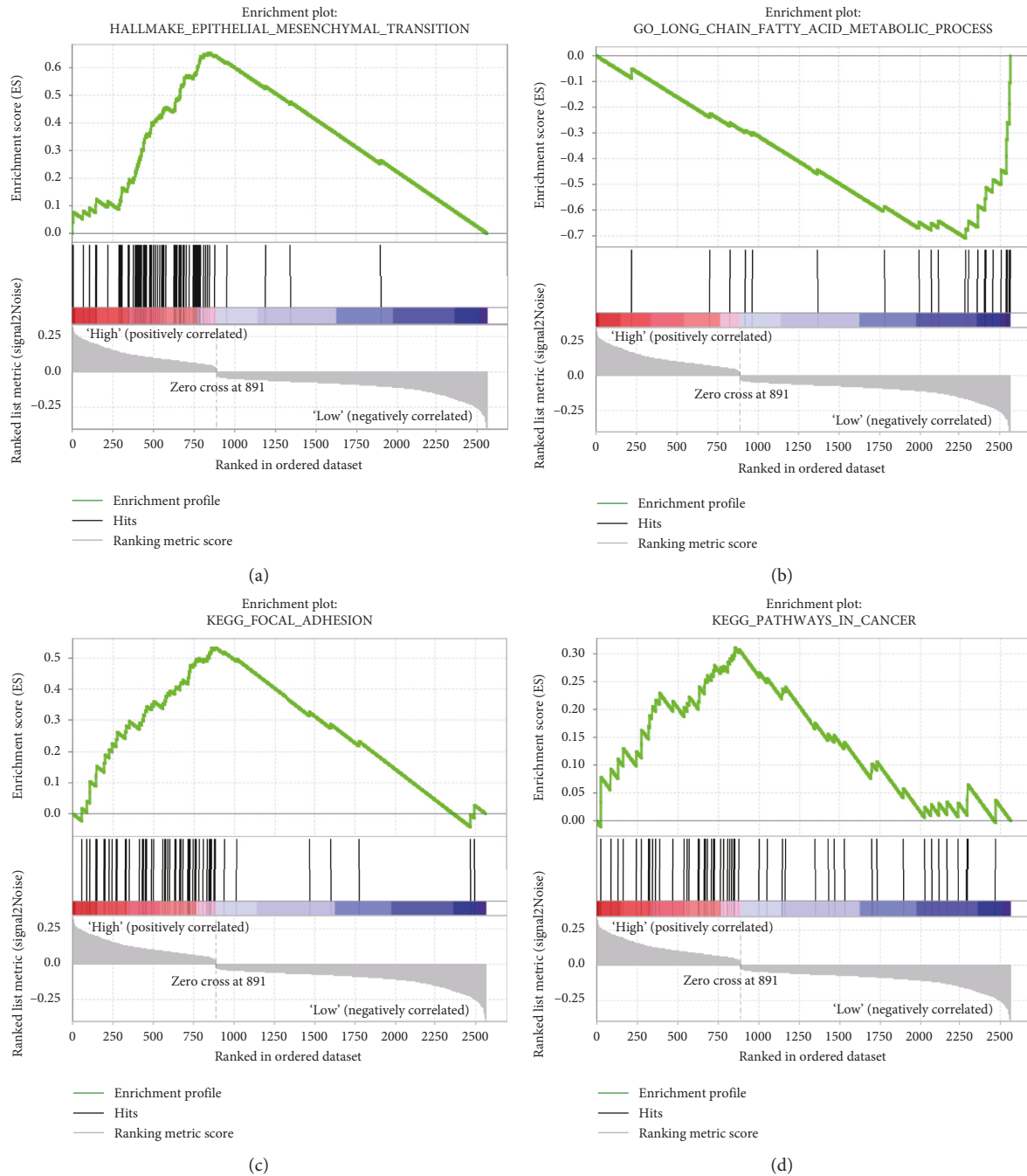


FIGURE 5: Predicting the function of genes in the signature. Gene set enrichment analysis (GSEA) showed that the flavoprotein signature was significantly associated with EMT pathways and long chain fatty acid metabolism (a, b). Two KEGG pathways (focal adhesion and cancer-related pathways) were significantly enriched in the enriched gene sets (c, d) ($P < 0.05$, $FDR < 0.05$).

the Ral/RALBP1-dependent pathway. Liu et al. confirmed that SYNJ2BP influences tumor growth and metastasis by activating the DLL4 pathway in hepatocellular carcinoma [52]. SYNJ2BP also plays an important role in breast cancer and renal cell carcinoma metastasis [53, 54]. Although a series of previous articles have revealed the potential value of flavoproteins and their interacting proteins in cancer prognosis prediction, such as CTTN, SRC, and GPD2, using

the combination of flavoproteins and their interacting proteins in predicting ESCC prognosis has not been elucidated clearly. Here, we analyzed the mRNA expression profiles of patients with ESCC downloaded from GEO and applied the RSFVH algorithm and ROC to pick out flavoproteins and their interacting proteins and reduce the high dimension. Next, we identified a signature including several flavoproteins and their interacting proteins, which

are strongly associated with the overall survival. Then, we constructed time-dependent ROC curves to assess the sensitivity and specificity of variables and calculated the corresponding AUC.

Functionally, we knocked down the flavoprotein signature by transfecting siRNA into ESCC cells. Next, the functionally well-defined CTTN and SRC were used as positive controls to compare the effect of the remaining four genes on proliferation and migration of transfected ESCC cells. Similar to knockdown of CTTN and SRC, ESCC cell growth and motility are significantly reduced following knockdown of GGH, GPD2, PYROXD2, and SYNJ2BP. Among these genes, GPD2 knockdown has the most significant effect on inhibiting the proliferation and migration of ESCC cells. The GPD2 gene encodes the mitochondrial glycerol-3-phosphate dehydrogenase, which is localized to the outer surface of the inner mitochondrial membrane. Mitochondrial glycerol-3-phosphate dehydrogenase, as a component of the glycerophosphate shuttle, functions at the crossroads of glycolysis, oxidative phosphorylation, and fatty acid metabolism. Mitochondrial glycerol-3-phosphate dehydrogenase regulates both the glycerol-3-phosphate and malate-aspartate shuttles, which play important roles in tumor metabolism [55–58]. GSEA analyses also suggest that the flavoprotein signature mainly affects the function of tumor cells by affecting metabolic pathways. The precise role played by GPD2 in ESCC needs further study. This study still has many limitations. For example, we only studied the flavoprotein signature as a whole, but we did not learn the mechanism of one or several genes. In addition, our study only stayed at the RNA level, but not at the protein level. Other aspects will be considered in future research.

In summary, this is the first study to investigate a signature, comprised of flavoproteins and their interacting proteins, in patients with esophageal squamous cell carcinoma. Furthermore, abnormal expression of the flavoprotein signature promotes proliferation and migration of ESCC cells. These results implicate components of the flavoprotein signature as efficient prognostic markers and potential targets in gene therapy for ESCC.

Abbreviations

AUC:	Area under the curve
CI:	Confidence interval
CTTN:	Cortactin
ESCC:	Esophageal squamous cell carcinoma
GEO:	Gene Expression Omnibus
GGH:	Gamma-glutamyl hydrolase
GO:	Gene ontology
GPD2:	Glycerol-3-phosphate dehydrogenase 2
HR:	Hazard ratio
KEGG:	Kyoto Encyclopedia of Genes and Genomes
OS:	Overall survival
PCG:	Protein coding gene
PYROXD2:	Pyridine nucleotide-disulphide oxidoreductase domain 2

ROC:	Receiver operating characteristic
SD:	Standard deviation
SRC:	Non-receptor tyrosine kinase
SYNJ2BP:	Synaptojanin 2 binding protein.

Data Availability

No data were used to support this study.

Conflicts of Interest

The authors declare that there are no conflicts of interest.

Authors' Contributions

Liu Peng and Jin-Cheng Guo contributed equally to this study. Liu Peng and Jin-Cheng Guo were responsible for data collection, data analysis, interpretation, and drafting. Lin Long and Feng Pan performed qRT-PCR analysis of ESCC samples. Jian-Mei Zhao provided technical support for bioinformatics. En-Min Li and Li-Yan Xu were responsible for study design and study supervision. All authors read and approved the final manuscript.

Acknowledgments

The authors thank Dr. Stanley Li Lin from the Department of Cell Biology and Genetics of Shantou University Medical College for assistance in revising the manuscript. This study was supported by the Natural Science Foundation of China-Guangdong Joint Fund (grant nos. U1301227 and U1601229) and the National Science Foundation of China (grant nos. 81472613 and 81772532).

References

- [1] W. Chen, R. Zheng, P. D. Baade et al., "Cancer statistics in China, 2015," *CA: A Cancer Journal for Clinicians*, vol. 66, no. 2, pp. 115–132, 2016.
- [2] L. A. Torre, F. Bray, R. L. Siegel, J. Ferlay, J. Lortet-Tieulent, and A. Jemal, "Global cancer statistics, 2012," *CA: A Cancer Journal for Clinicians*, vol. 65, no. 2, pp. 87–108, 2015.
- [3] J.-J. Xie, J.-C. Guo, Z.-Y. Wu et al., "Integrin $\alpha 5$ promotes tumor progression and is an independent unfavorable prognostic factor in esophageal squamous cell carcinoma," *Human Pathology*, vol. 48, pp. 69–75, 2016.
- [4] S.-S. Li, Y.-W. Xu, J.-Y. Wu et al., "Plasma riboflavin level is associated with risk, relapse, and survival of esophageal squamous cell carcinoma," *Nutrition and Cancer*, vol. 69, no. 1, pp. 21–28, 2017.
- [5] S. Ghisla and V. Massey, "Mechanisms of flavoprotein-catalyzed reactions," *European Journal of Biochemistry*, vol. 181, no. 1, pp. 1–17, 1989.
- [6] D. J. Stuehr, H. J. Cho, N. S. Kwon, M. F. Weise, and C. F. Nathan, "Purification and characterization of the cytokine-induced macrophage nitric oxide synthase: an FAD- and FMN-containing flavoprotein," *Proceedings of the National Academy of Sciences*, vol. 88, no. 17, pp. 7773–7777, 1991.
- [7] M. Eli, D.-S. Li, W.-W. Zhang et al., "Decreased blood riboflavin levels are correlated with defective expression of

- RFT2gene in gastric cancer,” *World Journal of Gastroenterology*, vol. 18, no. 24, pp. 3112–3118, 2012.
- [8] J. K. Bassett, G. Severi, A. M. Hodge et al., “Dietary intake of B vitamins and methionine and colorectal cancer risk,” *Nutrition and Cancer*, vol. 65, no. 5, pp. 659–667, 2013.
- [9] H.-t. Yang, P.-c. Chao, and M.-c. Yin, “Riboflavin at high doses enhances lung cancer cell proliferation, invasion, and migration,” *Journal of Food Science*, vol. 78, no. 2, pp. H343–H349, 2013.
- [10] J. K. Bassett, A. M. Hodge, D. R. English, R. J. MacInnis, and G. G. Giles, “Plasma phospholipids fatty acids, dietary fatty acids, and breast cancer risk,” *Cancer Causes & Control*, vol. 27, no. 6, pp. 759–773, 2016.
- [11] F. Siassi and P. Ghadirian, “Riboflavin deficiency and esophageal cancer: a case control-household study in the Caspian Littoral of Iran,” *Cancer Detection and Prevention*, vol. 29, no. 5, pp. 464–469, 2005.
- [12] F. B. Straub, “Isolation and properties of a flavoprotein from heart muscle tissue,” *Biochemical Journal*, vol. 33, no. 5, pp. 787–792, 1939.
- [13] W. P. Dijkman, G. De Gonzalo, A. Mattevi, and M. W. Fraaije, “Flavoprotein oxidases: classification and applications,” *Applied Microbiology and Biotechnology*, vol. 97, no. 12, pp. 5177–5188, 2013.
- [14] M. Medina, P. Ferreira, and M. Martinez-Julvez, “Editorial (hot topic: flavoproteins and flavoenzymes with biomedical and therapeutic impact),” *Current Pharmaceutical Design*, vol. 19, no. 14, pp. 2497–2498, 2013.
- [15] P. Chaiyen and N. S. Scrutton, “Special issue: flavins and flavoproteins,” *The FEBS Journal*, vol. 282, no. 16, pp. 3001–3002, 2015.
- [16] R. M. Buey, J. B. Arellano, L. López-Maury et al., “Unprecedented pathway of reducing equivalents in a diflavin-linked disulfide oxidoreductase,” *Proceedings of the National Academy of Sciences*, vol. 114, no. 48, pp. 12725–12730, 2017.
- [17] J.-C. Guo, C.-Q. Li, Q.-Y. Wang et al., “Protein-coding genes combined with long non-coding RNAs predict prognosis in esophageal squamous cell carcinoma patients as a novel clinical multi-dimensional signature,” *Molecular BioSystems*, vol. 12, no. 11, pp. 3467–3477, 2016.
- [18] J. Li, Z. Chen, L. Tian et al., “LncRNA profile study reveals a three-lncRNA signature associated with the survival of patients with esophageal squamous cell carcinoma,” *Gut*, vol. 63, no. 11, pp. 1700–1710, 2014.
- [19] J. C. Guo, Y. Wu, Y. Chen et al., “Protein-coding genes combined with long noncoding RNA as a novel transcriptome molecular staging model to predict the survival of patients with esophageal squamous cell carcinoma,” *Cancer Communications*, vol. 38, no. 1, p. 4, 2018.
- [20] U. B. Mogensen, H. Ishwaran, and T. A. Gerds, “Evaluating random forests for survival analysis using prediction error curves,” *Journal of Statistical Software*, vol. 50, no. 11, pp. 1–23, 2012.
- [21] H. Ishwaran and M. Lu, “Standard errors and confidence intervals for variable importance in random forest regression, classification, and survival,” *Statistics in Medicine*, vol. 38, no. 3, pp. 558–582, 2018.
- [22] H. H. Cao, S. Y. Zhang, J. H. Shen et al., “A three-protein signature and clinical outcome in esophageal squamous cell carcinoma,” *Oncotarget*, vol. 6, no. 7, pp. 5435–5448, 2015.
- [23] S.-Y. Gao, E.-M. Li, L. Cui et al., “Sp1 and AP-1 regulate expression of the human GeneVIL2in esophageal carcinoma cells,” *Journal of Biological Chemistry*, vol. 284, no. 12, pp. 7995–8004, 2009.
- [24] X. D. Zhang, J. J. Xie, L. D. Liao et al., “12-O-Tetradecanoylphorbol-13-Acetate induces up-regulated transcription of variant 1 but not variant 2 of VIL2 in esophageal squamous cell carcinoma cells via ERK1/2/AP-1/sp1 signaling,” *PLoS One*, vol. 10, no. 4, Article ID e0124680, 2015.
- [25] J.-C. Guo, Y.-M. Xie, L.-Q. Ran et al., “L1CAM drives oncogenicity in esophageal squamous cell carcinoma by stimulation of ezrin transcription,” *Journal of Molecular Medicine*, vol. 95, no. 12, pp. 1355–1368, 2017.
- [26] X.-D. Zhang, G.-W. Huang, Y.-H. Xie et al., “The interaction of lncRNA EZR-AS1 with SMYD3 maintains overexpression of EZR in ESCC cells,” *Nucleic Acids Research*, vol. 46, no. 4, pp. 1793–1809, 2018.
- [27] L. Long, X.-X. Pang, F. Lei et al., “SLC52A3 expression is activated by NF-kappaB p65/Rel-B and serves as a prognostic biomarker in esophageal cancer,” *Cellular and Molecular Life Sciences*, vol. 75, no. 14, pp. 2643–2661, 2018.
- [28] F.-M. Zeng, X.-N. Wang, H.-S. Shi et al., “Fascin phosphorylation sites combine to regulate esophageal squamous cancer cell behavior,” *Amino Acids*, vol. 49, no. 5, pp. 943–955, 2017.
- [29] R. L. Camp, M. Dolled-Filhart, and D. L. Rimm, “X-tile: a new bio-informatics tool for biomarker assessment and outcome-based cut-point optimization,” *Clinical Cancer Research*, vol. 10, no. 21, pp. 7252–7259, 2004.
- [30] J.-C. Guo, S.-S. Fang, Y. Wu et al., “CNIT: a fast and accurate web tool for identifying protein-coding and long non-coding transcripts based on intrinsic sequence composition,” *Nucleic Acids Research*, vol. 47, no. W1, pp. W516–W522, 2019.
- [31] A. Subramanian, P. Tamayo, V. K. Mootha et al., “Gene set enrichment analysis: a knowledge-based approach for interpreting genome-wide expression profiles,” *Proceedings of the National Academy of Sciences*, vol. 102, no. 43, pp. 15545–15550, 2005.
- [32] D. J. Stuehr, J. Tejero, and M. M. Haque, “Structural and mechanistic aspects of flavoproteins: electron transfer through the nitric oxide synthase flavoprotein domain,” *FEBS Journal*, vol. 276, no. 15, pp. 3959–3974, 2009.
- [33] E. Jortzik, L. Wang, J. Ma, and K. Becker, “Flavins and flavoproteins: applications in medicine,” in *Methods in Molecular Biology*, vol. 1146, pp. 113–157, Springer, Berlin, Germany, 2014.
- [34] A. B. Reynolds, S. B. Kanner, A. H. Bouton et al., “SRChing for the substrates of Src,” *Oncogene*, vol. 33, no. 37, pp. 4537–4547, 2014.
- [35] V. Martini, C. Gattazzo, F. Frezzato et al., “Cortactin, a Lyn substrate, is a checkpoint molecule at the intersection of BCR and CXCR4 signalling pathway in chronic lymphocytic leukaemia cells,” *British Journal of Haematology*, vol. 178, no. 1, pp. 81–93, 2017.
- [36] M.-L. Luo, X.-M. Shen, Y. Zhang et al., “Amplification and overexpression of CTTN (EMS1) contribute to the metastasis of esophageal squamous cell carcinoma by promoting cell migration and anoikis resistance,” *Cancer Research*, vol. 66, no. 24, pp. 11690–11699, 2006.
- [37] A. M. Weaver, “Cortactin in tumor invasiveness,” *Cancer Letters*, vol. 265, no. 2, pp. 157–166, 2008.
- [38] D. Jia, Y. Jing, Z. Zhang et al., “Amplification of MPZL1/PZR promotes tumor cell migration through Src-mediated phosphorylation of cortactin in hepatocellular carcinoma,” *Cell Research*, vol. 24, no. 2, pp. 204–217, 2014.
- [39] Y. Song, Y.-d. Dong, W.-l. Bai, and X.-l. Ma, “Silencing of Src by siRNA inhibits laryngeal carcinoma growth through the

- Src/PI-3 K/Akt pathway in vitro and in vivo," *Tumor Biology*, vol. 35, no. 9, pp. 9009–9014, 2014.
- [40] F.-P. Xu, Y.-H. Liu, X.-L. Luo et al., "Overexpression of SRC-3 promotes esophageal squamous cell carcinoma aggressiveness by enhancing cell growth and invasiveness," *Cancer Medicine*, vol. 5, no. 12, pp. 3500–3511, 2016.
- [41] X. Zhang, K. Liu, T. Zhang et al., "Cortactin promotes colorectal cancer cell proliferation by activating the EGFR-MAPK pathway," *Oncotarget*, vol. 8, no. 1, pp. 1541–1554, 2017.
- [42] G. Koike, P. V. Vooren, M. Shiozawa et al., "Genetic mapping and chromosome localization of the rat mitochondrial glycerol-3-phosphate dehydrogenase gene, a candidate for non-insulin-dependent diabetes mellitus," *Genomics*, vol. 38, no. 1, pp. 96–99, 1996.
- [43] H. Daoud, N. Gruchy, J.-M. Constans et al., "Haploinsufficiency of the GPD2 gene in a patient with non-syndromic mental retardation," *Human Genetics*, vol. 124, no. 6, pp. 649–658, 2009.
- [44] E. V. S. Hessel, H. A. van Lith, I. G. Wolterink-Donselaar et al., "Mapping of aFEB3homologous febrile seizure locus on mouse chromosome 2 containing candidate genesScn1aandScn3a," *European Journal of Neuroscience*, vol. 44, no. 11, pp. 2950–2957, 2016.
- [45] G. Singh, "Mitochondrial FAD-linked glycerol-3-phosphate dehydrogenase: a target for cancer therapeutics," *Pharmaceuticals*, vol. 7, no. 2, pp. 192–206, 2014.
- [46] G. Nicholson, M. Rantalainen, J. V. Li et al., "A genome-wide metabolic QTL analysis in Europeans implicates two loci shaped by recent positive selection," *PLoS Genetics*, vol. 7, no. 9, Article ID e1002270, 2011.
- [47] I. Montoliu, U. Genick, M. Ledda et al., "Current status on genome-metabolome-wide associations: an opportunity in nutrition research," *Genes & Nutrition*, vol. 8, no. 1, pp. 19–27, 2013.
- [48] M.-G. Hong, R. Karlsson, P. K. E. Magnusson et al., "A genome-wide assessment of variability in human serum metabolism," *Human Mutation*, vol. 34, no. 3, pp. 515–524, 2013.
- [49] M. Jin, K. Kawakami, Y. Fukui et al., "Different histological types of non-small cell lung cancer have distinct folate and DNA methylation levels," *Cancer Science*, vol. 100, no. 12, pp. 2325–2330, 2009.
- [50] N. Melling, M. Rashed, C. Schroeder et al., "High-level gamma-glutamyl-hydrolase (GGH) expression is linked to poor prognosis in ERG negative prostate cancer," *International Journal of Molecular Sciences*, vol. 18, no. 2, p. 286, 2017.
- [51] M. Terashima, W. Ichikawa, A. Ochiai et al., "TOP2A, GGH, and PECAM1 are associated with hematogenous, lymph node, and peritoneal recurrence in stage II/III gastric cancer patients enrolled in the ACTS-GC study," *Oncotarget*, vol. 8, no. 34, pp. 57574–57582, 2017.
- [52] X. Liu, J. Zhou, N. Zhou, J. Zhu, Y. Feng, X. Miao et al., "SYNJ2BP inhibits tumor growth and metastasis by activating DLL4 pathway in hepatocellular carcinoma," *Journal of Experimental & Clinical Cancer Research*, vol. 35, no. 1, p. 115, 2016.
- [53] G. C. Brito, Â. A. Fachel, A. L. Vettore et al., "Identification of protein-coding and intronic noncoding RNAs down-regulated in clear cell renal carcinoma," *Molecular Carcinogenesis*, vol. 47, no. 10, pp. 757–767, 2008.
- [54] M. Wang, H. Wu, S. Li et al., "SYNJ2BP promotes the degradation of PTEN through the lysosome-pathway and enhances breast tumor metastasis via PI3K/AKT/SNAI1 signaling," *Oncotarget*, vol. 8, no. 52, pp. 89692–89706, 2017.
- [55] M. Kaneko, M. Kurokawa, and S. Ishibashi, "Binding and function of mitochondrial glycerol kinase in comparison with those of mitochondrial hexokinase," *Archives of Biochemistry and Biophysics*, vol. 237, no. 1, pp. 135–141, 1985.
- [56] P. Kugler, "Microphotometric determination of enzymes in brain sections," *Histochemistry*, vol. 93, no. 5, pp. 537–540, 1990.
- [57] R. Ansell, K. Granath, S. Hohmann, J. M. Thevelein, and L. Adler, "The two isoenzymes for yeast NAD⁺-dependent glycerol 3-phosphate dehydrogenase encoded byGPD1 and GPD2have distinct roles in osmoadaptation and redox regulation," *The EMBO Journal*, vol. 16, no. 9, pp. 2179–2187, 1997.
- [58] T. Mráček, Z. Drahota, and J. Houštěk, "The function and the role of the mitochondrial glycerol-3-phosphate dehydrogenase in mammalian tissues," *Biochimica et Biophysica Acta (BBA) - Bioenergetics*, vol. 1827, no. 3, pp. 401–410, 2013.

Research Article

Spica Prunellae Extract Enhances Fluorouracil Sensitivity of 5-Fluorouracil-Resistant Human Colon Carcinoma HCT-8/5-FU Cells via TOP2 α and miR-494

Yi Fang ^{1,2}, Chi Yang,³ Ling Zhang,^{1,2} Lihui Wei,^{1,2} Jiumao Lin ^{1,2}, Jinyan Zhao,^{1,2} and Jun Peng ^{1,2}

¹Academy of Integrative Medicine, Fujian University of Traditional Chinese Medicine, Fuzhou 350122, China

²Fujian Key Laboratory of Integrative Medicine on Geriatrics, Fujian University of Traditional Chinese Medicine, Fuzhou 350122, China

³Institute of Edible Fungi, Fujian Academy of Agricultural Sciences, Fuzhou 350003, China

Correspondence should be addressed to Jun Peng; pjunlab@hotmail.com

Received 10 May 2019; Revised 12 July 2019; Accepted 9 August 2019; Published 30 September 2019

Guest Editor: Amal El-Naggar

Copyright © 2019 Yi Fang et al. This is an open access article distributed under the Creative Commons Attribution License, which permits unrestricted use, distribution, and reproduction in any medium, provided the original work is properly cited.

The use of 5-fluorouracil (5-FU) has been proven benefits, but it also has adverse events in colorectal cancer (CRC) chemotherapy. In this study, we explored the mechanism of 5-FU resistance by bioinformatics analysis of the NCBI public dataset series GSE81005. Fifteen hub genes were screened out of 582 different expressed genes. Modules of the hub genes in protein-protein interaction networks gathered to TOP2 α showed a decrease in HCT-8 cells but an increase in 5-FU-resistant HCT-8/5-FU cells with 5-FU exposure. Downregulation of TOP2 α with siRNA or miR-494 transfection resulted in an increase of cytotoxicity and decrease of cell colonies to 5-FU for HCT-8/5-FU cells. Moreover, we found that an ethanol extract of Spica Prunellae (EESP), which is a traditional Chinese medicine with clinically beneficial effects in various cancers, was able to enhance the sensitivity of 5-FU in HCT-8/5-FU cells and partly reverse the 5-FU resistance effect. It significantly helped suppress cell growth and induced cell apoptosis in HCT-8/5-FU cells with the expression of TOP2 α being significantly suppressed, which increased by 5-FU. Consistently, miR-494, which reportedly regulates TOP2 α , exhibited reverse trends in EESP/5-FU combination treatment. These results suggested that Spica Prunellae may be beneficial in the treatment of 5-FU-resistant CRC patients.

1. Introduction

Colorectal cancer (CRC, also known as colon cancer) is one of the most commonly diagnosed cancers. The GLOBOCAN 2018 data estimates of cancer incidence and mortality showed that CRC is the third most commonly diagnosed cancer, with an incidence of 10.2% and a mortality of 9.2% [1]. Presently, the treatment for CRC includes surgery, radiation, and chemotherapy palliative care [2]. Chemotherapy drugs for the treatment of CRC include capecitabine, oxaliplatin, fluorouracil (5-FU), leucovorin (folinic acid), and irinotecan. Among these chemotherapy agents, 5-FU is most commonly used for CRC [3]. Treatment with 5-FU has been shown to reduce tumor size by approximately 50% in patients with advanced CRC and prolong their median

survival by 5 months [4]. However, since the late 1990s, studies have revealed that 5-FU treatment can lead to therapy resistance [5, 6] accompanied by hand-foot syndrome, cardiotoxicity [7], and gastrointestinal side effects [3]. Therefore, combination chemotherapy has become widely used in chemotherapeutic regimens [8]. Nevertheless, this therapeutic strategy might be partly beneficial; however, problems, such as new chemotherapeutic resistance or unacceptable side effects, can still occur. Therefore, explored of the resistance mechanism for 5-FU would benefit for searching the new safe and acceptable resistance-reversal medications.

In this case, natural products have great advantages because they have relatively fewer adverse effects. Herbal medicines applied to chemotherapy could improve chemotherapeutic

efficacy and/or reduce induced toxicities in patients [9]. In addition, our previous studies have demonstrated that some herbal medicines suppressed cell growth, induced cell apoptosis, inhibited CRC angiogenesis, and overcame 5-FU resistance [10–12]. Therefore, herbal extracts might be feasible to increase chemotherapeutic efficacy and reduce the possibility of drug resistance and side effects.

Prunella vulgaris L. is a widely distributed perennial herb in the family Lamiaceae. In China, the spike of this herb, Spica Prunellae, is well known as a traditional Chinese medicine for its effects on heat clearing, dispersing swelling, and dissipating binds [13]. The herb has been reported to promote cancer cell apoptosis [14] and to suppress cell growth [15], vascular inflammation [16], tumor angiogenesis [17], and tumor volume [14, 18]; it has also been used in the treatment of cancers, such as breast cancer [19]. Recently, as a novel herbal medicine, LA16001, which is composed of *Prunella vulgaris* L., was found to prevent cisplatin-induced anorexia [20]. Extracts from other Lamiaceae plants, such as rosemary (*Rosmarinus officinalis*), have been shown to enhance the antitumor effect of 5-FU in 5-FU-resistant SW620-5FU-R cells [21]. Both *Rosmarinus officinalis* and *Prunella vulgaris* L. belong to the Labiatae family, and their marker compound is rosmarinic acid [22, 23], which has been shown to exhibit antioxidant [24], anti-inflammatory [25], and anticancer activities [26].

The aim of this study was to understand the resistance mechanism for 5-FU in depth and provide a clue for the searching of effective medications. Through bioinformatics analysis, DNA topoisomerase 2- α (TOP II α , TOP2 α) was important in the 5-FU resistance. Moreover, we found it was involved in the 5-FU sensitivity enhancement of EESP. In the fact, Spica Prunellae was suggested as a potential reversal agent for treating 5-FU-resistant patients. In addition, searching for medications which could down-regulate TOP2 α expression would be a benefit clue for the therapy of 5-FU-resistant patients.

2. Materials and Methods

2.1. Identification of Key Genes Associated with 5-FU Sensitivity. We chose a public and freely available gene expression profile (GSE81005) from the US NCBI Gene Expression Omnibus database to screen differentially expressed genes between HCT-8/5-FU and HCT-8 cells treated following 5-FU treatment. We searched for differentially expressed genes firstly by comparing data between the treatment of 5-FU for 24/48 h in HCT-8/5-FU cells or HCT-8 cells and control groups, secondly comparing the differentially expressed genes between HCT-8/5-FU cells and HCT-8 cells, and thirdly obtaining the DEGs by searching the common DEGs between 24 h and 48 h treatment. DEGs were detected by the R (3.4.1) software. The adjusted *P* values were used to reduce the false-positive rate by using the Benjamini and Hochberg false discovery rate method by default. An adjusted *P* value of <0.05 was set as the cutoff criterion. Metascape was used to conduct pathway and process enrichment analysis of the DEGs using default settings [27]. STRING was employed to map the DEGs,

which could detect the potential relationship among those DEGs. A maximum number of interactors=0 and a confidence score ≥ 0.4 were set as the cutoff criteria. The Molecular Complex Detection (MCODE) app in Cytoscape was used further to screen modules in the PPI network with a cutoff=2, *k*-core=2, node score cutoff=0.2, and max. depth=100. Expression patterns of TOP2A in colon adenocarcinoma cancer and normal tissues were demonstrated by the available data from gene expression profiling interactive analysis (GEPIA) and R2 (<https://hgserver1.amc.nl/cgi-bin/r2/main.cgi?&species=hs>), which is a free publicly accessible web-based genomics analysis and visualization platform.

2.2. Transfection of siRNA or miR-494. siRNA and its siRNA control (Genepharma, Shanghai, China) or miR-494 mimics and miRNA negative control (Guangzhou RiboBio Co., LTD, Guangzhou, China) were synthesized. Cells were plated in 96 or 6 wells, and they were transfected with siRNA or miR-494 mimics at 50 nM at 30%–40% cell confluence following the instruction of Lipofectamine RNAiMAX (Thermo Fisher Scientific Inc., MA, USA). Then, cell viability was detected by performing a 3-(4,5-dimethylthiazol-2-yl)-2,5-diphenyltetrazolium bromide colorimetric assay (ELX800; BioTek, Winooski, USA) at 570 nm each day, or cells were collected for the western blot or gene expression validation in 48 h.

2.3. Western Blot. Proteins were extracted into RIPA buffer (CW BIO, Beijing, China), separated in 10% sodium dodecyl sulfate-polyacrylamide gel electrophoresis, and then transferred to 0.22 μ m NC membranes (Millipore, MA, USA). The membranes were blocked and probed with antibodies against TOP2 α , β -actin, and the anti-rabbit IgG, HRP-linked antibody (Proteintech Group, Inc., Taiwan, China). The bands were detected with BeyoECL Plus (Beyotime Institute of Biotechnology, Shanghai, China) or Super ECL Star (US Everbright Inc., Suzhou, China). Image Lab Software (Bio-Rad, Hercules, CA, USA) was used to analyze the band intensity.

2.4. Gene Expression Validation. Total RNA was extracted with TRIzol (Takara, Dalian, China). Then, a nanodrop spectrophotometer (Thermo Fisher Scientific Inc., MA, USA) was used to assess the RNA quantity and quality. TOP2A primers for examination by real-time polymerase chain reaction (PCR) were designed from NCBI/Primer-BLAST, and GAPDH primers were obtained from PrimerBank (<https://pga.mgh.harvard.edu/primerbank/>). The miRNA primers were obtained from (General Biosystems, NC, USA). Reverse transcriptase- (RT-) PCR was performed for miRNA examination by Mir-X™ miRNA First Strand Synthesis according to the SYBR® qRT-PCR User Manual (Takara, Dalian, China) and for mRNA detection by using a PrimeScript™ RT reagent Kit. Real-time PCR was outperformed by using a TB Green™ Premix Ex Taq™ II (Takara, Dalian, China) for miRNA and a SYBR™ Select Master Mix (Life Technologies,

Shanghai, China). The 2- $\Delta\Delta$ Ct method was used to analyze the expression levels.

2.5. EESP Stock Solution Preparation and Cell Culture. EESP stock solution was prepared as previously described [15]. Human carcinoma HCT-8 cells and HCT-8/5-FU cells (KeyGEN Biotech, Nanjing, China) were cultured at 37°C in a humidified incubator with 5% CO₂ in RPMI medium 1640 (KeyGEN Biotech, Nanjing, China) supplemented with 10% FBS (Hyclone, Carlsbad, USA), 100 U/mL of penicillin, and 100 μ g/mL of streptomycin (Life Technologies, Shanghai, China). HCT-8/5-FU cells were cultured in the above-mentioned medium with the addition of 15 μ g/mL of 5-FU (Shanghai Amino Acids Company, Shanghai, China).

2.6. Reversal Effect Assays. Two cell lines were seeded into 96-well plates at a density of 1×10^4 cells/well. After 24 h, the cells were treated following various concentrations of EESP, 5-FU, or EESP plus 5-FU combination for 48 h. Then, the cell viabilities were evaluated. SPSS 16.0 software was used to calculate the cell survival rate and IC₅₀ value. The resistance index (RI) of HCT-8/5-FU cells to EESP or 5-FU, reversal fold (RF), and relative reversal rate (RRR%) were calculated according to the following formulas:

$$RI = IC_{50} \text{ of HCT-8/5-FU cells (EESP or 5-FU)} / IC_{50} \text{ of HCT-8 cells (EESP or 5-FU)}$$

$$RF = IC_{50} \text{ of HCT-8/5-FU cells (5-FU)} / IC_{50} \text{ of HCT-8/5-FU cells (EESP + 5-FU)}$$

$$RRR\% = (IC_{50} \text{ of HCT-8/5-FU cells (5-FU)} - IC_{50} \text{ of HCT-8/5-FU cells (5-FU + EESP)}) / IC_{50} \text{ of HCT-8/5-FU cells (5-FU)} - IC_{50} \text{ of HCT-8 cells (5-FU)}$$

2.7. Colony Formation. The HCT-8 and HCT-8/5-FU cells were seeded into 6-well plates at a density of 4×10^5 cells/well. After transfection or treatment with 5-FU (3.2 mM) with/without EESP (0.25 mg/mL or 0.5 mg/mL) or EESP (0.25 mg/mL or 0.5 mg/mL) for 48 h, the cells were harvested and reseeded into fresh 12-well plates at a density of 500 cells/well. With 2 weeks of maintenance in RPMI medium 1640 supplemented with 10% FBS, penicillin, and streptomycin, the formed colonies were fixed with 4% polyoxymethylene and stained with 0.01% crystal violet.

2.8. Apoptosis Detection. After treatment with 5-FU (3.2 mM) and with/without EESP (0.25 mg/mL or 0.5 mg/mL) or EESP (0.25 mg/mL or 0.5 mg/mL) for 48 h in 6-well plates, apoptosis of cells was detected by using an AnnexinV-FITC Apoptosis Detection Kit (KeyGEN Biotech, Nanjing, China), as described in a previous study [15].

2.9. Statistical Analysis. Data are presented as the mean \pm SD. The statistical significance of differences was assessed by Student's *t*-test or one-way ANOVA in SPSS 16.0 software. The level of statistical significance was set to * $P < 0.05$, ** $P < 0.01$, and *** $P < 0.001$.

3. Results

3.1. Identification of DEGs and Hub Genes. The potential molecular mechanisms were studied by searching for DEGs and hub genes. R (3.4.1) software was applied to detect DEGs in the US National Center for Biotechnology Information Gene Expression Omnibus GSE81005 dataset. Since the main difference between HCT-8/5-FU cells and HCT-8 cells was the 5-FU sensitivity, we analyzed hub genes during 5-FU intervention. We identified 1478 and 2316 DEGs in 5-FU treatment for 24 h and 48 h, respectively. We identified 582 DEGs in both the 24 h and 48 h 5-FU treatment groups. DEGs were functional and pathway enrichment analyzed using online tools in Metascape (<http://metascape.org/>), and the top 20 enrichment items were shown. As shown in Figures 1(a) and 1(b), the upregulated DEGs were enriched in brain development, mitotic prometaphase, cofactor metabolic process, etc., while the downregulated DEGs were enriched in PID P53 downstream pathway, cellular response to extracellular stimulus, negative regulation of cell proliferation, etc. To determine the essential genes involved in the 5-FU associated mechanism, the top 15 hub genes with a high degree of connectivity were screened (see Table S1). Then, an associated PPI network was created on the basis of the information in the STRING database (Figure 1(c)). The top 2 modules were selected by MCODE to find the key modules in the PPI network. The results revealed that TOP2A was involved in both the modules (Figures 1(d) and 1(e)). This suggested that TOP2A might be a key gene for 5-FU resistance of colorectal cancer.

TOP2 α was involved in the enhancement of 5-FU sensitivity to HCT-8/5-FU.

As TOP2 α was involved in both the modules, we speculate that it should be important in 5-FU resistance. Firstly, the expression levels of TOP2 α were analyzed in a public database. Compared with normal tissues, the tumor samples appeared to have higher levels in the expression profiling of TOP2 α (Figures 2(a) and 2(b)). These results suggested that overexpression of TOP2 α might be a signal for tumor development. In view of this fact, we wondered if TOP2 α overexpression might also be associated with 5-FU resistance. The expression levels of TOP2 α between HCT-8 and HCT-8/5-FU cells exposed to 5-FU were compared. The results showed that TOP2 α was significantly downregulated in HCT-8 cell lines but was upregulated in HCT-8/5-FU cell lines (Figures 2(c), 2(d), and 2(e)). To further confirm the role of TOP2 α in 5-FU resistance, siRNA of TOP2 α and miR-494 which was reported to target TOP2 α [28] was used to knock down the expression of TOP2 α . The efficiency of siRNA was shown in Figure S1. Compared to the negative control, siRNA or miR-494 transfection enhanced the 5-FU sensitive and cytotoxicity for HCT-8/5-FU cells (Figures 2(f) and 2(g)). Their transfection could also increase the cytotoxicity for HCT-8/5-FU cells, and miR-494 enhanced the 5-FU sensitivity for HCT-8/5-FU cells (Figures 2(h)–2(j)). But there was no significant difference in siRNA groups in the presence of 5-FU. These results indicated that TOP2A was involved in 5-FU resistance.

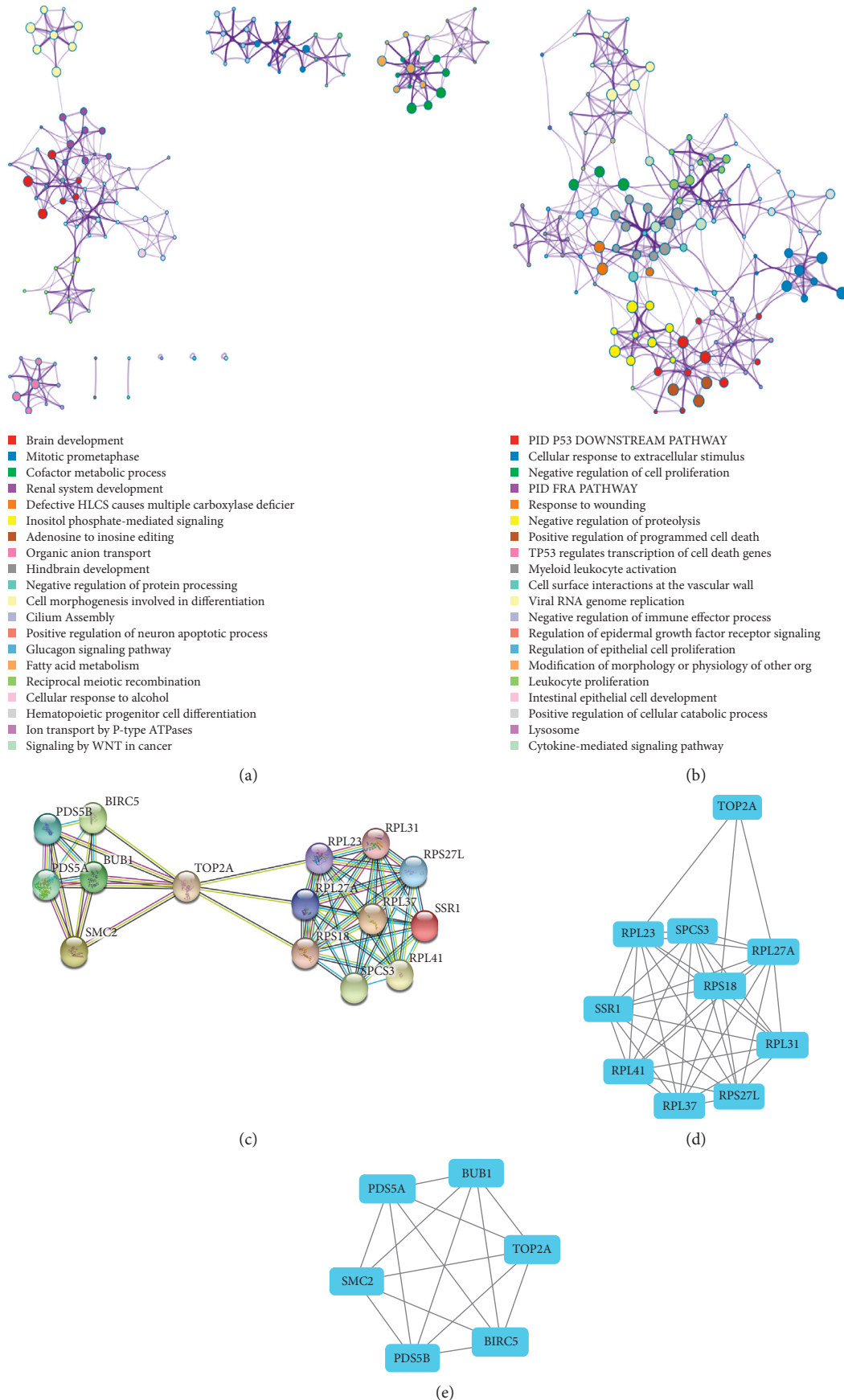


FIGURE 1: Identification of DEGs and hub genes. Enriched ontology clusters of (a) upregulated and (b) downregulated DEGs colored by cluster ID. (c) The PPI network of the top 15 hub genes. (d, e) Selection of the top 2 modules by using the MCODE plug-in to detect significant modules in this PPI network.

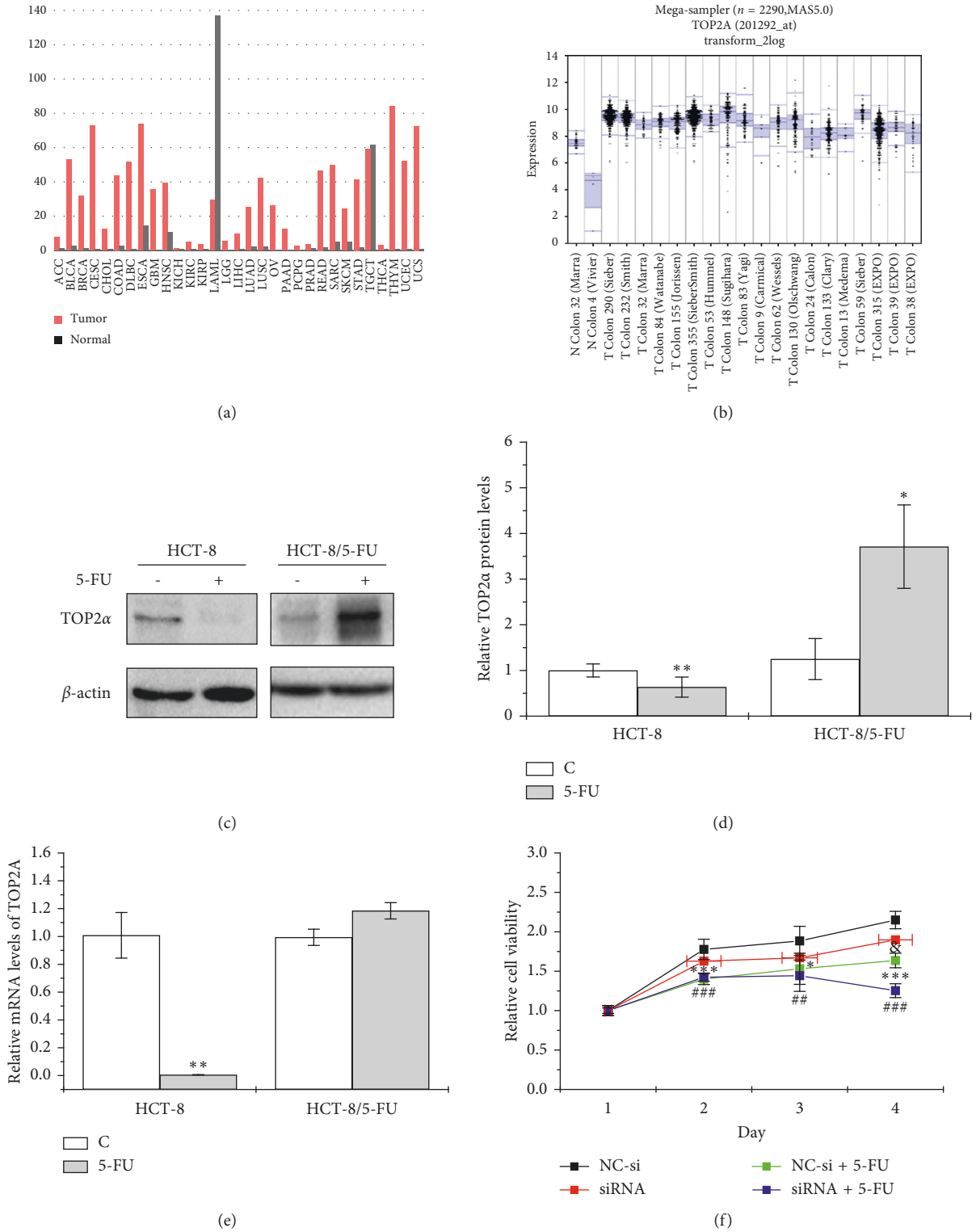


FIGURE 2: Continued.

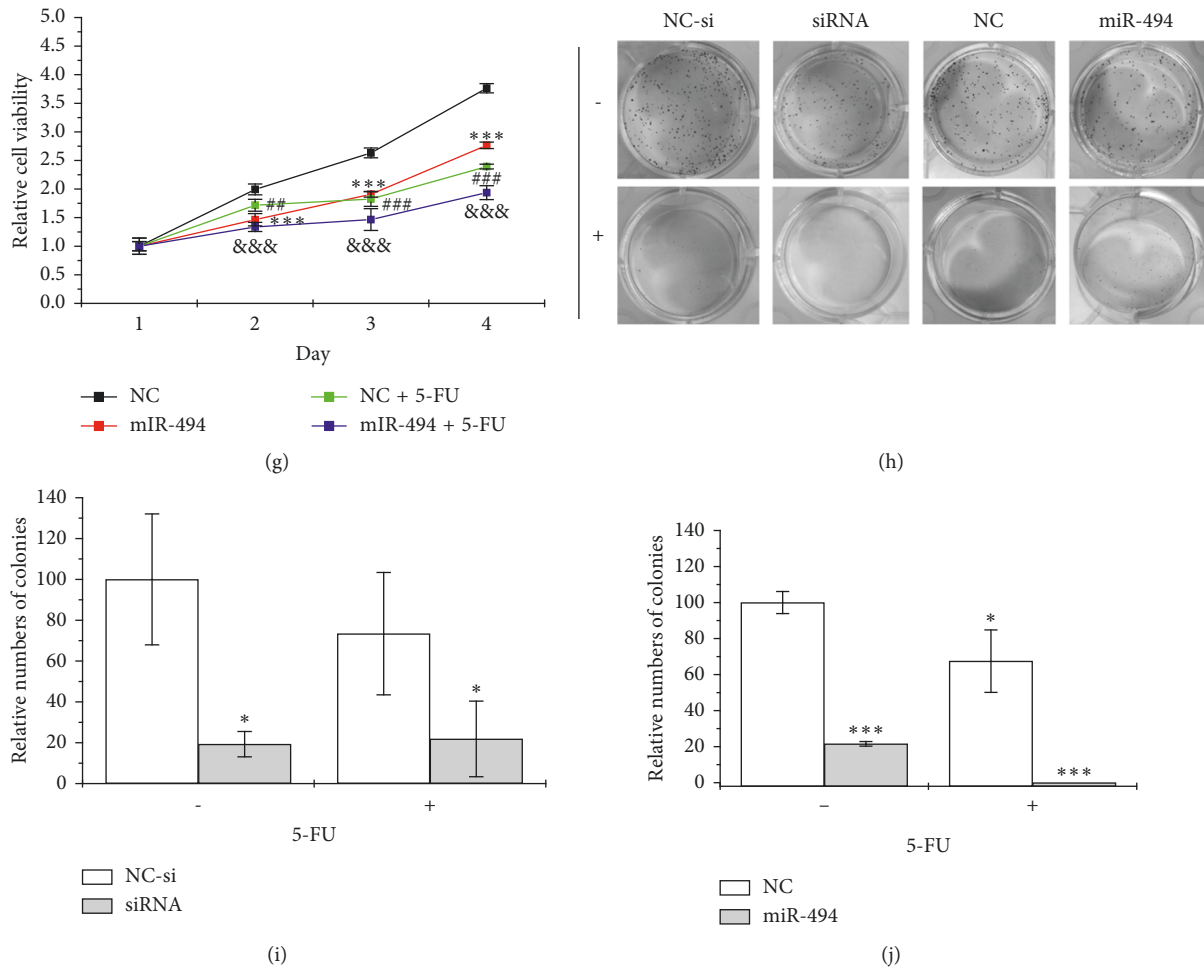


FIGURE 2: Overexpression of TOP2 α mediates the 5-FU resistance. (a, b) Analysis of TOP2 α expression levels in the GEPIA database and Mega-sampler in the TCGA database. (c) Detection of relative protein levels for HCT-8 and HCT-8/5-FU cells treated with or without 5-FU (3.2 mM) for 48 h by western blot and (d) quantification. (e) Real-time PCR evaluation of the mRNA levels of TOP2A. The data from western blot and real-time PCR are normalized to GADPH. Relative cell viability of HCT-8/5-FU cells transfected with (f) siRNA or (g) miR-494 and then treated with or without 5-FU (3.2 mM) for different time periods (1, 2, 3, and 4 days). (h) Cell colonies for HCT-8/5-FU cells transfected with siRNA or miR-494 and then treated with or without 5-FU (3.2 mM) for 48 h and (i, j) their relative numbers for cell colonies were analyzed. Compared with the negative control group, for siRNA or miR-494 transfection, * $P < 0.05$, ** $P < 0.01$, and *** $P < 0.001$; for negative control treatment with the 5-FU group (NC + 5-FU), # $P < 0.05$, ## $P < 0.01$, and ### $P < 0.001$; for siRNA or miR-494 transfection and treatment with the 5-FU group (NC + 5-FU), & $P < 0.05$, && $P < 0.01$, and &&& $P < 0.001$.

3.2. HCT-8/5-FU Cells Were Suitable for the Study of 5-FU Modulation with EESP. Given that the resistance index (RI) is a significant metric for evaluation of 5-FU-resistant cells to anticancer drugs, we examined the RI for EESP and 5-FU treatment. Compared with parental HCT-8 cells, HCT-8/5-FU cells showed a 257.4-fold increase in resistance to 5-FU and a 1.03-fold increase in resistance to EESP (Table 1). These results suggested that HCT-8/5-FU cells were resistant to 5-FU but not resistant to EESP; therefore, HCT-8/5-FU cells were suitable for the further study of 5-FU modulation with EESP.

3.3. Reversal Effect of EESP on 5-FU in HCT-8/5-FU Cells. For the evaluation of the reversal effect of EESP on 5-FU, two low concentrations of EESP (0.25 mg/mL and 0.5 mg/mL) with weakly cytotoxicity (inhibition rate < 20%) were chosen

TABLE 1: Inhibitory effects of EESP and 5-FU on HCT-8 and HCT-8/5-FU cells for 48 h ($n = 3$).

Cell line	^a IC ₅₀	
	EESP (mg/mL)	5-FU (mM)
HCT-8	0.77 ± 0.07	0.60 ± 0.13
HCT-8/5-FU	0.75 ± 0.09	154.46 ± 14.07
RI	1.03	257.40

^aIC₅₀ represents semi-inhibitory concentration of modulators.

according to the evaluation of cell cytotoxicity with 5-FU in MTT assays. The results showed that EESP increased the sensitivity of HCT-8/5-FU cells to 5-FU by 3.88-fold (at 0.25 mg/mL) and 20.68-fold (at 0.5 mg/mL), respectively (Table 2). The relative reversal rates for these 2 concentrations of EESP were 74.56% and 95.53%, respectively. These results demonstrated that the combination of EESP

with 5-FU increased the 5-FU sensitivity in HCT-8/5-FU drug-resistant cells although 0.25 mg/mL and 0.50 mg/mL of EESP combined separately with 5-FU each only partially reversed the effect of 5-FU.

3.4. EESP Enhanced 5-FU Cell Sensitivity in HCT-8/5-FU Cells via Cell Colony Formation Suppression and Cell Apoptosis Induction. To study the effects of EESP on the 5-FU sensitivity of colon carcinoma cells, 5-FU-resistant HCT-8/5-FU cells were treated at 0.25 mg/mL and 0.5 mg/mL of EESP separately with 5-FU at 3.2 mM or 0.25 mg/mL and 0.5 mg/mL of EESP alone for 48 h. There was no significant difference in the number of cell colonies between the 5-FU group and the control group. However, following treatment with 0.25 mg/mL and 0.5 mg/mL EESP combined with 5-FU, the number of cell colonies significantly decreased (Figures 3(a) and 3(c)). Furthermore, it was interesting that EESP in 0.25 mg/mL combined with 5-FU could enhance the suppression effect compared with 0.25 mg/mL of EESP alone groups. Similar results were also observed in the detection of cell apoptosis (Figures 3(b) and 3(d)). The combination of 5-FU with EESP in 0.5 mg/mL notably increased the apoptotic populations of HCT-8/5-FU cells relative to those in the 5-FU or EESP group. Results suggested that combination of EESP and 5-FU in low cytotoxicity concentration leads a better effect for enhancement of 5-FU sensitivity in HCT-8/5-FU cells. So in our following study, we chose to study its mechanism by EESP combined with 5-FU groups. These results together clearly implied that EESP enhanced 5-FU cell sensitivity in HCT-8/5-FU cells via suppression of cell colony formation and cell apoptosis induction.

3.5. EESP Enhanced 5-FU Sensitivity in HCT-8/5-FU by Downregulating the Expression of TOP2 α . Our results showed that EESP suppressed the expression of TOP2 α protein significantly, which increased by 3.2 mM of 5-FU (Figures 4(a) and 4(b)). Similar results were shown in the transcription level analysis (Figure 4(c)). Because TOP2 α was a downstream target for miR-494 [28], we decided to investigate its probable effects in the function of EESP. Levels of miR-494 were detected in HCT-8 and HCT-8/5-FU cells with or without 5-FU treatment. The expression level of miR-494 was increased following 3.2 mM 5-FU treatment in HCT-8 cells, but there was no difference in HCT-8/5-FU cells (Figure 4(d)). Furthermore, treatment with 0.5 mg/mL of EESP combined with 5-FU in HCT-8/5-FU cells significantly increased the levels of miR-494 (Figure 4(e)). In addition, combination with 5-FU seemed to enhance EESP effect for TOP2 α and miR-494 (Figure S2), which was consistent with the results of cell colonies depression. Taken together, the results suggested that EESP suppressed TOP2 α expression and promoted the levels of miR-494, which could partially reverse 5-FU resistance in HCT-8/5-FU cells.

4. Discussion

With the presence of 5-FU resistance, some chemical reversal molecules, such as bufalin [29], 2',4'-dihydroxy-6'-

TABLE 2: Potency of EESP in enhancing cytotoxicity of 5-FU in HCT-8/5-FU cells ($n = 3$).

Anticancer drugs	IC ₅₀	RF ^a	RRR% ^b
0.25 mg/mL EESP + 5-FU	49.46 ± 2.14	3.88	74.56
0.50 mg/mL EESP + 5-FU	7.47 ± 1.91	20.68	95.53

^aRF and ^bRRR% represent reversal effect of modulators. The greater the RF magnitude, the more significant the effect. When RRR% $\geq 100\%$, the modulator totally reversed the effect of 5-FU; when RRR% $< 100\%$, the modulator only partially reversed the effect of 5-FU.

methoxy-3',5'-dimethylchalcone [30], oroxylin A [31], schizandrin A [32], and tyroservatide [33], were studied in 5-FU-resistant cell lines. However, these chemical agents might be restricted in clinical applications because of the single mechanism, poor selectivity, or unacceptable side effects.

As a chemotherapy agent, 5-FU is an analog of uracil [34] that inhibits thymidylate synthase and incorporates into DNA and RNA as the 5-FU metabolites [34]. 5-FU induces cell apoptosis through p53. Moreover, its sensitivity has been correlated with membrane-associated proteins, such as MDR3, MDR4, and MAT-8 [35, 36]. In addition, a recent study demonstrated that genes in drug metabolism-cytochrome P450 and pyrimidine metabolic pathways with promoter hypermethylation and concordant expression were silenced in HCT-8/5-FU cells [37]. Among fifteen hub genes in the PPI network, nine of them were related to protein synthesis and protein translocation. They consisted of seven genes associated with ribosome function: 5 ribosome proteins (RPL23, RPL27A, RPL37, RPL31, and RPL41) and 2 ribosome binding proteins (RPS18 and RPS27L). And the other two were translocation-associated proteins: signal peptidase complex subunit 3 and signal sequence receptor subunit 1. There were also three DNA replication-associated proteins (DNA topoisomerase TOP2A and sister chromatid cohesion proteins PDS5A and PDS5B). The rest of them were mitotic checkpoint serine/threonine kinase 1 (*BUB1* gene) which participated in mitosis, chromosome condensation protein of structural maintenance of chromosomes protein 2 (*SMC-2* gene), or baculoviral IAP repeat-containing 5 (*BIRC5* gene). These genes indicated that DNA replication, protein synthesis, and protein translocation were active in 5-FU-resistant cells. Identifying the key protein might be a favorable way to reverse 5-FU resistance. In our study, TOP2 α was selected since it was involved in both the modules. Besides, it was also reported as a character in new induction of 5-FU-resistant cell lines for its level was always altered in 5-FU-resistant cancers [38]. Furthermore, the other two hub genes, RPL37 and RPL23, were identified in the expression profiling of the cDNA-based microarray in response to 5-FU in a breast cancer cell [36] though without subsequent validation. So we considered that other genes were still valuable for further research. Additionally, because the resistance mechanism of 5-FU is complex as noted above and Chinese medicine with multiple compounds always targets many pathways, we suspected that EESP might have a role through other genes or pathways associated with 5-FU resistance besides regulation of TOP2 α .

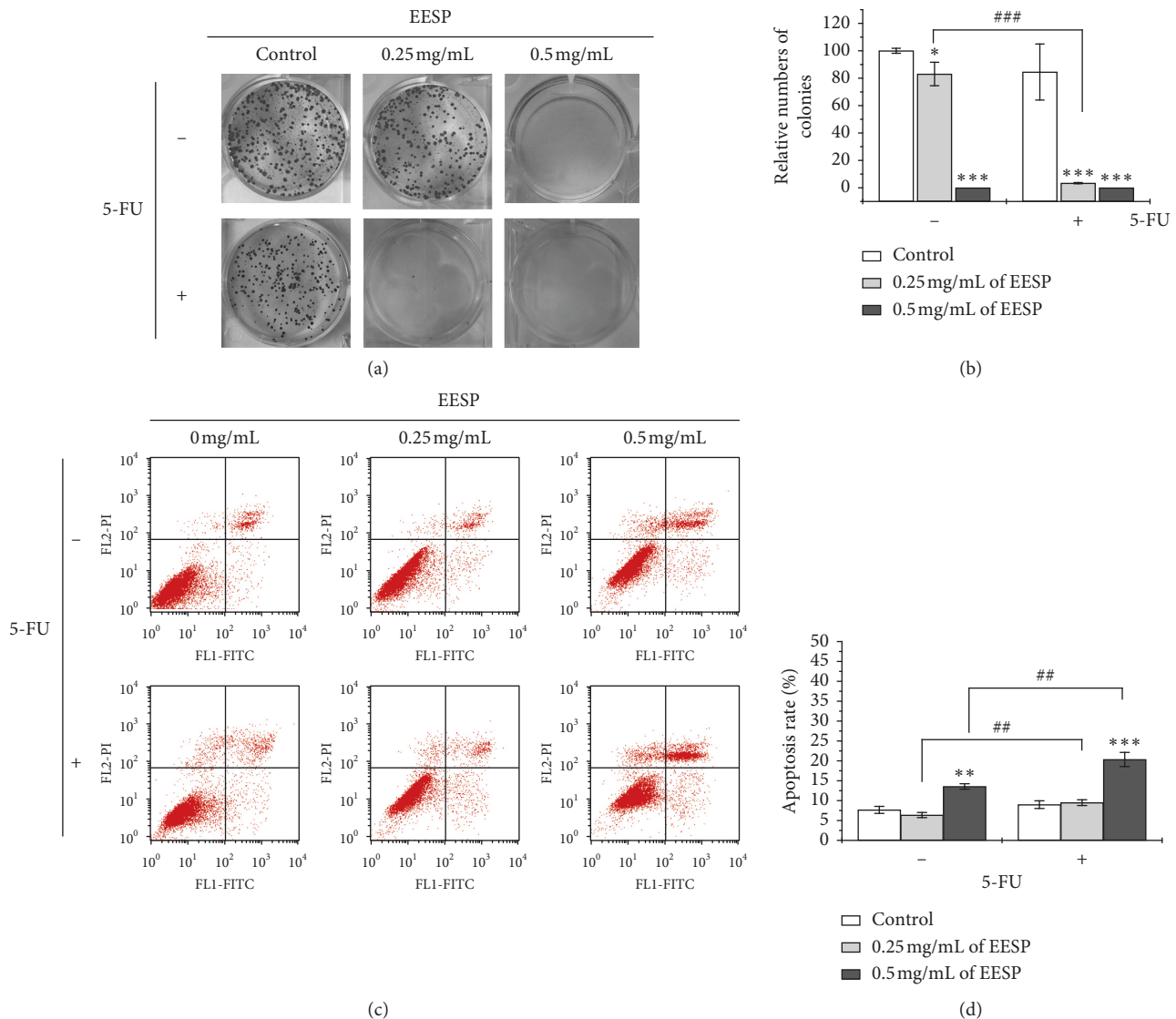


FIGURE 3: EESP combined with 5-FU suppressed the colony formation ability and induced apoptosis of HCT-8/5-FU cells. (a) After treatment with 5-FU (3.2 mM) with/without EESP (0.25 mg/mL or 0.5 mg/mL) or EESP (0.25 mg/mL or 0.5 mg/mL) for 48 h HCT-8/5-FU cells were fixed with methanol and stained with 0.01% crystal violet. (b) The numbers of colony formation were calculated from (a). (c) Treatment of HCT-8/5-FU cells with 5-FU (3.2 mM) with/without EESP (0.25 mg/mL or 0.5 mg/mL) or EESP (0.25 mg/mL or 0.5 mg/mL) for 48 h cell staining with annexin V/PI and analysis by using fluorescence-activated cell sorting. (d) Statistical analysis of the data from (c). Compared with the control group, * $P < 0.05$, ** $P < 0.01$, and *** $P < 0.001$; for 5-FU group, # $P < 0.05$, ## $P < 0.01$, and ### $P < 0.001$.

TOP2 α is a DNA helicase encoded by the TOP2A gene, which is located in chromosome 17. TOP2 α can instantaneously break and connect double-stranded DNA chains and regulate and alter the topological states of DNA during transcription and replication. Some type IIA topoisomerase inhibitors, including epipodophyllotoxins and anthracyclines, were selected for related diseases [39]. Mutation or overexpression of TOP2 α was associated with chemotherapeutic resistance to some drugs, such as etoposide, irinotecan, and 5-FU [40–42]. In our study, we also confirmed the gene's pivotal role in 5-FU resistance by bioinformatics analysis. Besides TOP2 α , topoisomerase-I, another protein from the topoisomerase family, has also been observed to be overexpressed in the tumor recurrences of patients with colorectal cancer who had received 5-FU-based

adjuvant chemotherapy [42, 43]. We suggest that some other members in the topoisomerase family probably take part in the 5-FU-resistance mechanism or in the function of Spica Prunellae.

In our study, the protein level of TOP2 α in HCT-8/5-FU cells after 5-FU exposure increased significantly, whereas its transcription level showed no difference from that in the control group (Figures 2(c)–2(e)). Since the levels of miR-494 was not change in the 5-FU exposure too (Figure 4(d)), it does not exclude the possibility that resistance to 5-FU for HCT-8/5-FU cells in this concentration of 5-FU was not in the activation of transcriptional levels but in the inhibition of protein degradation as a compensatory effect to protect cells. Of course, this hypothesis would be confirmed in the future

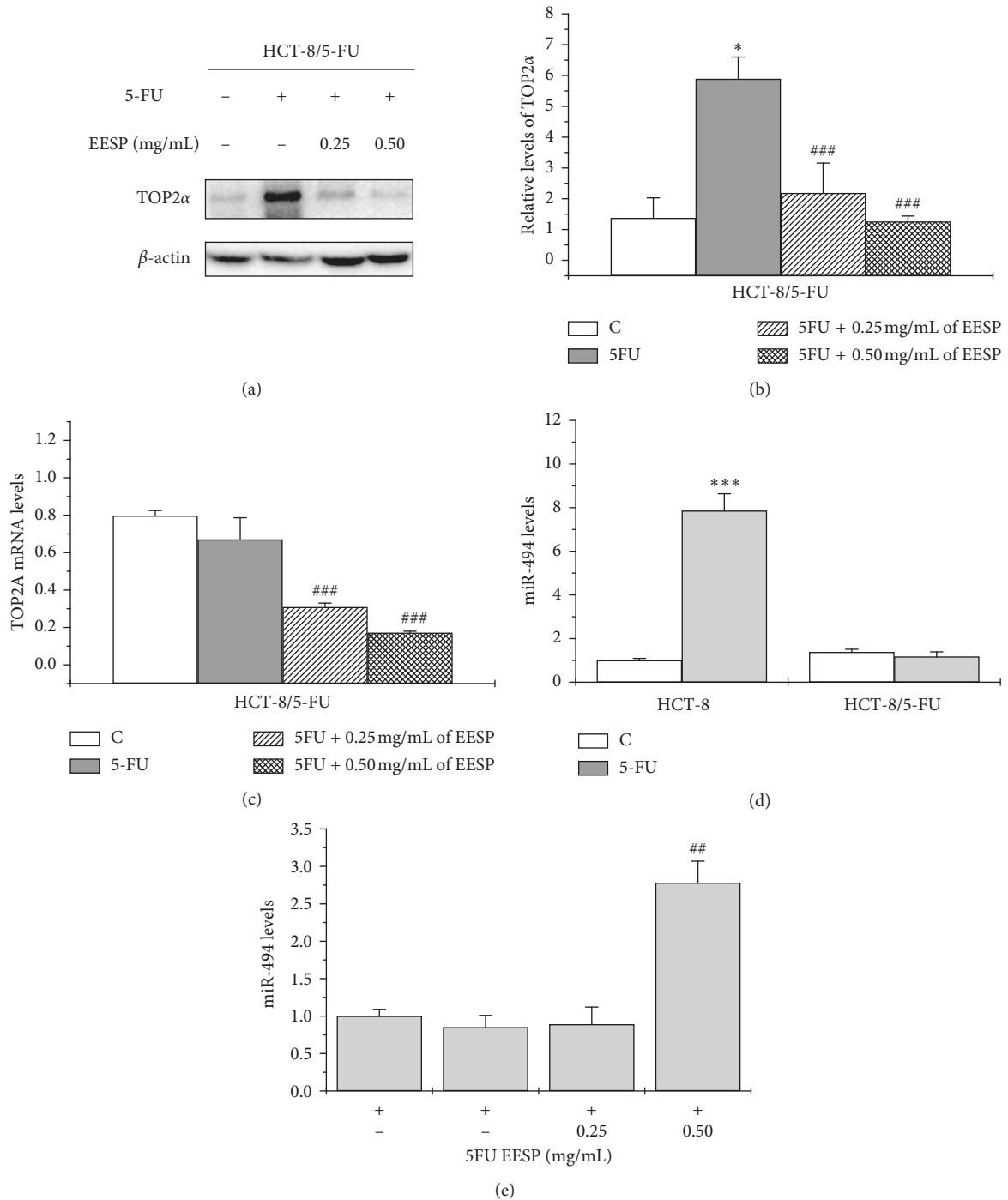


FIGURE 4: EESP enhanced the 5-FU sensitivity of HCT-8/5-FU cells through inhibition of TOP2α. (a) Detection of relative protein levels for HCT-8 and HCT-8/5-FU cells treated with 5-FU (3.2 mM), with or without EESP (0.25 mg/mL or 0.5 mg/mL), for 48 h by western blot and (b) quantification. (c) Real-time PCR evaluation of the mRNA levels of TOP2A. The data from western blot and real-time PCR were normalized to GADPH. (d) Detection of levels of miR-494 by real-time PCR in HCT-8 and HCT-8/5-FU cells treated with 3.2 mM of 5-FU for 48 h (e) Relative levels of miR-494 in HCT-8/5-FU cells treated with 5-FU (3.2 mM), with or without EESP (0.25 mg/mL or 0.5 mg/mL), for 48 h. Data were normalized to U6. Compared with control, * $P < 0.05$, ** $P < 0.01$, and *** $P < 0.001$; compared with the 5-FU (3.2 mM) treatment alone group, # $P < 0.05$, ## $P < 0.01$, and ### $P < 0.001$.

by performing a cyclohexamide chase assay [44]. Moreover, in our study, we also observed that EESP could enhance 5-FU sensitivity of HCT-8/5-FU cells by cell apoptosis induction; considering that EESP contained multicomponents which

helped it play multiroles, there must be some apoptosis pathways involved.

A recent study found that TOP2α is activated by Y-box binding protein-1 in transcriptional level, which is a

multifunctional oncoprotein containing an evolutionarily conserved cold shock domain and dysregulates a wide range of genes involved in cell proliferation and survival, drug resistance, and chromatin destabilization by cancer [44]. So there is a possibility for EESP being suppressed by the expression of TOP2 α via YBX1. Of course, this assumption needs to be confirmed by further investigation. Since our study suggested that TOP2 α might be a marker for 5-FU resistant, it could be an index for selection of more effective treatments for 5-FU resistant patients. Additionally, we also recommend trying the medications like TOP2 α inhibitors or other medicines like Spica Prunellae (with less side effects and charges) in the clinical therapy might achieve some new hope to change the bottleneck period for 5-FU resistance.

MicroRNAs (miRNAs) are a group of small noncoding RNA molecules. They are crucial in every period of life or cancer development. Previous studies have demonstrated that TOP2 α was one of the targets for miR-494 [28]. miR-494 has a global regulatory role in the cell cycle process by binding to the open reading frame and downregulating TOP2 α and PTTG1 [28]. Fortunately, we noticed that EESP enhanced 5-FU sensitivity by downregulating TOP2 α and miR-494. We suggest that EESP probably suppressed expression of TOP2A via upregulation of miR-494. This mechanism will be confirmed by miRNA mimics and inhibitors in a planned future study. Furthermore, because more than two of these miRNAs are involved in the regulation of TOP2 α or drug-resistance mechanisms, they would be valuable to study in the future.

5. Conclusions

Chemotherapy is a common phenomenon during the treatment of colorectal cancer. In our study, we aimed to find some key genes involved in chemotherapy resistance of colorectal cancer. An important gene, TOP2A, was obtained for 5-FU resistance of colorectal cancer by bioinformatics analysis. Our study showed that TOP2 α is a potentially important protein in the 5-FU-resistance mechanism and Spica Prunellae partly reversed 5-FU resistance by downregulating TOP2 α and upregulating levels of miR-494. Furthermore, we believe that Spica Prunellae has more advantages in clinical therapy for 5-FU-resistant patients because it is safer and has fewer adverse effects than chemical agents have.

Data Availability

The gene expression profile data supporting this ontology clusters enrichment and PPI work are from previously reported studies and datasets, which have been cited. The processed data are available at the US NCBI Gene Expression Omnibus database. The expression patterns data supporting expression patterns of TOP2A in colon adenocarcinoma cancer and normal tissues are from previously reported studies and datasets, which have been cited. The processed data are available at gene expression profiling interactive analysis (GEPIA) and R2 (<https://hgserver1.amc.nl/cgi392bin/r2/main.cgi?&species=hs>).

Conflicts of Interest

The authors declare that there are no conflicts of interest regarding the publication of this paper.

Acknowledgments

This research was funded by the National Natural Science Foundation of China (grant no. 81603413) and Department of Education, Fujian Province (grant no. JAT160244). The authors thank Wei Lin for providing EESP powder. The authors also appreciate Aling Shen for his suggestion on manuscript writing.

Supplementary Materials

Table S1: top 15 hub genes with higher degree of connectivity. Figure S1: transfection of siRNA and miR-494 downregulated levels of TOP2 α in HCT-8/5-FU cells. (A) miR-494 levels were detected by real time PCR after transfection of its mimics for 48 h. (B) Analysis of TOP2A mRNA levels. (C) TOP2 α protein levels in HCT-8/5-FU cells after transfection of siRNA and miR-494 mimics for 48 h. (D) Quantification of (C). Compared with the negative control group, * $P < 0.05$, ** $P < 0.01$, and *** $P < 0.001$. (*Supplementary Materials*)

References

- [1] B. Freddie, J. Ferlay, I. Soerjomataram, R. L. Siegel, L. A. Torre, and A. Jemal, "Global cancer statistics 2018: GLOBOCAN estimates of incidence and mortality worldwide for 36 cancers in 185 countries," *CA: A Cancer Journal for Clinicians*, vol. 68, no. 6, pp. 394–424, 2018.
- [2] I. Massa, O. Nanni, F. Foca et al., "Chemotherapy and palliative care near end-of life: examining the appropriateness at a cancer institute for colorectal cancer patients," *BMC Palliative Care*, vol. 17, no. 1, p. 86, 2018.
- [3] I. C. Nordman, S. Iyer, A. M. Joshua, and S. J. Clarke, "Advances in the adjuvant treatment of colorectal cancer," *ANZ Journal of Surgery*, vol. 76, no. 5, pp. 373–380, 2010.
- [4] P. Thirion, S. Michiels, J. P. Pignon et al., "Modulation of fluorouracil by leucovorin in patients with advanced colorectal cancer: an updated meta-analysis," *Saudi Dental Journal*, vol. 26, no. 2, pp. 68–73, 2014.
- [5] M. Inaba, Y. Naoe, and J. Mitsushashi, "Mechanisms for 5-fluorouracil resistance in human colon cancer DLD-1 cells," *Biological & Pharmaceutical Bulletin*, vol. 21, no. 6, pp. 569–573, 1998.
- [6] A. Mori, S. Bertoglio, A. Guglielmi et al., "Activity of continuous-infusion 5-fluorouracil in patients with advanced colorectal cancer clinically resistant to bolus 5-fluorouracil," *Cancer Chemotherapy and Pharmacology*, vol. 33, no. 2, pp. 179–180, 1993.
- [7] J. D. Sara, J. Kaur, R. Khodadadi et al., "5-fluorouracil and cardiotoxicity: a review," *Therapeutic Advances in Medical Oncology*, vol. 10, Article ID 175883591878014, 2018.
- [8] J. Tol, M. Koopman, A. Cats et al., "Chemotherapy, bevacizumab, and cetuximab in metastatic colorectal cancer," *New England Journal of Medicine*, vol. 360, no. 6, pp. 563–572, 2009.

- [9] S.-H. Liu and Y.-C. Cheng, "Old formula, new Rx: the journey of PHY906 as cancer adjuvant therapy," *Journal of Ethnopharmacology*, vol. 140, no. 3, pp. 614–623, 2012.
- [10] A. Shen, H. Chen, Y. Chen et al., "Pien tze huang overcomes multidrug resistance and epithelial-mesenchymal transition in human colorectal carcinoma cells via suppression of TGF- β pathway," *Evidence-based Complementary and Alternative Medicine*, vol. 2014, Article ID 679436, 10 pages, 2013.
- [11] Q. Li, X. Wang, A. Shen et al., "Hedyotis diffusa Willd overcomes 5-fluorouracil resistance in human colorectal cancer HCT-8/5-FU cells by downregulating the expression of P-glycoprotein and ATP-binding cassette subfamily G member 2," *Experimental and Therapeutic Medicine*, vol. 10, no. 5, pp. 1845–1850, 2015.
- [12] J. Lin, J. Feng, H. Yang et al., "Scutellaria barbata D. Don inhibits 5-fluorouracil resistance in colorectal cancer by regulating PI3K/AKT pathway," *Oncology Reports*, vol. 38, no. 4, pp. 2293–2300, 2017.
- [13] C. P. Commission, *Pharmacopoeia of the People's Republic of China*, Chemical Industry Press, Beijing, China, 2005.
- [14] W. Lin, L. Zheng, Q. Zhuang et al., "Spica Prunellae promotes cancer cell apoptosis, inhibits cell proliferation and tumor angiogenesis in a mouse model of colorectal cancer via suppression of stat3 pathway," *BMC Complementary and Alternative Medicine*, vol. 13, no. 1, p. 144, 2013.
- [15] Y. Fang, L. Zhang, J. Feng, W. Lin, Q. Cai, and J. Peng, "Spica Prunellae extract suppresses the growth of human colon carcinoma cells by targeting multiple oncogenes via activating miR-34a," *Oncology Reports*, vol. 38, no. 3, pp. 1895–1901, 2017.
- [16] S. M. Hwang, Y. J. Lee, J. J. Yoon et al., "Prunella vulgaris suppresses HG-induced vascular inflammation via Nrf2/HO-1/eNOS activation," *International Journal of Molecular Sciences*, vol. 13, no. 1, pp. 1258–1268, 2012.
- [17] W. Lin, L. Zheng, J. Zhao et al., "Anti-angiogenic effect of Spica Prunellae extract in vivo and in vitro," *African Journal of Pharmacy and Pharmacology*, vol. 5, no. 24, pp. 2647–2654, 2011.
- [18] X. Mao, G. Wang, W. Zhang, and S. Li, "Study on inhibitory effect of Spica Prunellae extract on T Lymphoma cell EL-4 tumor," *African Journal of Traditional, Complementary and Alternative Medicines*, vol. 10, no. 5, pp. 318–324, 2013.
- [19] J. Zhao, D. Ji, X. Zhai, L. Zhang, X. Luo, and X. Fu, "Oral administration of Prunella vulgaris L improves the effect of taxane on preventing the progression of breast cancer and reduces its side effects," *Frontiers in Pharmacology*, vol. 9, p. 806, 2018.
- [20] S.-M. Woo, K. M. Lee, G. R. Lee et al., "Novel herbal medicine LA16001 ameliorates cisplatin-induced anorexia," *Molecular Medicine Reports*, vol. 17, no. 2, pp. 2665–2672, 2018.
- [21] M. González-Vallinas, S. Molina, G. Vicente et al., "Antitumor effect of 5-fluorouracil is enhanced by rosemary extract in both drug sensitive and resistant colon cancer cells," *Pharmacological Research*, vol. 72, pp. 61–68, 2013.
- [22] M. González-Vallinas, G. Reglero, and A. Ramírez de Molina, "Rosemary (*Rosmarinus officinalis* L.) extract as a potential complementary agent in anticancer therapy," *Nutrition and Cancer*, vol. 67, no. 8, pp. 1223–1231, 2015.
- [23] L. Fang, N. Lin, and Y. Wu, "Simultaneous determination of four active components in Spica Prunellae by HPLC," *China Journal of Chinese Materia Medica*, vol. 35, no. 5, pp. 616–619, 2010.
- [24] A. M. Popov, A. N. Osipov, E. A. Korepanova, O. N. Krivoschapko, and A. A. Artiukov, "Study of antioxidant and membrane activity of rosmarinic acid using different model systems," *Biophysics*, vol. 58, no. 5, pp. 775–785, 2013.
- [25] C. Colica, L. Di Renzo, V. Aiello, A. De Lorenzo, and L. Abenavoli, "Rosmarinic acid as potential anti-inflammatory agent," *Reviews on Recent Clinical Trials*, vol. 13, no. 4, pp. 240–242, 2018.
- [26] M. K. Swamy, U. R. Sinniah, and A. Ghasemzadeh, "Anti-cancer potential of rosmarinic acid and its improved production through biotechnological interventions and functional genomics," *Applied Microbiology and Biotechnology*, vol. 102, no. 18, pp. 7775–7793, 2018.
- [27] Y. Zhou, B. Zhou, L. Pache et al., "Metascape provides a biologist-oriented resource for the analysis of systems-level datasets," *Nature Communications*, vol. 10, no. 1, p. 1523, 2019.
- [28] S. Yamanaka, N. R. Campbell, F. An et al., "Coordinated effects of microRNA-494 induce G₂/M arrest in human cholangiocarcinoma," *Cell Cycle*, vol. 11, no. 14, pp. 2729–2738, 2012.
- [29] W. Gu, L. Liu, F.-F. Fang, F. Huang, B.-B. Cheng, and B. Li, "Reversal effect of bufalin on multidrug resistance in human hepatocellular carcinoma BEL-7402/5-FU cells," *Oncology Reports*, vol. 31, no. 1, pp. 216–222, 2014.
- [30] H.-y. Huang, J.-l. Niu, L.-m. Zhao, and Y.-h. Lu, "Reversal effect of 2',4'-dihydroxy-6'-methoxy-3',5'-dimethylchalcone on multi-drug resistance in resistant human hepatocellular carcinoma cell line BEL-7402/5-FU," *Phytomedicine*, vol. 18, no. 12, pp. 1086–1092, 2011.
- [31] H.-Y. Yang, L. Zhao, Z. Yang et al., "Oroxynin A reverses multi-drug resistance of human hepatoma BEL7402/5-FU cells via downregulation of P-glycoprotein expression by inhibiting NF- κ B signaling pathway," *Molecular Carcinogenesis*, vol. 51, no. 2, pp. 185–195, 2012.
- [32] D. Kong, D. Zhang, X. Chu, and J. Wang, "Schizandrin A enhances chemosensitivity of colon carcinoma cells to 5-fluorouracil through up-regulation of miR-195," *Biomedicine & Pharmacotherapy*, vol. 99, pp. 176–183, 2018.
- [33] L.-x. Shi, R. Ma, R. Lu et al., "Reversal effect of tyroservatide (YSV) tripeptide on multi-drug resistance in resistant human hepatocellular carcinoma cell line BEL-7402/5-FU," *Cancer Letters*, vol. 269, no. 1, pp. 101–110, 2008.
- [34] D. B. Longley, D. P. Harkin, and P. G. Johnston, "5-Fluorouracil: mechanisms of action and clinical strategies," *Nature Reviews Cancer*, vol. 3, no. 5, pp. 330–338, 2003.
- [35] H. Zembutsu, Y. Ohnishi, T. Tsunoda et al., "Genome-wide cDNA microarray screening to correlate gene expression profiles with sensitivity of 85 human cancer xenografts to anticancer drugs," *Cancer Research*, vol. 62, no. 2, pp. 518–527, 2002.
- [36] P. J. Maxwell, D. B. Longley, T. Latif et al., "Identification of 5-fluorouracil-inducible target genes using cDNA microarray profiling," *Cancer Research*, vol. 63, no. 15, pp. 4602–4606, 2003.
- [37] Y. Shen, M. Tong, Q. Liang et al., "Epigenomics alternations and dynamic transcriptional changes in responses to 5-fluorouracil stimulation reveal mechanisms of acquired drug resistance of colorectal cancer cells," *The Pharmacogenomics Journal*, vol. 18, no. 1, pp. 23–28, 2018.
- [38] N. Namwat, P. Amimanan, W. Loilome et al., "Characterization of 5-fluorouracil-resistant cholangiocarcinoma cell lines," *Chemotherapy*, vol. 54, no. 5, pp. 343–351, 2008.
- [39] J. L. Delgado, C.-M. Hsieh, N.-L. Chan, and H. Hiasa, "Topoisomerases as anticancer targets," *Biochemical Journal*, vol. 475, no. 2, pp. 373–398, 2018.

- [40] A. Coss, M. Tosetto, E. J. Fox et al., "Increased topoisomerase II α expression in colorectal cancer is associated with advanced disease and chemotherapeutic resistance via inhibition of apoptosis," *Cancer Letters*, vol. 276, no. 2, pp. 228–238, 2009.
- [41] Y. X. Liu, Y. Hsiung, M. Jannatipour, Y. Yeh, and J. L. Nitiss, "Yeast topoisomerase II mutants resistant to anti-topoisomerase agents: identification and characterization of new yeast topoisomerase II mutants selected for resistance to etoposide," *Cancer Research*, vol. 54, no. 11, pp. 2943–2951, 1994.
- [42] N. Tsavaris, A. Lazaris, C. Kosmas et al., "Topoisomerase I and II α protein expression in primary colorectal cancer and recurrences following 5-fluorouracil-based adjuvant chemotherapy," *Cancer Chemotherapy and Pharmacology*, vol. 64, no. 2, p. 399, 2009.
- [43] P. Gouveris, A. C. Lazaris, T. G. Papathomas et al., "Topoisomerase I protein expression in primary colorectal cancer and recurrences after 5-FU-based adjuvant chemotherapy," *Journal of Cancer Research and Clinical Oncology*, vol. 133, no. 12, pp. 1011–1015, 2007.
- [44] K. Michihiko, T. Shibata, K. Watari, and M. Ono, "Oncogenic Y-box binding protein-1 as an effective therapeutic target in drug-resistant cancer," *Cancer Science*, vol. 110, no. 5, pp. 1536–1543, 2019.

Research Article

Risk of Developing Hepatocellular Carcinoma following Depressive Disorder Based on the Expression Level of Oatp2a1 and Oatp2b1

Yan Chen ^{1,2}, Jiongshan Zhang,² Mengting Liu,¹ Zengcheng Zou,² Fenglin Wang,² Hao Hu,¹ Baoguo Sun ¹, and Shijun Zhang ¹

¹Department of Traditional Chinese Medicine, The First Affiliated Hospital, Sun Yat-sen University, 58, Zhongshan Road II, Guangzhou, 510080, China

²Department of Traditional Chinese Medicine, The Third Affiliated Hospital, Sun Yat-sen University, Guangdong Key Laboratory of Liver Disease Research, 600, Tianhe Road, Guangzhou, 510630, China

Correspondence should be addressed to Baoguo Sun; sunbaoguo666@126.com and Shijun Zhang; 2806973376@qq.com

Received 4 April 2019; Revised 31 May 2019; Accepted 9 June 2019; Published 29 July 2019

Guest Editor: Chengsheng Wu

Copyright © 2019 Yan Chen et al. This is an open access article distributed under the Creative Commons Attribution License, which permits unrestricted use, distribution, and reproduction in any medium, provided the original work is properly cited.

Background. Accumulating evidence from prospective epidemiological studies has showed that depression disorder (DD) is a risk factor for cancer. The aim of this study is to explore the association of DD and the overall occurrence risk of hepatocellular carcinoma (HCC) and the mechanism. **Methods.** In this study, 60 mice were randomly divided into four groups: Control group, DD group, HCC group, HCC-DD group. Mice received a chronic dose of reserpine to establish depression model, followed by Diethylnitrosamine and Carbon tetrachloride administration to establish HCC models. Behavioral depression was assessed by sucrose preference test (SPT) and the expression of Serotonin 1A (5-HT1A) receptor in the hippocampal. The expression of Oatp2a1 and Oatp2b1 in the digestive system tissues was detected by PCR and western blotting. **Results.** Reserpine-administrated mice had a reducing sucrose preference at Day 14 compared with blank mice ($P < 0.05$). The expression of 5-HT1A receptor in the hippocampal was decreased in DD mice compared with blank mice. The survival analysis indicated that the HCC mice with DD have poorer survival rate compared with the HCC mice. Compared with HCC mice, the expression of Oatp2a1 and Oatp2b1 was lower in liver and stomach tissue and higher in hepatic carcinoma and colon tissue of HCC-DD mice ($P < 0.05$), and the expression of Oatp2a1 was higher in the spleen tissue of HCC-DD mice while the expression of Oatp2b1 was lower ($P < 0.05$). However, no difference was found in the expression of Oatp2a1 and Oatp2b1 in the small intestine tissue between HCC group and HCC-DD group. **Conclusions.** DD was the adverse factors for the overall occurrence risk of HCC. Mechanistically, be the downregulation of Oatp2a1 and Oatp2b1 in liver tissue induced by DD might be involved.

1. Introduction

Globally, HCC is the fifth most common cancer and is the second cause of cancer mortality [1]. Statistics shows a rising incidence of HCC from 1.5 per 100,000 persons to nearly 14 per 100,000 persons, and a 5-year survival under 12% in the last 40 years even in the low incidence of hepatitis B in the United States [2]. Although liver resection, transplantation, radiofrequency ablation (RFA), or even for ablative techniques of transcatheter arterial chemoembolization (TACE) have been improved and applied widely for HCC, HCC recurrence remains to be a challenge [3]. The molecular targeted

therapies are the only treatment modalities for patients with advanced HCC. Sorafenib provides a meaningful survival benefit in patients with advanced HCC; however, as other molecular targeted drugs developed, they still have serious side effects [4]. Therefore, increasing researchers focus on exploring the pathogenic factors and etiopathogenesis of HCC, aiming at provide suitable treatment or even preventing HCC.

Studies suggested that the long time chronic social defeat stress induced by life style changing contributes to the pathogenesis of major DD [5]. An interesting study demonstrated that the increasing comparisons on Facebook may induce

feelings of envy, which may be related to DD [6]. DD is not only the leading cause of decrement in health utility in general population, but also in the cancer patients [7]. The researchers have found that hepatoma-burden might induce depressive-related behavior and antidepressants might not only palliate depression symptoms but also modify disease processes in the auxiliary treatment of cancer. Moreover, the antidepressants of selective serotonin reuptake inhibitors (SSRIs) may possibly reduce the risk of HCC in HBV-infected patients in a dose-responsive manner [8, 9].

Recently, growing evidence from prospective epidemiological studies has showed that DD is a risk factor for cancer. The study suggested that DD may be related to increased risk of ovarian cancer [10]. Gut-derived serotonin induced by depression could promote breast cancer bone metastasis through the RUNX2/PTHrP/RANKL pathway in mice, and DD might be responsible for progression of malignancy and thus accelerate the metastasis formation in cancer patients [11]. Another study showed a close relationship between DD and the overall occurrence risk of HCC without mentioning its underlying mechanism [12]. And the relationship between DD and HCC has been seldom reported so far.

Organic anion transporters (Oatps) as a superfamily of transporter proteins is globally expressed throughout tissues and organs of human body with different abundance and the organs and tissues of digestive system no exception [13]. Oatp family proteins mainly carry out the uptake of small molecules and exert important functions to maintain the homeostasis of human body under physiological condition [14]. Oatp proteins in digestive system are involved in absorbing nutrients and ions, excreting bile acids, and metabolise toxins [14–18]. Thus, dysfunction of Oatp proteins in digestive system may easily mediate the initiation and progression of tumors [19]. The study reported that Oatp2a1 is likely to promote tumorigenesis by PGE₂ uptake into the endothelial cells; blockade of Oatp2a1 is an additional pharmacologic strategy to improve colon cancer outcomes [20]. The expression of Oatp2b1 mRNA was increased in bone tumors [21]. Oatp2 is mainly expressed on the sinusoidal membrane of human hepatocytes and transporting both unconjugated and conjugated bilirubin from plasma into the liver [22]. In liver, Oatp2 is in charge of the uptake and glucuronidation of bilirubin in hepatocytes; mutation of Oatp2 may be involved in the development of hyperbilirubinemia [23]. It plays an important role in the excretion of bilirubin and liver toxin [24]. We hypothesize that, as the important members of transporter proteins to excrete bilirubin and liver toxin, Oatp2a1 and Oatp 2b1 may also be relevant to HCC.

Recently, the disordered tissue microenvironment and imbalanced internal environment which is further enhanced by the causes of metabolic have been proposed as the pathogenic factors of HCC [25]. DD, caused by the stress from physiological, psychological, and physical factors, has an adverse impact on human body homeostasis [26]. To our knowledge, DD has an adverse impact on human body homeostasis and has a relationship with HCC, Oatp 2a1, and Oatp 2b1 as the important members of transporter proteins in the internal environment are closely related with the occurrence of digestive system tumors; internal environment

disorder is the important factor for HCC. Therefore, we will observe the expression of Oatp 2a1 and Oatp 2b1 on HCC-DD mice and explore the relationship between DD and HCC at the molecular level in body internal environment in this study.

2. Materials and Methods

2.1. Experimental Animals. In total 60 specific pathogen-free (SPF) C57BL/6 mice (male; weight, 18±2g; series No.: 44008500008530) were purchased from the Animal Experimental Center of Sun Yat-sen University (Certification No.: SYXK (Guangdong) 2012-0081; Guangzhou, China).

2.2. Chemicals. Reserpine injection (lot number: 1210111) was purchased from Jinyao Amino Acids Co., Ltd., (Tianjin, China). Diethylnitrosamine (CAS 55-18-5, N-nitrosodiethylamine, DEN) was purchased from Sigma-Aldrich Shanghai Trading Co., Ltd., (Shanghai, China). Carbon tetrachloride (CAS 56-23-5, CCl₄) and olive oil (CAS 8001-25-0) were purchased from Aladdin biological technology co., Ltd., (Shanghai, China). Rabbit polyclonal to 5HT1A Receptor antibody (ab85615) was provided by Abcam Co., Ltd., (USA). Goat anti-rabbit IgG-HRP (sc-2004) was provided by Santa Cruz Biotechnology, Inc. (USA).

2.3. Experimental Design. After one-week acclimatization, sixty mice were randomly divided into four groups as follows (n=15 per group): (A) Control group, (B) DD group, (C) HCC group, and (D) HCC-DD group. At phase one, thirty mice (Group B and Group D) were accepted DD model procedure; then sixty mice (the all groups) were evaluated by Sucrose Preference Test at the same time. At the second phase, fifteen blank mice (Group C) and fifteen DD animals (Group D) were used to establish HCC model one week after phase one.

2.4. Induction of DD Animal Model. A chronic dose of reserpine administration was used to establish the animal model of DD according to the previous study [27]. The mice received a daily dose of reserpine (0.28 mg/kg i.p.) for 14 days; then the DD models were evaluated by Sucrose Preference Test.

2.5. SPT. Three days before the reserpine administration, the animals were placed in a cage with two bottles of 1% sucrose solution for 24 h to serve as a baseline. Then animals were presented with a 1% sucrose solution bottle and a water bottle for 24 h and two water bottles for another 24 h in order to adapt. Sucrose preference test was carried out on the 7th day and the 14th day. Animals were free to access two bottles containing 1% sucrose solution and water for 24 h, respectively. The consumed sucrose solution and water was recorded. The sum of water consumption and sucrose consumption was defined as total intake. The percentage of sucrose intake was calculated using the following equation: % sucrose preference = sucrose intake × 100 / total intake [28].

2.6. Induction of HCC in Animal Model. HCC was induced by four steps. Firstly, animals received single (i.p.) injection of DEN (95 mg/kg) diluted in saline (100 mg/ml). After that, promotion was induced by intragastric administration of CCl₄ as a single necrogenic dose (5 ml/kg diluted in olive oil at a ratio of 1:4) twice a week from the fourth day. Then all the animals were intraperitoneal injection of diluted DEN once with a reduced dose 50 mg/kg at the third week. Finally, animals had intragastric administration by the increased dose of CCl₄ (8 ml/kg, diluted in olive oil at a ratio of 1:4) twice a week from the fourth week until the 20 weeks. This was followed by feeding the animals the basal diet till the end of the study [29].

2.7. Sample Collection. Mice were sacrificed by cervical dislocation after they were anesthetized using 10% chloral hydrate (3.5 ml/kg, i.p.); all the brains, the livers, the spleens, the stomachs, the small intestines, and the colons were collected. One part of the samples were stored at -80°C for the following researches; the other parts of the samples were fixed with 4% paraformaldehyde and then embedded in paraffin for immunohistochemistry. Meanwhile, when the mice reached the ethical limits of animal care (the body weight loss 20%, chills or ascites), they were sacrificed by cervical dislocation under anesthesia immediately in order to relieve suffering and the samples were collected.

2.8. Immunohistochemistry (IHC). The hippocampi were separated from the brains which were fixed with 4% paraformaldehyde. Then, the hippocampi tissues were dehydrated and set in paraffin. After dewaxing by xylene, ethanol, and distilled water, the sections were put into citrate buffer solution and heated in a microwave oven. The slides were blocked using 6.5% BSA at room temperature and incubated in diluted primary antibody (1:500) at 4°C overnight. After washing thrice in PBS, the sections were incubated with diluted secondary antibody (1:1,000) for 1 h at room temperature. After washing with distilled water the sections were counterstained with Harris hematoxylin solution dehydrated, cleared in xylene, and mounted with synthetic resin mounting medium and coverslip. Brown-yellow stain was positive staining [30].

2.9. Fluorescence-Based Quantitative RT-PCR Reactions. The levels of Oatp 2a1 and Oatp 2b1 mRNA in the digestive system tissues were analyzed by Real-Time quantitative-PCR. The total RNA was extracted using Trizol, and the DNA was obtained by reverse transcription with a BIO-RAD quantitative PCR instrument. The quantitative standard curve was prepared based on a gradient of positive standard with a negative control of sterile double-distilled water. The following probes and primers were used for mRNA analysis: Oatp2a1:forward primer:5'-CTC CCG TCC ATC TTC CTC ATC T-3', reverse primer:5'-AGA ACT GTA CTC CAA TGG CAA ACG A-3'; Oatp2b1:forward primer:5'-GGT GGC TGG GCT TCC TCA TCT-3', reverse primer: 5'-CCA AGA CCT TCC GCC TGA AAT GA-3'; GAPDH:forward primer:5'-AGA AGG TGG TGA AGC AGG CAT C-3',

reverse primer:5'-CGA AGG TGG AAG AGT GGG AGT TG-3'. The PCR conditions were as follows: 94°C for 30s was operated for 1 cycle, then 94°C for 5 s, 55°C for 15 s, and 72°C for 10 s were repeated for 40 cycles, and after that 60°C for 15 s and 95°C for 15 s were operated for 1 cycle.

2.10. Western-Blotting. The Oatp 2a1 and Oatp 2b1 protein expression in the digestive system tissues were analyzed by western blot. Tissue lysates were clarified by centrifugation at 4°C, 12000r/min for 30 minutes. Protein extract was separated on 10% sodium dodecyl sulphate-polyacrylamide gel electrophoresis. And then it was electrophoretically transferred onto a PDVF membrane (Millipore, Etten-Leur, The Netherlands) for 90 min at 100V. Subsequently, the PVDF membrane which had been blocked in 5% nonfat milk for 1 h at room temperature was incubated with primary antibodies. The primary antibodies Slco2a1(Santa Cruz biotechnology, USA) and Slco2b1(Abcam, USA), GAPDH (ABclonal Biotechnology, USA), were diluted in 1:1000, 1:500 and 1:5000, respectively at 4°C overnight;. And the secondary antibody Horseradish peroxidase (HRP) (Zhongshanjinjiao Biotechnology, Beijing, China) was diluted in 1:5000 at room temperature for 1h. The membranes were washed with TBST, and the proteins were analysed by using ECL chemiluminescence.

2.11. Statistical Analysis. The data were analyzed using the Statistical Product and Service Solutions (SPSS17.0) software package for Windows. The survival time was analyzed using the Kaplan-Meier and Log-Rank (Mantel-Cox) test. The normally distributed data were analyzed using an independent t-test. A Wilcoxon nonparametric test was used while normal distribution was not assumed. P<0.05 was considered to indicate a statistically significant difference.

3. Results

3.1. Effects of the DD Model Established by Reserpine. Sucrose preference test is an important method to assess behavioral depression. Reserpine-administrated mice (DD group and HCC-DD group) did not significantly differ from blank mice (Control group and HCC group) in sucrose preference at Day 7 but had a reducing sucrose preference at Day 14 compared with blank mice (P<0.05, Figures 1(a) and 1(b)). Between-group analyses showed that reserpine-exposed animals weighed significantly less compared to blank animals through Day 4 till Day 14 (P<0.05, Figure 1(c)). In addition, the data of food intake of DD animals was also less compared to blank animals through Day 4 till Day 14 (P<0.05, Figure 1(d)).

5-HT1A receptor of the hippocampal is an admittedly important biological marker of DD. The expression level of 5-HT1A receptor in the CA1 region of the hippocampus was detected by IHC. DD triggered the decrease in 5-HT1A receptor expression in the CA1 region of the hippocampus compared with blank mice without DD (Figure 2).

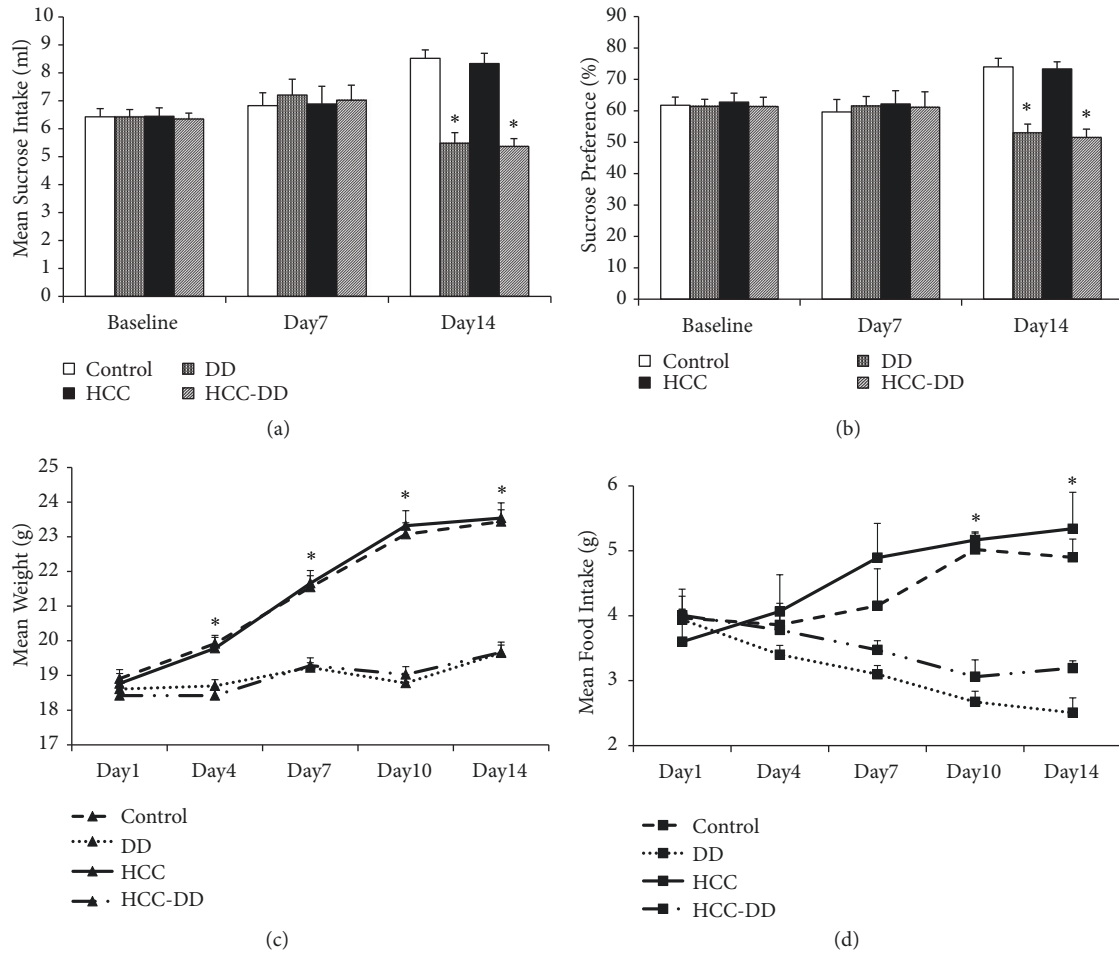


FIGURE 1: Sucrose preference test. Control, Control group; DD, DD group; HCC, HCC group; HCC-DD, HCC-DD group. * $P < 0.05$ vs. Control group and HCC group. (a) Sucrose intake; (b) sucrose preference; (c) body weight; (d) food intake.

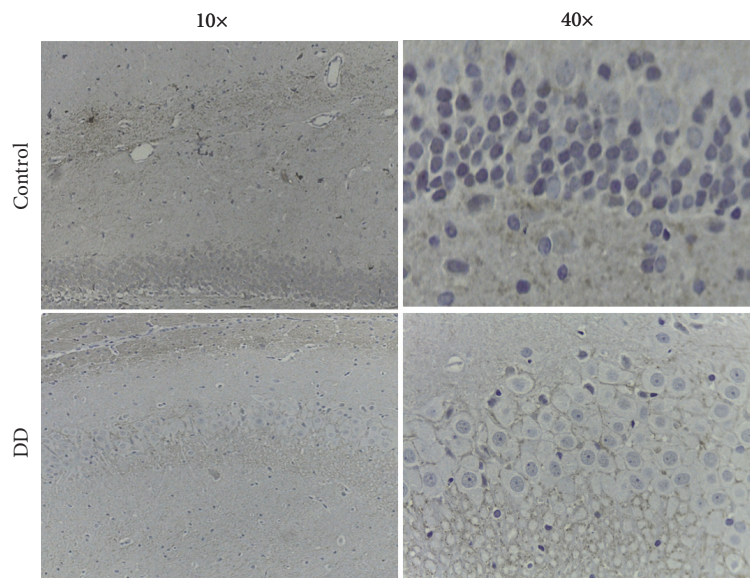


FIGURE 2: Change in the hippocampal 5-HT1A receptor expression of mice by immunohistochemistry (IHC).

TABLE 1: Liver weight, spleen weight, stomach weight, and body weight (n=15, mean ± standard deviation).

Group	Liver	Spleen	Stomach	Body weight
Control	1.45 ± 0.06	0.09 ± 0.00	0.21 ± 0.02	26.67 ± 0.84
DD	1.53 ± 0.05	0.11 ± 0.00	0.20 ± 0.01	28.82 ± 1.07
HCC	0.83 ± 0.08 * #	0.15 ± 0.03*	0.15 ± 0.01 * #	15.94 ± 0.87 * #
HCC-DD	1.19 ± 0.07 * #&	0.11 ± 0.01	0.17 ± 0.01	20.99 ± 1.00 * #&

Control, Control group; DD, DD group; HCC, HCC group; HCC-DD, HCC-DD group. *P<0.05 vs. Control group; #P<0.05 vs. DD group; &P<0.05 vs. HCC group.

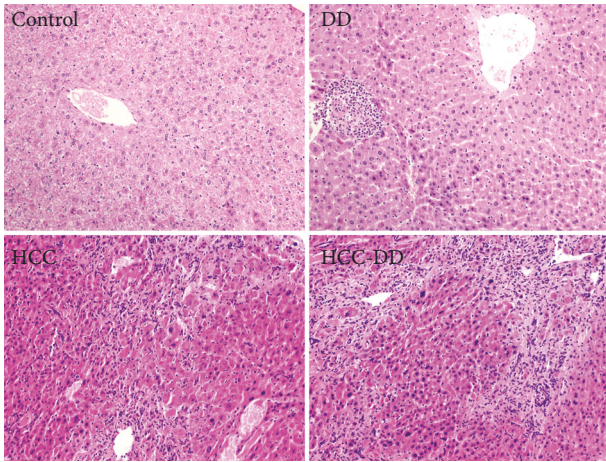


FIGURE 3: HE stain of the liver tissue. Scale, 200X. Control, Control group; DD, DD group; HCC, HCC group; HCC-DD, HCC-DD group.

3.2. Pathological Analysis of Hepatic Carcinoma. The liver tissues in all groups were analyzed at the end of the building of HCC at the 20th week. The hematoxylin-eosin (H&E) staining results showed that the constructions of hepatocytes were in normal situation with full-constructed hepatic lobes, aligned nuclei, radially distributed hepatic cords, and apparent hepatic sinusoids in the Control group and DD group mice. The liver tissue in HCC group and HCC-DD group showed the carcinoma cells were of all sizes, multinucleated tumor giant cells, and funicular slice distributed and accumulated irregularly without the normal hepatocytes constructions. The Edmondson-Steiner classification of the liver tissue in HCC group was the III level while the HCC-DD group was the IV level. The results showed that the malignant degree of the tumor tissue was higher in HCC-DD (Figure 3).

3.3. Weight and Survival Analysis. The spleen weight of the HCC group was the highest, and the stomach weight of the HCC group was the lowest (P<0.05, Table 1). Liver weight and body weight of the HCC group and HCC-DD group were lower than other groups; they were higher in HCC-DD group compared with HCC group because of the increased tumor size inside the HCC-DD liver (P<0.05, Table 1). The survival analysis indicated that the HCC-DD mice have poorer survival rate when compared with the HCC mice (P <0.05, Figure 4).

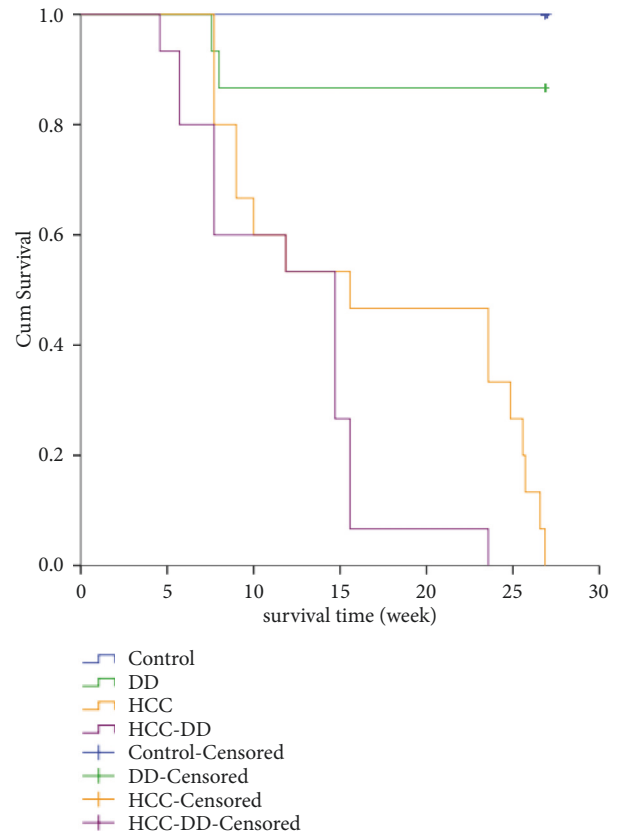


FIGURE 4: Survival analysis. Kaplan-Meier and Log-Rank (Mantel-Cox) Pairwise Comparison test of survival distributions for different levels of each group. Control-Censored and DD-Censored: when the study was completed on the 20th week, there were alive mice in Control group (n = 15) and DD group (n = 13), but the survival time was not observed. Control, Control group; DD, DD group; HCC, HCC group; HCC-DD, HCC-DD group.

3.4. The Expression Levels of Oatp2a1 and Oatp2b1

3.4.1. The mRNA Levels of Oatp2a1 and Oatp2b1. The expression level of liver Oatp2a1 mRNA in DD group was the lowest in all the groups; it was lower in HCC-DD group compared with HCC group. For the Oatp2b1 mRNA, the expression level was decreased in DD group compared with control group; the expression level was also decreased in HCC-DD group compared with HCC group (P<0.05, Figure 5(a)). In the spleen tissue, the expression level of Oatp2a1 mRNA in HCC-DD group was the highest, while the DD group was the

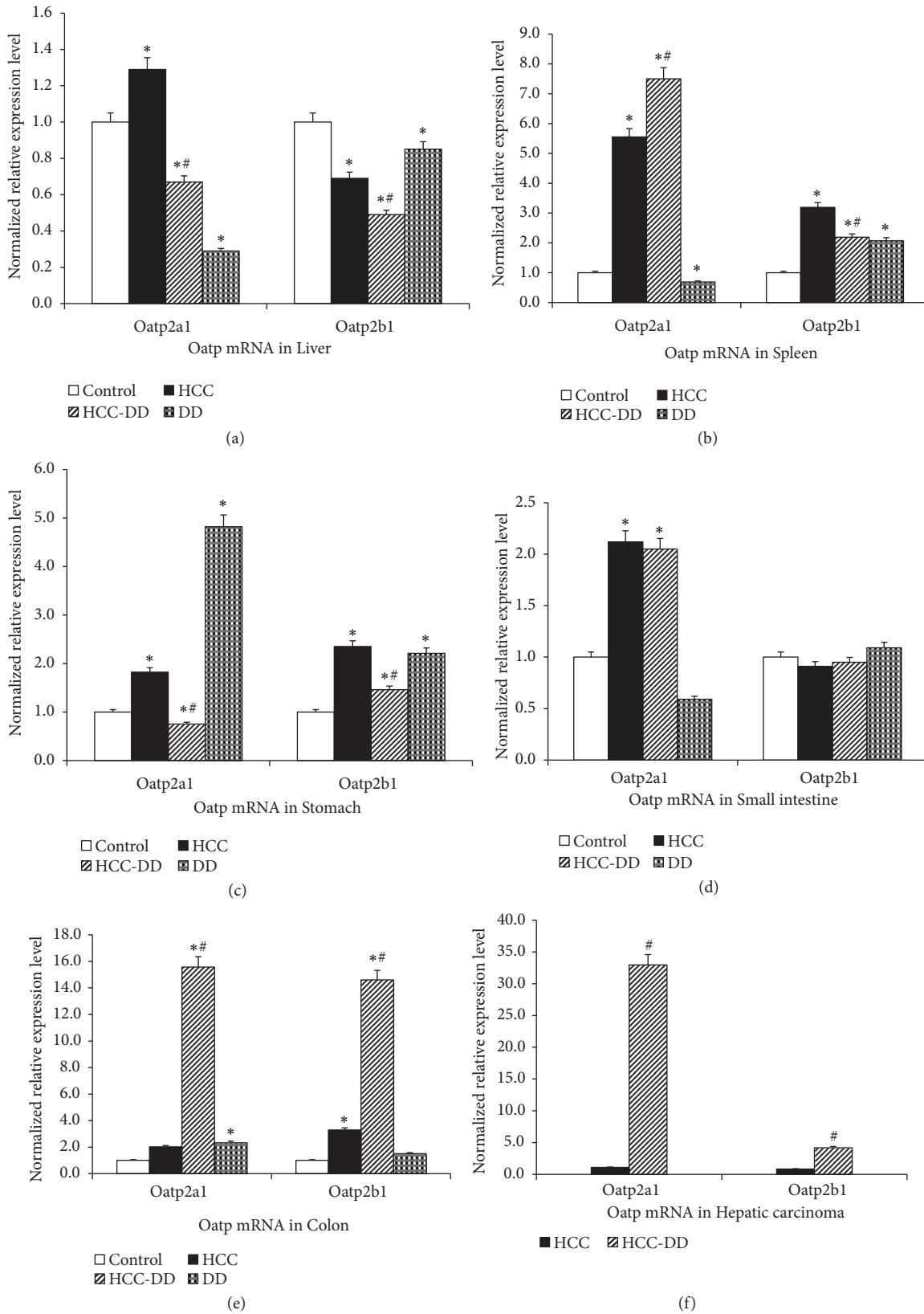


FIGURE 5: The expression level of Oatp2a1 and Oatp2b1 mRNA in digestive system tissues. (a) liver tissue; (b) spleen tissue; (c) stomach tissue; (d) small intestine tissue; (e) colon tissue; (f) hepatic carcinoma tissue. Control, Control group; DD, DD group; HCC, HCC group; HCC-DD, HCC-DD group. * $P < 0.05$ vs. Control group; # $P < 0.05$ vs. HCC group.

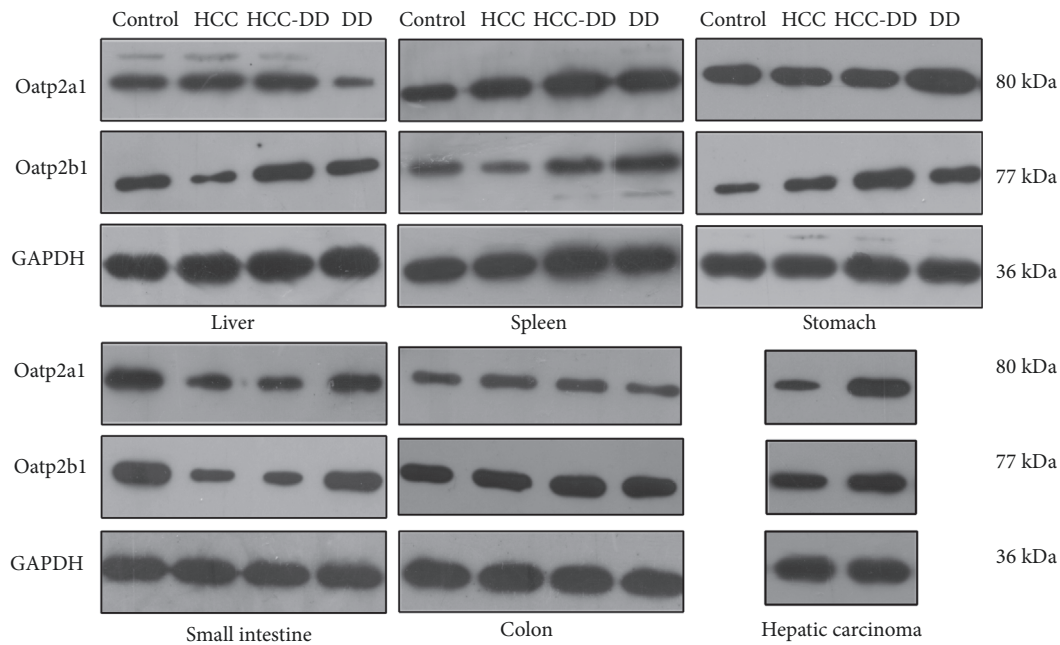


FIGURE 6: The expression level of Oatp2a1 and Oatp2b1 protein in digestive system tissues. Control, Control group; HCC, HCC group; HCC-DD, HCC-DD group; DD, DD group; GAPDH, glyceraldehyde 3-phosphate dehydrogenase.

lowest; for Oatp2b1 mRNA, it was the highest in HCC group ($P < 0.05$, Figure 5(b)). In the stomach tissue, the expression levels of Oatp2a1 mRNA and Oatp2b1 mRNA were lower in HCC-DD group compared with HCC group; they were increased in DD group compared with Control group and the expression of Oatp2a1 mRNA in DD group was the highest ($P < 0.05$, Figure 5(c)). In the small intestine tissue, for the Oatp2a1 mRNA, the expression levels in HCC group and HCC-DD group were higher than Control group ($P < 0.05$, Figure 5(d)); however, no difference was found in all groups for Oatp2b1 mRNA. In the colon tissue, for both Oatp2a1 mRNA and Oatp2b1 mRNA, the expression level in HCC-DD group was the highest ($P < 0.05$, Figure 5(e)). Compared with HCC group, the expression of Oatp2a1 mRNA and Oatp2b1 mRNA of hepatic carcinoma was increased in HCC-DD group ($P < 0.05$, Figure 5(f)).

3.4.2. The Protein Levels of Oatp2a1 and Oatp2b1. The expression levels of Oatp2a1 and Oatp2b1 in different groups and tissues showed a different trend. The levels of both Oatp2a1 and Oatp2b1 protein were almost consistent with the levels of Oatp2a1 and Oatp2b1 mRNA (Figures 6 and 7). In the liver tissue, the expression levels of Oatp2a1 and Oatp2b1 were decreased in the DD group compared with Control group, and they were decreased in the HCC-DD group compared with HCC group. In the spleen tissue, the expression level of Oatp2a1 protein in DD group was lower than Control group, while it was increased in HCC-DD group compared with HCC group; for the Oatp2b1 protein, the trend was the reversed. In the stomach tissue, the expression level of Oatp2a1 protein and Oatp2b1 protein in DD group was higher than Control group, while they were decreased in HCC-DD group compared with HCC group. In the small intestine

tissue, the expression level of Oatp2a1 protein in DD group was lower than Control; however no difference was found in all groups for Oatp2b1 protein. Compared with HCC group, the expression levels of Oatp2a1 and Oatp2b1 in the colon tissue and hepatic carcinoma tissue were increased significant in HCC-DD group.

4. Discussion

DD shows relatively high prevalence rates; it is ranked by the World Health Organization (WHO) as the highest global cause of “years of life lived with disability” for all age groups [31]. Cancer patients usually live under chronic stress caused by diagnosis-related strong emotional experience and depression. The study indicated a subsequent risk of DD in patients with HCC, and the risk increased for those with female gender, aged 40 to 59 and aged 60 to 79, with metastasis, with HCV, or with liver cirrhosis [32, 33]. In spite of the fact that no association was detected between DD and risk of HCC in people aged 65 years or older in Taiwan without the data of the younger people, other studies have found an etiological association [12, 34].

Studies have shown that reserpine is widely used to establish mouse depression model [35]. Reserpine is not lethal. Chronic rather than an acute dose of reserpine was used convincingly in the study to induce DD animals. SPT was used for this study, since previous studies have shown that sucrose consumption is a weak and inconsistent index of reward responsiveness in DD [36]. 5-HT_{1A} receptor is closely related to emotional disorders; it is an admittedly important biological markers of DD [37]. This study showed the effect of reduced sucrose consumption in DD group and HCC-DD group at Day 14. Besides, DD group and HCC-DD

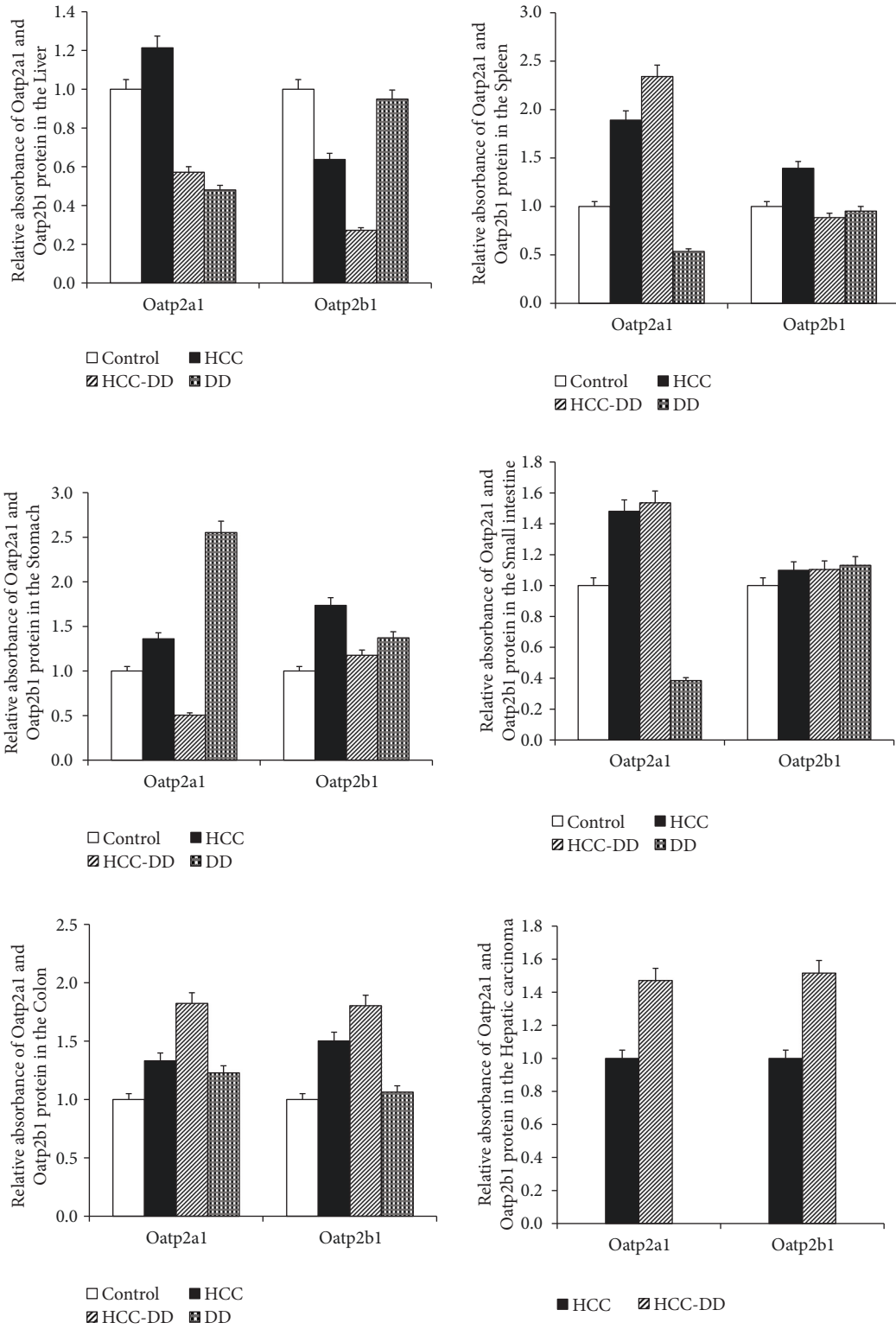


FIGURE 7: The relative absorbance of Oatp2a1 and Oatp2b1 protein in digestive system tissues. Control, Control group; HCC, HCC group; HCC-DD, HCC-DD group; DD, DD group.

group had lower body weight and food intake compared with Control group and HCC group. The expression of 5-HT_{1A} receptor in the CA1 region of the hippocampus of the DD mice was decreased compared with the blank mice. These results suggested that DD animal models are successfully established after reserpine administration (0.28 mg/kg i.p.) for 14 consecutive days.

Animal models are crucial tools in the study of HCC. Chemically induced HCC which has an irreversible process characterization by structural DNA changes is closer to human HCC, and DEN induced HCC model is the most frequently used [38]. In this study, DEN and CCl₄ were used to establish HCC models as a classic HCC animal model for 20 weeks. The H&E staining results indicated the HCC occurred in the HCC group and HCC-DD group. The survival analysis indicated that there was no significance difference between Control group and DD group in the survival rate, liver weight, spleen weight, stomach weight, and body weight. The results suggested that the effect of DD did not continue for 20 weeks or did not enough affect the mice growth. The survival rate of HCC-DD group was poorer than HCC group. The body weights of the HCC group and HCC-DD group were lower than other groups. And the body weight of HCC-DD group with a higher liver weight was higher than HCC group; it was due to increased tumor size inside the HCC-DD liver. The comparison of survival rate, body weight, and liver weight indicated that DD might be beneficial to the growth of the tumor in HCC-DD mice.

DD and tumor growth could suppress the immune function of mice to different degrees and change the body microenvironment [39]. Immune dysregulation may be a central feature common to DD which induced decreased natural killer cell cytotoxicity and elevated IL-6, TNF α , and CRP [40]. At the molecular level, the DD induce the production and secretion of dopamine, catecholamines, and glucocorticoids, which influence the body internal environment and promote proliferation, apoptosis susceptibility, and migration/invasion potential of cancer cells [26]. Recent studies demonstrate that some Oatps are up- or downregulated in several cancers and that Oatp expression might affect cancer development, Oatps could be valuable targets for anticancer therapy [41]. Oatp 2a1 and Oatp 2b1 as members of the solute carrier (SLC) transporters family also undertake the responsibility [20, 21].

Oatp2 is mainly expressed on the sinusoidal membrane of hepatocytes and transporting bilirubin from plasma into the liver. It plays an important role in the excretion of bilirubin and liver toxin. The results showed that, compared with Control group, the expression levels of Oatp2a1 were decreased in liver tissue, spleen tissue, and small intestine tissue in DD group while it increased in colon tissue and stomach tissue; the expression levels of Oatp2b1 were increased in spleen tissue, stomach tissue and colon tissue in DD group. That suggested the DD could regulate the expression of Oatp2a1 and Oatp2b1 in digestive system tissues especial in liver tissue. The expression levels of Oatp2a1 and Oatp2b1 were decreased in liver tissue in HCC-DD group compared with HCC group. However, the study found that downregulation of OATP2 may be involved in the development of hyperbilirubinemia

and hepatotoxicity [42]. So, the reason of bigger tumor size and poorer survival rate of HCC-DD mice might be the decreased Oatp2a1 and Oatp2b1 in the internal environment of depression. In other words, the lower level of Oatp2a1 and Oatp2b1 from the DD might be beneficial to the growth of the tumor in HCC-DD mice. And the toxin metabolism disordered by the decreased expression of Oatp2a1 and Oatp2b1 in liver of HCC-DD. The accumulation of toxins in the tissue of hepatocellular carcinoma might result in an increase of expression of Oatp2a1 and Oatp2b1 in compensatory activity, so they were higher in hepatic carcinoma tissue from HCC-DD mice.

5. Conclusions

Indeed, there was a positive relationship between DD and the overall occurrence risk of HCC. The pathogenic factors might be an imbalanced body homeostasis caused by DD. At the molecular levels, the decreased expression of Oatp2a1 and Oatp2b1 by DD might be involved. However, further studies are needed to explore the role of the Oatp2a1 and Oatp2b1 played in the progression of cancer.

Data Availability

The datasets used and/or analysed during the current study are available from the corresponding author on reasonable request.

Ethical Approval

The whole experimental procedure was performed in the Animal Experimental Center of Sun Yat-sen University (Guangzhou, China). All the procedure was monitored strictly by the Institutional Animal Care and Use Committee (IACUC), Sun Yat-sen University according to the "3R" principles with humanism care to the experimental animals (Ethical Approval No.: IACUC-2013-1002).

Conflicts of Interest

The authors declare that they have no competing interests.

Authors' Contributions

Yan Chen and Jiongshan Zhang contributed equally to this work. Shijun Zhang and Baoguo Sun designed the study and obtained the funding. Yan Chen and Jiongshan Zhang performed the project and wrote the original draft and a review. Mengting Liu and Hao Hu edited the manuscript. Zengcheng Zou and Fenglin Wang analyzed the data. All authors read and approved the final manuscript.

Acknowledgments

This work was supported by the National Natural Science Foundation of China (NO. 81673909, No.81873248,

No. 81373500), Guangdong Science and Technology Department (NO. 2018A030310276, NO. 2017A030313739, NO. 2017A030313723, NO. 2014A020212391, NO. 2013B021800266), and the basic scientific research operation expense of Sun Yat-sen University in Guangdong province (NO. 18zxt09).

References

- [1] R. B. Ladju, D. Pascut, M. N. Massi, C. Tiribelli, and C. H. C. Sukowati, "Aptamer: A potential oligonucleotide nanomedicine in the diagnosis and treatment of hepatocellular carcinoma," *Oncotarget*, vol. 9, no. 2, pp. 2951–2961, 2018.
- [2] N.J. Mehta, A.D. Celik, and M. G. Peters, "Screening for hepatocellular carcinoma: What is missing?" *Hepatology Communications*, vol. 1, no. 1, pp. 18–22, 2017.
- [3] M. Najjar, S. Agrawal, J. Emond, and K. Halazun, "Pretreatment neutrophil–lymphocyte ratio: useful prognostic biomarker in hepatocellular carcinoma," *Journal of Hepatocellular Carcinoma*, vol. 5, pp. 17–28, 2018.
- [4] J. M. Llovet and V. Hernandez-Gea, "Hepatocellular carcinoma: reasons for phase iii failure and novel perspectives on trial design," *Clinical Cancer Research*, vol. 20, no. 8, pp. 2072–2079, 2014.
- [5] C. Menard, M. L. Pfau, G. E. Hodes et al., "Social stress induces neurovascular pathology promoting depression," *Nature Neuroscience*, vol. 20, no. 12, pp. 1752–1760, 2017.
- [6] A. Pera, "Psychopathological processes involved in social comparison, depression, and envy on facebook," *Frontiers in Psychology*, vol. 9, p. 22, 2018.
- [7] D. Fujisawa, H. Inoguchi, H. Shimoda et al., "Impact of depression on health utility value in cancer patients," *Psycho-Oncology*, vol. 25, no. 5, pp. 491–495, 2016.
- [8] C. Chang, M. Hsieh, T. Yang et al., "Selective serotonin reuptake inhibitors and the risk of hepatocellular carcinoma in hepatitis B virus-infected patients," *Cancer Management and Research*, vol. 9, pp. 709–720, 2017.
- [9] H. Qi, J. Ma, Y. Liu et al., "Allostatic tumor-burden induces depression-associated changes in hepatoma-bearing mice," *Journal of Neuro-Oncology*, vol. 94, no. 3, pp. 367–372, 2009.
- [10] T. Huang, E. M. Poole, O. I. Okereke et al., "Depression and risk of epithelial ovarian cancer: Results from two large prospective cohort studies," *Gynecologic Oncology*, vol. 139, no. 3, pp. 481–486, 2015.
- [11] J. Zong, X. Wang, X. Zhou et al., "Gut-derived serotonin induced by depression promotes breast cancer bone metastasis through the RUNX2/PTHrP/RANKL pathway in mice," *Oncology Reports*, vol. 35, no. 2, pp. 739–748, 2016.
- [12] Y. Jia, F. Li, Y. Liu, J. Zhao, M. Leng, and L. Chen, "Depression and cancer risk: a systematic review and meta-analysis," *Public Health*, vol. 149, pp. 138–148, 2017.
- [13] K. M. Giacomini, S.-M. Huang, D. J. Tweedie et al., "Membrane transporters in drug development," *Nature Reviews Drug Discovery*, vol. 9, no. 3, pp. 215–236, 2010.
- [14] Y. Li, J. Lu, and J. W. Paxton, "The Role of ABC and SLC Transporters in the Pharmacokinetics of Dietary and Herbal Phytochemicals and their Interactions with Xenobiotics," *Current Drug Metabolism*, vol. 13, no. 5, pp. 624–639, 2012.
- [15] S. Gulec, G. J. Anderson, and J. F. Collins, "Mechanistic and regulatory aspects of intestinal iron absorption," *American Journal of Physiology-Gastrointestinal and Liver Physiology*, vol. 307, no. 4, pp. G397–G409, 2014.
- [16] K. Chan, S. M. Busque, M. Sailer et al., "Loss of function mutation of the Slc38a3 glutamine transporter reveals its critical role for amino acid metabolism in the liver, brain, and kidney," *Pflügers Archiv - European Journal of Physiology*, vol. 468, no. 2, pp. 213–227, 2016.
- [17] T. Suga, H. Yamaguchi, T. Sato, M. Maekawa, J. Goto, and N. Mano, "Preference of conjugated bile acids over unconjugated bile acids as substrates for OATPIB1 and OATPIB3," *PLoS ONE*, vol. 12, no. 1, Article ID e0169719, 2017.
- [18] T. Sato, H. Yamaguchi, T. Kogawa, T. Abe, and N. Mano, "Organic anion transporting polypeptides 1B1 and 1B3 play an important role in uremic toxin handling and drug-uremic toxin interactions in the liver," *Journal of Pharmacy & Pharmaceutical Sciences*, vol. 17, no. 4, pp. 475–484, 2014.
- [19] J. Xie, X. Y. Zhu, L. M. Liu, and Z. Q. Meng, "Solute carrier transporters: potential targets for digestive system neoplasms," *Cancer Management and Research*, vol. 10, pp. 153–166, 2018.
- [20] T. Nakanishi, Y. Ohno, R. Aotani et al., "A novel role for OATP2A1/SLCO2A1 in a murine model of colon cancer," *Scientific Reports*, vol. 7, no. 1, 2017.
- [21] R. Liedauer, M. Svoboda, K. Wlcek, and eral, "Different expression patterns of organic anion transporting polypeptides in osteosarcomas, bone metastases and aneurysmal bone cysts," *Oncology Reports*, vol. 22, no. 6, pp. 1485–1492, 2009.
- [22] X. Y. Qu, L. N. Tao, S. X. Zhang et al., "The role of Ntcp, Oatp2, Bsep and Mrp2 in liver injury induced by Dioscorea bulbifera L. and Diosbulbin B in mice," *Environmental Toxicology and Pharmacology*, vol. 51, pp. 16–22, 2017.
- [23] J. Min, L. Jie, Y. Caiyun, L. Ying, and Y. Xuefang, "Gene mutation in neonatal jaundice – mutations in UGT1A1 and OATP2 genes," *The Indian Journal of Pediatrics*, vol. 83, no. 7, pp. 723–725, 2016.
- [24] L. Wang, M. Zhou, C. Chen et al., "Increased renal clearance of rocuronium compensates for chronic loss of bile excretion, via upregulation of Oatp2," *Scientific Reports*, vol. 7, no. 1, Article ID 40438, 2017.
- [25] D. N. Samonakis and E. A. Kouroumalis, "Systemic treatment for hepatocellular carcinoma: Still unmet expectations," *World Journal of Hepatology*, vol. 9, no. 2, p. 80, 2017.
- [26] M. Surman and M. E. Janik, "Stress and its molecular consequences in cancer progression," *Postepy Higieny i Medycyny Doswiadczalnej*, vol. 71, pp. 485–499, 2017.
- [27] H. Ikram and D. J. Haleem, "Repeated treatment with reserpine as a progressive animal model of depression," *Pakistan Journal of Pharmaceutical Sciences*, vol. 30, no. 3, pp. 897–902, 2017.
- [28] T. Yan, B. He, S. Wan et al., "Antidepressant-like effects and cognitive enhancement of Schisandra chinensis in chronic unpredictable mild stress mice and its related mechanism," *Scientific Reports*, vol. 7, no. 1, Article ID 6903, 2017.
- [29] H. Luo, Y. Chen, B. Sun, T. Xiang, and S. Zhang, "Establishment and evaluation of the orthotopic hepatocellular carcinoma and drug-induced hepatocellular carcinoma in mice with spleen-deficiency syndrome in traditional chinese medicine," *African Journal of Traditional, Complementary and Alternative Medicines*, vol. 14, no. 1, pp. 165–173, 2016.
- [30] K. Cao, C. Shen, Y. Yuan et al., "SiNiSan ameliorates the depression-like behavior of rats that experienced maternal separation through 5-HT1A receptor/CREB/BDNF pathway," *Frontiers in Psychiatry*, vol. 10, p. 160, 2019.
- [31] A. Bhattacharya and W. C. Drevets, "Role of neuro-immunological factors in the pathophysiology of mood

- disorders: Implications for novel therapeutics for treatment resistant depression.” *Current Topics in Behavioral Neurosciences*, vol. 31, pp. 339–356, 2017.
- [32] C. Chang, S. Chen, C. Liu, and E. Villa, “Risk of developing depressive disorders following hepatocellular carcinoma: a nationwide population-based study,” *PLoS ONE*, vol. 10, no. 8, p. e0135417, 2015.
- [33] S. Polis and R. Fernandez, “Impact of physical and psychological factors on health-related quality of life in adult patients with liver cirrhosis: a systematic review protocol,” *JBIC Database of Systematic Reviews and Implementation Reports*, vol. 13, no. 1, pp. 39–51, 2015.
- [34] S.-W. Lai, C.-L. Lin, K.-F. Liao, and W.-C. Chen, “No association between depression and risk of hepatocellular carcinoma in older people in Taiwan,” *ISRN Psychiatry*, vol. 2013, Article ID 901987, 3 pages, 2013.
- [35] H. Yu, D. Lv, M. Shen et al., “BDNF mediates the protective effects of scopolamine in reserpine-induced depression-like behaviors via up-regulation of 5-HTT and TPH1,” *Psychiatry Research*, vol. 271, pp. 328–334, 2019.
- [36] M. S. Riaz, M. O. Bohlen, B. W. Gunter, Q. Henry, C. A. Stockmeier, and I. A. Paul, “Attenuation of social interaction-associated ultrasonic vocalizations and spatial working memory performance in rats exposed to chronic unpredictable stress,” *Physiology & Behavior*, vol. 152, pp. 128–134, 2015.
- [37] L. J. Steinberg, M. D. Underwood, M. J. Bakalian et al., “5-HT1A receptor, 5-HT2A receptor and serotonin transporter binding in the human auditory cortex in depression,” *Journal of Psychiatry & Neuroscience*, vol. 44, no. 4, pp. 1–8, 2019.
- [38] L. He, D. Tian, P. Li, and X. He, “Mouse models of liver cancer: Progress and recommendations,” *Oncotarget*, vol. 6, no. 27, pp. 23306–23322, 2015.
- [39] Y. T. Lu, J. Li, X. Qi et al., “Effects of Shugan Jianpi Formula on myeloid-derived suppression cells-mediated depression breast cancer mice,” *Chinese Journal of Integrative Medicine*, 2016.
- [40] J. Blume, S. D. Douglas, and D. L. Evans, “Immune suppression and immune activation in depression,” *Brain, Behavior, and Immunity*, vol. 25, no. 2, pp. 221–229, 2011.
- [41] A. Obaidat, M. Roth, and B. Hagenbuch, “The expression and function of organic anion transporting polypeptides in normal tissues and in cancer,” *Annual Review of Pharmacology and Toxicology*, vol. 52, pp. 135–151, 2012.
- [42] A. Q. Alkhedaide, “Preventive effect of *Juniperus procera* extract on liver injury induced by lithocholic acid,” *Cellular and Molecular Biology*, vol. 64, no. 13, pp. 63–68, 2018.